UNIVERSITY OF CALIFORNIA
RIVERSIDE

Analysis of SUMO Function in WUS-Mediated Stem Cell Maintenance

A Dissertation submitted in partial satisfaction
of the requirements for the degree of

Doctor of Philosophy

in

Plant Biology

by

Stephen Andrew Snipes

March 2016

Dissertation Committee:

Dr. Venugopala Reddy Gonehal, Chairperson
Dr. Patricia Springer
Dr. Zhenbiao Yang

The Dissertation of Stephen Andrew Snipes is approved:

_____

_____

_____

Committee Chairperson

University of California, Riverside

Acknowledgements

I would first like to thank Dr. Venu Reddy Gonehal for his superb tutelage and advisement throughout my graduate school career. He has been extremely supportive throughout this endeavor both scientifically and financially, and has provided essential advice to help focus and improve my doctoral research plan. I owe so much of my scientific career to the lessons he has taught me. I also would like to thank my dissertation committee members, Dr. Patricia Springer and Dr. Zhenbiao Yang, who have also provided valuable comments and advice throughout my doctoral studies. These professors along with Dr. Xuemei Chen, Dr. Linda Walling, and Dr. Howard Judelson all provided critical comments to my dissertation proposal that helped shaped my research into a fruitful pursuit through my qualifying exam. I would also like to thank Dr. Thomas Girke for his help with introducing me to bioinformatics analysis approaches that I was able to employ in my research.

I would also like to thank many postdoctoral and graduate student researchers who provided great assistance and discussion throughout my doctoral career. Dr. Mariano Perales, Dr. Ram Yadav, Dr. Mercedes Diaz-Mendoza, Dr. Kaori Miyawaki, Dr. Ricardo Moreno, Dr. Aaron Devries, and Kevin Rodriguez all provided great assistance to my experimental design and troubleshooting research problems that arose throughout my tenure. I also had the help of an exceptional undergraduate student, Taher Baijee, who was extremely helpful with functional screening analysis and many other research projects. I would finally like to thank my fellow graduate students, friends and family for providing scientific and emotional support throughout my graduate school career.

ABSTRACT OF THE DISSERTATION

Analysis of SUMO Function in WUS-Mediated Stem Cell Maintenance

by

Stephen Andrew Snipes

Doctor of Philosophy, Graduate Program in Plant Biology
University of California, Riverside, March 2016
Dr. Venugopala Reddy Gonehal, Chairperson

The Shoot Apical Meristem of plants harbors a small population of undifferentiated stem cells that is responsible for propagating all of the post-embryonic organ development through the differentiation of a subset of these stem cell daughters. WUSCHEL is a homeodomain transcription factor that moves from its domain of expression to act in a non-cell autonomous manner to promote stem cell maintenance and repress differentiation promoting factors in the stem cell domain. The mechanisms regulating this non cell autonomous behavior are poorly understood. Protein interactions are important in modulating the function of target proteins, and this study sought to identify factors that regulate this WUSCHEL activity by uncovering the WUSCHEL-protein interaction network through a yeast two-hybrid interaction screen in tandem with a high throughput sequencing approach. A total of 119 putative WUS-interactors were identified, and a subset of 62 was functionally characterized through a RNAi reverse genetics suppressor screen in the *clv3-2 pWUS::eGFP-WUS* background. The four interactors TCTP, FLOR1, AT3G12300, and AT1G67035 were shown to suppress the c*lv3-2* phenotype, and all of these except FLOR1 reduced the accumulation of WUS in the SAM. SUMO, a regulator of protein localization, transcriptional activity, and stability

via post-translational modifications and non-covalent protein interactions was also identified in the yeast two-hybrid screen. Molecular analysis revealed an interaction between WUS and SUMO1/SUMO2 occurs across a broad sequence that includes a homodimerization motif, a transcriptional enhancer motif, and a motif that regulates both target gene repression and nuclear accumulation. Genetic analysis with *sumo1/2* lines revealed smaller meristems and reduced accumulation of eGFP-WUS. Additionally, an inducible form of WUS lacked the ability to strongly activate expression of *CLV3* in the *sumo1/2* background.

These data reveal a potential network of WUS interactors that could facilitate new understanding in the modulation of WUS function. The interaction between WUS and SUMO links an essential highly conserved protein regulator to WUS-mediated stem cell maintenance, and provides a fascinating avenue for future study of protein complex modulation of WUS function.

Table of Contents

Introduction

Structure of the SAM and WUS Function ---------- 1

SUMO Regulation of Protein Function ---------- 4

Systems for Detection of Protein-Protein Interactions ---------- 7

High Throughput Sequencing for Analysis of Large Scale DNA Datasets -------- 11

RNAi Regulation of Target Gene Expression ---------- 13

Confocal Microscopy and Fluorescent Proteins as Molecular Biology Tools ---- 14

Dissertation Objectives ---------- 16

Chapter 1: A High Throughput Sequencing Approach Reveals a Possible WUSCHEL Protein-Protein Interaction Network

Introduction ---------- 17

Results ---------- 20

Discussion ---------- 27

Methods ---------- 31

Chapter 2: A Reverse Genetics Screen of WUS PPIs Reveals Factors with Possible Functional Roles in WUS Mediated SAM Maintenance

Introduction ---------- 59

Results ---------- 63

Discussion ---------- 68

Methods ---------- 73

Chapter 3: Biochemical and Genetic Analysis of the WUS-SUMO1/SUMO2 Interaction Reveals a Role for SUMO1/SUMO2 in WUS-Mediated SAM Maintenance

Introduction ---------- 96

Results ---------- 99

Discussion ---------- 114

Methods ---------- 123

References ---------- 135

List of Figures

Introduction

Figure 0.1: General Structure and Features of the SAM ---------- 2

Figure 0.2: SUMOylation and Non-covalent SUMO-Protein Interactions --------- 6

Figure 0.3: Methods for Identifying Protein-Protein Interactions---------- 8

Figure 0.4: Confocal Microscopy for SAM Imaging ----------15

Chapter 1: A High Throughput Sequencing Approach Reveals a Possible WUSCHEL Protein-Protein Interaction Network

Figure 1.1: Overview of Y2H screening and independent confirmation of WUS PPIs----------22

Figure 1.2: Analysis of WUS PPIs based on GO Slim and cell type expression data ----------26

Figure S1.1: Y2H transactivation assay, library screening, and negative WUS PPIs----------38

Figure S1.2: Sequence analysis of a WUS PPI subset and negative BiFC controls ----------39

Figure S1.3: Network of WUS PPIs----------40

Chapter 2: A Reverse Genetics Screen of WUS PPIs Reveals Factors with Possible Functional Roles in WUS Mediated SAM Maintenance

Figure 2.1: Filtering of 119 WUS PPIs Into a Subset of 62 for Screening with RNAi----------62

Figure 2.2: Phenotypes of RNAi Partial *clv3-2* Suppressor Lines ----------65

Figure 2.3: Confocal Images of pYU501 Lines with clv3-2 Suppression Phenotypes ---------- 66

Figure 2.4: Semi-quantitative Analysis of eGFP-WUS Accumulation and SAM Size in RNAi Partial *clv3-2* Suppressor Phenotypes ---------- 67

Figure S2.1: Semi-quantitative Analysis of eGFP-WUS and SAM Size in RNAi Lines ---------- 77

Chapter 3: Biochemical and Genetic Analysis of the WUS-SUMO1/SUMO2 Interaction Reveals a Role for SUMO1/SUMO2 in WUS-Mediated SAM Maintenance

Figure 3.1: Selective Mapping the Interaction Region of WUS and SUMO1/SUMO2 ---------- 102

Figure 3.2: BiFC and Co-IP Interactions of WUS-SUMO1/SUMO2 ---------- 107

Figure 3.3: Phenotypes of *sumo1/2* Plants ---------- 108

Figure 3.4: Accumulation of WUS and WUS Mutant Variants in *sumo1/2* ----- 110

Figure 3.5: Quantification of *pWUS::eGFP-WUS* in *Wt* and *sumo1/2* lines ---- 111

Figure 3.6: Response of *CLV3* Expression to Manipulation of WUS Levels in *sumo1/2* ---------- 116

Figure S3.1: Non-Selective Controls for Mapping the Interaction Region of WUS and SUMO1/SUMO2 ---------- 127

Figure S3.2: BiFC Controls of WUS-SUMO1/SUMO2 ---------- 128

Figure S3.3: Accumulation of WUS and WUS Mutant Variants in *sumo1/2* --- 129

Figure S3.4: Semi- Quantitation of *WUS* and *CLV3* Expression in *Wt* and *sumo1/2*

SAMs ---------- 130

Figure S3.5: Semi-Quantitative Analysis of eGFP-WUS and SAM Size in *sumo1/2* lines ---------- 131

List of Tables

Chapter 1: A High Throughput Sequencing Approach Reveals a Possible WUSCHEL Protein-Protein Interaction Network

Table 1.1: Selection Data for Y2H Screen ---- 41

Table 1.2: List of WUS PPIs with Unique Cell Type Localization ---- 41

Table S1.1: List of WUS PPIs with Their Cell Type, Functional Grouping, and Subcellular Localization ---- 44

Table S1.2: WUS PPI Clones Verified via Independent Sanger Sequencing ---- 58

Table S1.3: Primers ---- 58

Chapter 2: A Reverse Genetics Screen of WUS PPIs Reveals Factors with Possible Functional Roles in WUS Mediated SAM Maintenance

Table S2.1: WUS PPIs Used in RNAi Knockdown Reverse Genetics Screen ---- 78

Table S2.2: Primers ---- 92

Chapter 3: Biochemical and Genetic Analysis of the WUS-SUMO1/SUMO2 Interaction Reveals a Role for SUMO1/SUMO2 in WUS-Mediated SAM Maintenance

Table S3.1: Predicted SUMOylation and SIM Sites on WUS ---- 132

Table S3.2: Primers ---- 133

Introduction:

Structure of the SAM and WUS Function

Plant development is a complex process that integrates many diverse signaling mechanisms in a temporal and spatial specific manner. The two structures responsible for maintaining this development throughout the lifespan of the plant are the Root Apical Meristem (RAM) and the Shoot Apical Meristem (SAM), both of which house a small population of undifferentiated stem cells that are essential for the continued development of new organs (Sussex, 1952, Sussex, 1989, Barton and Poethig, 1993, Schoof et al., 2000). The SAM is comprised of three distinct cell layers, the epidermal L1 layer, the subepidermal L2 layer, and the inner corpus L3 layer (Sussex, 1989). At the center of the SAM across the L1-L3 layers, a small population of 20-30 undifferentiated stem cells forms the Central Zone (CZ) (Figure 0.1A) (Steeves and Sussex, 1989, Brand et al., 2000, Reddy, 2008). As these stem cells divide, one daughter cell is retained in the stem cell pool to facilitate continued propagation of the stem cells throughout the plant lifespan (Steeves and Sussex, 1989). The second stem cell daughter resulting from this anticlinal division is pushed away from the stem cell pool and begins to differentiate as subsequent cell divisions occur (Steeves and Sussex, 1989). Mutagenesis and ablation studies have demonstrated that the L1 and L2 layers that originate from these cell divisions form clonally distinct single cell layers (Reinhardt et al., 2003). The continued division of these cells displaces them into the Peripheral Zone (PZ), which is divided into two regions. The first of these is in the Inner Peripheral Zone (IPZ) and is an incomplete stage of differentiation which is reversible in the proper environment (Reddy, 2008). Further

divisions push these cells further towards the Outer Peripheral Zone (OPZ), in which the differentiation program is not easily reversible (Reddy, 2008).

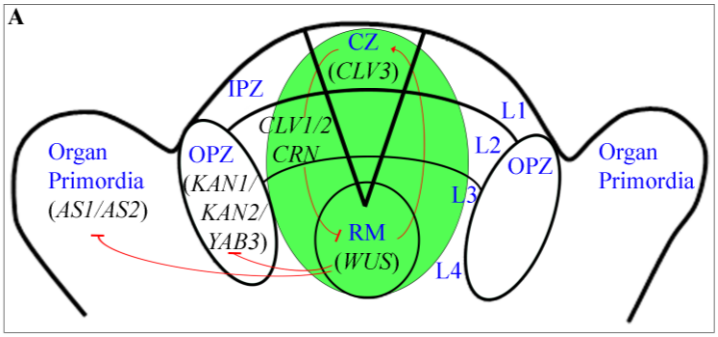

Figure 0.1: General Structure and Features of the SAM. A simplified sideview of the SAM shows the regions identified as the Rib Meirstem (RM), Central Zone (CZ), Inner Peripheral Zone (IPZ), Outer Peripheral Zone (OPZ), L1-L4 layers, and the developing Organ Primordia (A). *WUS* is expressed in the RM, and encodes a mobile protein which fills the space in green. WUS directly activates *CLV3* expression in the stem cell containing CZ, which encodes a small peptide that represses *WUS* expression through signalling mediated by the membrane bound receptor kinases CLV1/CLV2/CRN. WUS also represses the expression of differentiation promoting genes such as KAN1/KAN2, YAB3, and AS1/AS2. Red connections represent positive (arrows) and negative (lines) regulatory interactions, blue text represents SAM regions, and black text are genes.

Underneath the CZ in the L3 and L4 deeper layers, a small group of cells in the Rib Meristem (RM) is responsible for regulating the size of the CZ via the expression of the homeobox transcription factor WUSCHEL (WUS) (Mayer et al., 1998, Brand et al, 2000). WUS and the *KNOX* gene encoding SHOOT MERISTEMLESS (STM) are responsible for repressing the expression of independent sets of differentiation inducing genes in the CZ (Lenhard et al., 2002). Many of these genes, such as *KANADI1/KANADI2*, *ASYMMETRIC LEAVES1/ASYMMETRIC LEAVES2*, and *YABBY3* are direct transcriptional regulators of leaf patterning, polarity and development (Yadav et al. 2013). Mutations in both *wus* and *stm* result in a loss of SAM identity that demonstrates their essential function in SAM and stem cell maintenance (Schoof et al., 2000, Lenhard et al., 2002).

Additionally, WUS is a mobile protein that is able to act non cell autonomously to directly bind and activate the expression of *CLV3* in the CZ, which encodes a small 96

AA protein that is enzymatically cleaved and post-translationally arabinosylated to form a mature functional signaling 13 residue peptide (Kondo et al., 2006, Ohyama et al., 2009, Yadav et al., 2013). This peptide moves through the apoplastic space and binds to the CORYNE/CLV1/CLV2 family of membrane bound leucine-rich repeat receptor kinases (LRR-RKs) to initiate a signaling cascade that in turn downregulates the expression of *WUSCHEL* and maintains a homeostatic population of stem cells in the CZ (Rojo et al., 2002, Guo et al., 2010). This was confirmed through genetic analysis using both *clv3* and an inducible *CLV3* RNAi knockdown system, which both yield SAM and stem cell domain expansion (Schoof et al., 2000, Reddy and Meyerowitz, 2005). Additionally, *wus clv3* double mutant phenotypes are similar to those of *wus* single mutants with terminated flattened SAMs, demonstrating the epistatic nature of *CLV3* in relation to *WUS*. The mechanisms by which WUS represses the expression of differentiation promoting genes while activating genes responsible for regulating the stem cell population are still relatively unclear at this juncture.

WUS movement is an essential part to this function, as 2xeGFP-WUS fusion protein expressed from its native promoter, which is too large to move out of the RM, fails to rescue the *wus* phenotype (Yadav et al., 2009). However, little is known about the regulation of this WUS movement out of the RM. Protein complexes are critically important to facilitate movement of proteins within a cell and across cells, indeed there are entire families of proteins dedicated to transport and localization, such as the importin α/β family, which regulates nuclear import and export (Yoneda et al., 1999, Bollman et al., 2003). The significance of protein complexes in movement has even been

demonstrated in a meristem context through the regulation of SHORT-ROOT (SHR) movement mediated by its co-factor SCARECROW (SCR) in the RAM (Nakajima et al., 2001, Gallagher et al., 2004, Cui et al., 2007). SHR is able to move from its expression in the stele of the root into the adjacent Quiescent Center (QC) and endodermis layer, where it is sequestered in the nucleus by SCR protein interaction (Nakajima et al., 2001, Gallegher et al., 2004, Cui et al., 2007). These concepts demonstrate the importance of further understanding the protein complexes that could regulate mobility and other critical functions of WUS in SAM maintenance.

SUMO Regulation of Protein Function

Protein regulation occurs via a wide array of post-translational modifications and protein interaction complexes, which provide essential functions to developmental processes. One of the most well understood regulators of protein function across eukaryotic taxa is UBIQUITIN (UBQ), a protein that was first discovered in research on the bovine thymus (Schlesinger et al., 1975). Further analysis revealed its presence in almost every cell type across eukaryotic taxa (Goldstein et al., 1975). Ubiquitination is a multi-step process involving a series of enzymatic steps regulated by the UBIQUITIN-ACTIVATING ENZYME (E1), UBIQUITIN-CONJUGATING ENZYMES (E2), and UBIQUITIN-PROTEIN LIGASES (E3) to direct the covalent attachment of the C-terminal G76 residue to a K residue on the target protein (Hershko et al., 1983). The main function of protein ubiquitination is targeted degradation via transport to the 26S proteasome or through exocytosis; however other functions such as transcription factor

regulation and DNA repair occur in small instances (Chau et al., 1989, Spence et al., 1995, Hofmann and Pickart, 1999, Kaiser et al., 2000).

A related SMALL UBIQUITIN-LIKE MODIFIER (SUMO) has been identified as another crucial regulator of protein function. SUMO has two main mechanisms through which it regulates target protein activity: SUMOylation, which functions in a manner similar to Ubiquitination, and non-covalent protein interactions through SUMO Interacting Motifs (SIMs) (Shen et al., 1996, Minty et al., 2000, Hecker et al., 2006). SUMOylation occurs in a similar multi-enzymatic process consisting of a SUMO-ACTIVATING ENZYME (E1), a SUMO-CONGUGATING ENZYME (E2), and SUMO LIGASES (E3) (Figure 0.2A) (Muller et al., 2001, Kurepa et al., 2003). In *A. thaliana* the SUMO E1s consists of SAE1/SAE2, and are essential for the ATP-dependent activation of SUMO (Kurepa et al., 2003). The SUMO E2 protein SCE1 is used to transfer the active SUMO from the E1 to the E3 members SIZ1/SIZ2 and HIGH PLOIDY2 (HPY2), which then covalently attach the C-terminal G92 of processed SUMO to a K residue on the target protein (Kurepa et al., 2003, Saracco et al., 2007, Ishida et al., 2009). Mutations in *sae1/sae2* or *sce1* are embryonic lethal, demonstrating the essential function of SUMOylation in plant development (Saracco et al., 2007). Mutations in *siz1/siz2* result in increased sensitivity to cold, and mutations in *hpy2* result in reduced cell division and expansion in the root (Muira et al., 2007, Huang et al., 2009). SUMOylation has several distinct differences from Ubiquitination, the first of which is the diverse set of functions that SUMOylation regulates including transcriptional activation, subcellular localization, chromatin modification, and protein complex binding (Tsuruzoe et al., 2006, Du et al.,

2008, Budhiraja et al., 2009, Bauer et al., 2010, Elrouby et al., 2013). Another unique aspect of SUMOylation is its highly reversible nature and the percentage of actively SUMOylated targets that is typically below 20% of the total target protein population at a given time (Mazur and van den Burg, 2012).

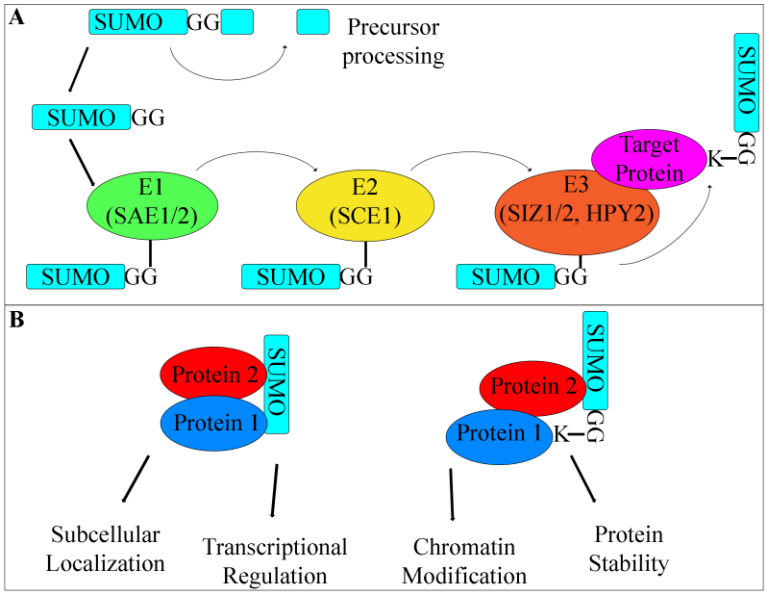

Figure 0.2: SUMOylation and Non-covalent SUMO-Protein Interactions. A general overview of the SUMOylation enzymatic steps (A). The SUMO protein is processed to expose the C-terminal G92, which is then transferred to the SAE1/SAE2 E1 complex. SUMO is then transferred to the SCE1 E2 complex, and finally to the SIZ1/SIZ2/HPY2 E3 complex. The E3 complex covalently attaches SUMO to the targeted protein. SUMO facilitates non-covalent protein-protein interactions that regulate diverse cellular processes through the stabilization of protein complexes that may or may not include SUMOylated proteins.

In addition to the covalent modifications of target proteins through SUMOylation, SUMO can also interact with target proteins in a non-covalent manner using a SIM (Figure 0.2B) (Hecker et al., 2006). This phenomenon is less well characterized than SUMOylation, yet still provides many essential functions. Protein-protein interaction analysis identified a set of STUbLs that are responsible for chromatin methylation (Elrouby et al., 2013). PIAS repression of target gene expression is enhanced by SUMO non-covalent interactions, a function that is of significant importance with respect to WUS-mediated repression of differentiation promoting factors (Ullmann et al., 2012). A combination of SUMOylation and non-covalent interactions can facilitate and stabilize

the interaction of various protein complexes, as shown with the requirement of Ran-GAP1 SUMOylation to facilitate its interaction between RanBP2 at the nuclear pore complex (Mahajan et al., 1997). This combined functionality is yet another feature that provides an intriguing and potentially relevant role to understanding WUS protein complex formation.

Systems for Detection of Protein-Protein Interactions

A critical feature in the regulation of protein function is the formation of multi-protein complexes that provide temporal and spatial functional specificity. Therefore, the identification of protein-protein interaction complexes is essential to understanding the complex networks and pathways within which a protein functions. Over the past several decades, several techniques have been developed to identify protein-protein interactions, and these approaches have greatly expanded our knowledge of protein regulation.

Co-immunoprecipitation is a rather straightforward process that extrapolates the techniques of immunoprecipitation (Beeckmans and Kanarek, 1981). Proteins isolated from a tissue sample are enriched via the presence of a specific antibody for the protein of interest. Then, the isolated target protein and its protein-protein interaction partners can be separated via a SDS-PAGE denaturing gel and an antibody specific to the second protein of interest can be used for detection of an interaction (Figure 0.3A) (Beeckmans and Kanarek, 1981, Farras et al., 2001). This procedure has undergone slight modifications over the past few decades, including the addition of tags with standardized antibodies such as HIS, HA, and FLAG epitopes to reduce the need for specific antibodies to each target protein (Field et al., 1988, Hopp et al., 1988, Hoffman and

Roeder, 1991). While this approach is useful for determining protein-protein interactions in native tissue, it suffers from an efficient high-throughput approach for protein-protein interaction analysis.

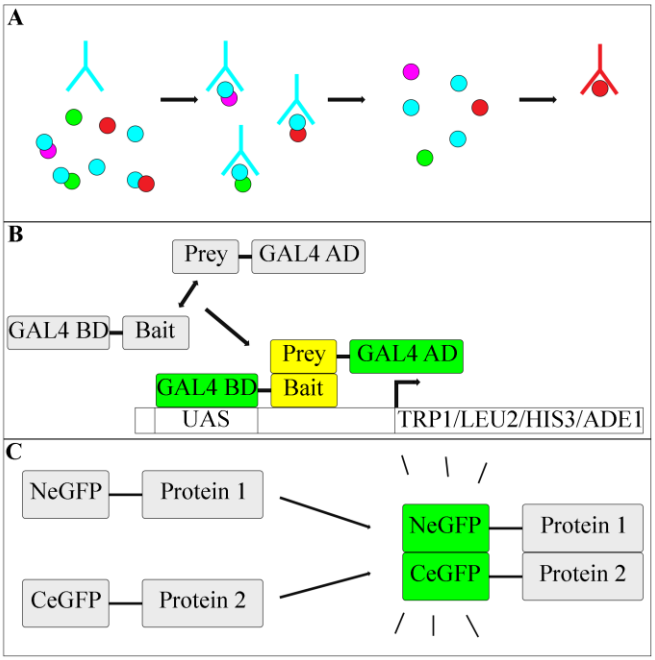

Figure 0.3: Methods for Identifying Protein-Protein Interactions. Co-IP involves the purification of a desired protein and any potential interacting partners (A). Then a second antibody specific to the targeted interactor is used to identify its presence in the pool of enriched protein-protein interaction complexes. Yeast two-hybrid experiments rely on a protein of interest (Bait) fused to the GAL4 DNA Binding Domain (BD) and a second protein of interest (Prey) fused to the GAL4 Activation Domain (AD) (B). Interaction between the two proteins of interest reconstitues a functional GAL4 transcriptional regulator that is able to activate the expression of auxotrophic selection markers to be used in yeast growth. BiFC relys on a similar mechanism to the yeast two hybrid system, but replaces the transcriptional regulator subunits with split halves of a fluorescent protein that only fluoresce when reconstituted via protein-protein interaction of the two target proteins (C).

The yeast two-hybrid approach was first developed to utilize the natural function of the GAL4 transcriptional regulator in *S. cerevisiae* (Fields and Song, 1989). The GAL4 protein is composed of two functional motifs: a N-terminal DNA binding element that recognizes a canonical UAS gene regulation sequence, and a C-terminal transcriptional activator motif (Fields and Song, 1989). Independently these motifs are not sufficient for activation of gene expression, yet working in tandem these two elements are functional (Fields and Song, 1989). Indeed, these motifs are functional even expressed as separate units as long as they are reconstituted in close proximity (Fields and Song, 1989). This

ability to function as separate units is essential to the yeast two-hybrid technique, as it allows each GAL4 motif to be expressed in a translational fusion with a protein of interest to generate a 'bait' protein fusion to the GAL4 DNA binding motif and a 'prey' protein fusion to the GAL4 transcriptional activation motif (Figure 0.3B) (Fields and Song, 1989). These constructs are co-transformed into yeast cells typically with mutations in several genes essential for AA biosynthesis such as *trp1, leu2, his3,* and *ade1;* and if the 'bait' and 'prey' proteins interact, the two functional GAL4 motifs are brought into proximity to reconstitute a functional complex that is able to regulate gene activation (Fields and Song, 1989). The presence of mutations in the AA biosynthesis genes are essential since functional variants of *TRP1, LEU2, HIS3,* and *ADE1* are used as auxotrophic selection markers for both the co-transformed constructs (such as *TRP1* and *LEU2* respectively in the system demonstrated in this work) and the reconstitution of a functional GAL4 complex brought about through positive protein-protein interactions (such as *HIS3* and *ADE1* in the system used in this work) (Fields and Song, 1989). Additionally, reporters using the *lacZ* gene can be used to perform β-galactosidase assays for visualization as a secondary confirmation of positive protein-protein interaction (Fields and Song, 1989).

This procedure is of vital importance to the progression of protein-protein interaction analysis and protein network development over the past several decades, and several iterations on this process have improved the technique even further (Fields and Song, 1989, James et al., 1996). The most essential of these is the development of a yeast two hybrid screening procedure, which allows cloning of large cDNA libraries as 'prey'

constructs and screening their encoded proteins for an interaction against a specific 'bait' protein (James et al., 1996, Gietz et al., 1997, Uetz et al., 2000, Ito et al., 2001). This provides an efficient method for identifying the network of proteins that interact with a protein of interest. Another essential variant is the introduction of the yeast one-hybrid system, which instead screens for protein-DNA interactions by replacing the 'bait' protein fusion with a DNA sequence to which the 'prey' protein fusion binds (Li and Herskowitz, 1993). Finally, the yeast three-hybrid approach introduces either a third intermediary protein or an RNA molecule to determine the requirement of the protein or RNA respectively in the formation of a complex with the 'bait' and 'prey' protein (Zhang and Lautar, 1996, Hook et al., 2005).

Other more recent tools for analysis of protein interactions include Bi-molecular Fluorescence Complementation (BiFC) and Forster Resonance Energy Transfer (FRET), both of which rely on 'bait' and 'prey' proteins fused to fluorescent proteins instead of GAL4 subunits (Day, 1998, Gordon et al., 1998, Hu et al., 2002). In BiFC experiments, two non-fluorescent subunits of a fluorescent protein such as YFP or eGFP are fused to a 'bait' and 'prey' protein and co-expressed in cells to visualize the reconstitution of a functional fluorescent protein when the 'bait' and 'prey' proteins interact (Figure 0.3C) (Hu et al., 2002, Walter et al., 2004, Kerppola et al., 2008). In FRET, a 'donor' molecule is excited through specific wavelength exposure, which then results in the emission of energy that is within the acceptable window to excite a nearby secondary 'acceptor' molecule, which then emits energy at a second unique wavelength (Gordon et al., 1998). Using two fluorophore 'donor' and 'acceptor' molecules in which the excitation and

emission wavelengths do not overlap, and the emission wavelength of the 'donor' does overlap with the 'acceptor' molecule, interaction of proteins fused to the 'donor' and 'acceptor' can be determined visually by exciting the 'donor' fluorophore and visualizing the specific emission spectra of the 'acceptor' fluorophore (Gordon et al., 1998). These techniques provide a useful alternative to identify protein-protein interactions that can also provide additional information, such as the subcellular localization of such a protein-protein interaction (Walter et al., 2004, Kerppola et al., 2008, Zhong et al., 2008).

High Throughput Sequencing for Analysis of Large Scale DNA Datasets

DNA sequencing technologies have advanced greatly in the past several decades since the introduction of chain terminating DNA polymerase sequencing (Sanger et al., 1977). This initial approach utilized the chemistry of deoxyribonucleotides (dNTPs) and the requirement of the 3'-hydroxyl group in the elongation of DNA sequences by DNA polymerase (Sanger et al., 1977). By introducing small concentrations of dideoxyribonucleotides (ddNTPs) of each base independently into separate aliquots of the same DNA polymerase reaction, randomly terminated sequences were generated that could then be visualized on an acrylamide gel to identify the order of the DNA bases responsible for terminating each reaction (Sanger et al., 1977). Then based on the order of sizes of these terminated DNA strands, the sequence of DNA molecules can be reconstituted (Sanger et al., 1977). Further advancements to this technique introduced fluorescent tags for systematic and efficient visualization of each ddNTP, which eliminated the requirement for independent reactions and tedious gel based visualization of the DNA sequences (Prober et al., 1987). Then the introduction of bacterial artificial

chromosomes (BACs) and yeast artificial chromosomes (YACs) provided a system for faster analysis of DNA sequences through restriction digest mapping and PCR amplification and sequencing (Green and Olson, 1990, Kim et al., 1996). These developments, along with shotgun sequencing techniques that involve the sequencing of random DNA elements that have typically been enzymatically or physically sheared and cloned into high-replication plasmid constructs, permitted important scientific milestones such as the sequencing of the Human and *A. thaliana* genomes among others (Green and Olson, 1990, Kim et al., 1996, Venter et al., 1998, Kaul et al., 2000).

It was not until the introduction of high throughput sequencing techniques that the exponential burst in DNA sequence data was observed. Several new approaches were developed in a short time span, and these so-called next generation sequence outputs are largely categorized by their instrumentation and methods into three prominent types: 454, Illumina/Solexa, and ABI/SOLiD (Shendure et al., 2005, Barbazuk et al., 2007, Dohm et al., 2008, Liu et al., 2012). With these approaches, millions of DNA sequence reads can be performed over a series of several days, greatly reducing the sequence generation time relative to previously described methods. 454 sequencing uses pyrosequencing, which involves detection of the pyrophosphate (PPi) that is released when a dNTP is incorporated into the DNA sequence (Liu et al., 2012). Bases are added individually and in succession, and those which are not incorporated are subsequently degraded. Synthesis of the PPi detected together with the order of dNTPs added to the reaction is used to generate the resulting DNA sequence (Liu et al., 2012). Illumina/Solexa technology is perhaps the most widely used and inexpensive technology, and it provides sequence reads

during synthesis. After DNA sequences are fixed in place by sequence adapters on a flowcell, bridge PCR is used to create clustered groups of each sequence (Dohm et al., 2008, Liu et al., 2012). Then, strand synthesis is performed with dNTPs that contain dyes to be imaged as the strand is elongated (Dohm et al., 2008). ABI/SOLiD sequencing undergoes sequencing by ligation, in which a pool of degenerate oligomers that are differentially color labeled at each base are ligated to the target sequence, via an anchor primer (Shendure et al., 2005, Liu et al., 2012). Through the ligase complementarity specificity, the sequence can be identified by the colors ligated, and this process is repeated sequentially (Shendure et al., 2005). Of these approaches, Illumina/Solexa sequencing currently produces the most cost effective and efficient approach, yielding sequence reads commonly over 500Gbp per run and over 98% accuracy, all with the lowest cost per base sequence per run (Liu et al., 2012). These techniques are driving the exponential growth of sequencing data and leading to new approaches to sequencing experiments. Some novel applications of high throughput sequencing approaches include RNA-seq to sequence the transcriptome, and ChiP-seq to sequence DNA elements bound to proteins of interest that are isolated via immunoprecipitation (Marioni et al., 2008, Visel et al., 2009).

RNAi Regulation of Target Gene Expression

The Central Dogma of molecular biology describes the transcription of DNA into RNA, the translation of RNA into proteins, and the self-replication of DNA itself (Crick, 1970). In this classical model, the DNA and consists of the hereditary elements, and the proteins serve as the functional units responsible for maintaining cell function. However,

the role of RNA outside of the conversion of genetic sequences into functional proteins was poorly understood. One key discovery of a unique RNA function was the identification of short 21-26nt RNA sequences in *C. elegans* that suppress gene expression (Fire et al., 1998, Grishok et al., 2001). In plants, these RNA interference (RNAi) elements are double stranded sequences that down-regulate the expression of a target gene by guiding a target mRNA to the ARGONAUTE (AGO) family of proteins via sequence complementarity to undergo enzymatic cleavage and subsequent degredation (Hamilton and Baulcombe, 1999, Grishok et al., 2001, Baumberger and Baulcombe, 2005). The discovery of these molecules and their function in plants led to a quick advancement in the understanding of RNA mediated posttranscriptional gene silencing (PTGS), and introduction of targeted RNAi molecules to genes such as *CLV3*, *AGAMOUS* (*AG*), *APETALA1*, and *PERIANTHIA* resulted in phenotypes similar to their respective genetic mutants (*clv3-2*, *ag-1*, *ap1-1*, *ap1-4*, *ap1-5*, and *crc-1* (Hamilton and Baulcombe, 1999, Chuang and Meyerowitz, 2000). In light of this, plant expression systems have been developed that use RNAi constructs to facilitate targeted downregulation of specific genes for phenotypic characterization and reverse genetic screening experiments such as the screen presented in this work (Ueno et al., 2007).

Confocal Microscopy and Fluorescent Proteins as Molecular Biology Tools

Microscopy has been an essential analytical tool throughout the field of biology, and the development of confocal microscopy techniques have proven critical to the dissection of genetic and protein systems in cells. The basic principle of confocal microscopy is to enhance the focal point of the objective lens by restricting the cone of

light returned to the viewer through a small pinhole (Figure 0.4A) (Webb 1996). Therefore, the focus of an optical plane is enhanced and the remaining depth of the sample is filtered from view. This permits clear visualization throughout a thick tissue, such as the SAM, that is otherwise unattainable with conventional light microscopy (Figure 0.4B-0.4C). Additionally, the non-invasive nature of this technology eliminates the need for tissue sectioning and permits high resolution live sample analysis.

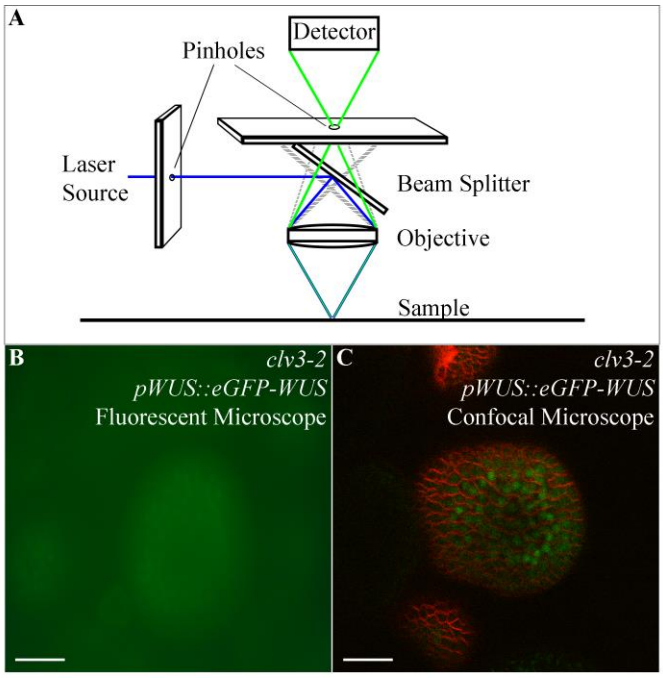

Figure 0.4: Confocal Miscroscopy for SAM Imaging. A simplified diagram of the confocal microscope design is shown (A). Laser light from the emission source is shown in blue and light reflected back to the detector is shown in green. Light that is filtered out by the pinhole is shown in thatched lines. Images of a *clv3-2 pWUS::eGFP-WUS* SAM using a fluorescent microscope (B) and a confocal microscope (C) demonstrate the high resolution images that confocal microscopy provides. Green signal is eGFP-WUS, red signal is FM4-64X plasma membrane bound dye. (Scale bars=50μm).

The engineering of fluorescent proteins as molecular biology tools has also been of critical importance since the first GFP molecule was isolated (Prasher et al., 1992, Chalfie et al., 1994). Fluorescent proteins are able to absorb light energy at specific wavelengths and emit a visible fluorescent signal that can be imaged by techniques such as confocal microscopy. This property has been incorporated in a wide variety of applications, perhaps the most prevalent being the analysis of gene expression and protein accumulation through direct fusions of fluorescent proteins to target promoter elements and protein coding

sequences, respectively (Chalfie et al., 1994). Since its application in cellular imaging techniques, many variants have been isolated and engineered that provide emission spectra across the visible spectrum, permitting the use of multiple fluorophores in combination with fluorescent dyes to visualize cellular dynamics (Figure 0.4C) (Shaner et al., 2005). The use of confocal microscopy to visualize fluorescent proteins continues to be vital to the dissection of complex biological systems such as the analysis of SAM and its regulatory components (Gallois et al., 2002, Reddy et al., 2004, Kim et al., 2005, Reddy and Meyerowitz, 2005, Reddy, 2008, Yadav et al., 2011).

Dissertation Objectives

WUS is an integral factor in the maintenance of stem cells, yet little is known about the protein co-regulators that help to specify its mobility and bifunctional regulation to promote SAM maintenance. To further the understanding of the essential proteins involved in WUS-mediated SAM maintenance and characterize their functions, this dissertation consists of three main objectives:

1. Identification of a set of WUS-interacting proteins that facilitate WUS function through a combined yeast two-hybrid/high throughput sequencing screen.
2. Functional characterization of the genetic relevance of a subset of identified WUS-interacting proteins through a targeted RNAi screen.
3. Molecular and genetic characterization of the WUS-SUMO interaction and its function in SAM maintenance.

Chapter 1: A High Throughput Sequencing Approach Reveals a Possible WUSCHEL Protein-Protein Interaction Network

Introduction

Plants are complex eukaryotic organisms, and exhibit a unique form of post-embryonic development in which new organs are continually produced throughout their life cycle. Post embryonic development in *A. thaliana* consists of two main phases: a vegetative phase and a reproductive phase (Laux et al., 1996). During the vegetative growth phase, a population of undifferentiated stem cells in the central zone (CZ) must be continually maintained through WUS-mediated repression of differentiation-promoting transcription factors such as KANADI1/2, ASYMMETRIC LEAVES2, YABBY3, and UNUSUAL FLORAL ORGANS (Laux et al., 1996, Mayer et al., 1998, Yadav et al., 2013). In addition, the rib meristem (RM) originating WUS self regulates its own expression through the non-cell autonomous direct activation of its own negative regulator, the signaling peptide CLV3, which signals through the CLAVATA1/CLAVATA2/CORINE signaling kinase cascade (Brand et al., 2000, Schoof et al., 2000, Guo et al. 2010, and Yadav et al., 2011). Additionally, once plants have transitioned to the reproductive phase, the stem cell population is eventually terminated through *AGAMOUS* (*AG*)-mediated direct recruitment of Polycomb-group Proteins (PcG) to *WUS* and AG mediated indirect silencing via *KNUCKLES* activation (Liu et al., 2011). WUS also regulates the activation of *AG*, therefore leading to its own termination in reproductive development (Ikeda et al., 2009). This bi-functional transcriptional activity

requires integration of several signals to provide specificity for activated and repressed WUS targets (Ikeda et al., 2009 and Yadav et al., 2013).

Additionally, WUS is responsible for regulating cell division rates in the SAM. Mitotic activity in the RM and CZ is the lowest, and this activity increases as cells divide away from the CZ and RM and into the peripheral zone (PZ) of the SAM (Reddy and Meyerowitz, 2005, Yadav et al., 2010). Higher levels of WUS protein in the RM and CZ appear to be responsible for this decrease in mitotic activity, as mis-expression of WUS in the PZ results in lowered cell division rates in these cell types (Yadav et al., 2010). Less is known mechanistically about this regulation, however integration of signaling from the hormone auxin is likely involved as downregulation of WUS in the SAM lead to increased auxin signaling and PIN transporter activity (Yadav et al., 2010).

The non-cell autonomous functions of WUS are also poorly understood at a mechanistic level. Morphogens and other non-cell autonomous signals have long been studied in animal systems, and include the *Drosophila* morphogen families KRUPPEL-LIKE FACTOR (*Klf*) and TRANSFORMING GROWTH FACTOR BETA (*Tgf-β*) (Matsumura et al., 2005, Reffey et al., 2001). These participate in protein-protein interaction signaling that regulates transcriptional function and specificity. In plants, the root apical meristem non-cell autonomous transcription factor SHORT-ROOT relies on interactions with SCARECROW for nuclear sequestration to define the SHORT-ROOT boundary (Cui et al., 2007, Koizumi et al., 2011). Likewise the non-cell autonomous floral transcription factor LEAFY (LFY) physically interacts with UNUSUAL FLORAL

ORGANS (UFO) to regulate expression of *APETALA3* (*AP3*) in floral meristems (Sessions et al., 2000, Chae et al., 2008).

In light of this information, previous analyses of WUS protein-protein interactors (PPIs) have been performed, yet only five interactome members have been identified and confirmed to date: TPL, TOPLESS-RELATED4 (TPR4), and HAIRY-MERISTEM1/2/4 (HAM1/2/4) (Kieffer et al., 2006, Zhou et al., 2015). To date these interactors have only been shown to function as cofactors involved in WUS-mediated repression (Causier et al., 2012, Zhou et al., 2015). However, the previously discussed diversity of WUS functions cannot be accounted for solely on the function of these transcriptional repressors. Therefore, in order to clarify the known WUS activities and identify possible new WUS functions, we sought to uncover additional players in the WUS PPI network.

An excellent tool for identification of PPIs is the yeast two-hybrid (Y2H) system (Gietz et al., 1997, Brückner et al., 2009). A 'bait' protein of interest is used to screen a pool of 'prey' unknown proteins to identify PPIs. This approach uses auxotrophic selection as a reporter in yeast, and can be easily and systematically scaled to screen the entire proteome of a tissue or organism. Y2H, combined with recent advances in high throughput sequencing analyses, allows for efficient generation of PPI networks with rapid speed for relatively low cost (Langmead et al., 2009, Yu et al., 2011). This study presents a putative WUS PPI network generated from a Y2H screen and followed by high throughput sequencing identification of WUS interactors. Then a network of WUS PPIs was developed based on GO Term analysis and the true/false positive rates were subsequently identified through independent retesting of a subset of putative interactors

via sequencing, Y2H, bi-molecular fluorescence complementation (BiFC), and co-immunoprecipitation (Co-IP). This WUS PPI network was then used to theorize new potential roles for WUS in plant development.

Results

WUS Expression and Transactivation Potential Require Special Optimization for Y2H Design

Prior to initiating the Y2H screen, a transactivation experiment was performed to optimize the screen parameters. WUS full-length CDS was PCR amplified and cloned into the MCS of pGBKT7 to generate the bait construct (Table S1.3). Because WUS is itself a transcription factor, transactivation, or the activation of auxotrophic selection reporters without the presence of both bait and prey constructs, was observed on SD-(L/W/H) plates which provide all necessary nutrients for yeast growth except the essential amino acids L, W, and H. To combat this effect, the HIS3 gene product inhibitor 3-amino-1,2,4-triazole (3AT) was added to the SD-(L/W/H) media in concentrations of 0mM, 10mM, and 25mM to determine that the optimal concentration to reduce WUS transactivation is 10mM 3-AT (Figure S1.1A-S1.1D) (Gietz et al., 1997). All future Y2H experiments were performed under these conditions unless otherwise stated.

WUS is expressed in only 25-35 cells in the SAM, and as such the cDNA used to generate the prey library needed to be enriched to ensure representation of spatially appropriate PPIs (Mayer et al., 1998). Library cDNA synthesis was performed by Clontech using RNA isolated from *Wt* and double mutant *apetala1-1 cauliflower1-1* SAMs, which convert floral meristems into SAMs forming a cauliflower-like structure

(Bowman et al., 1993). Generated cDNA was amplified and size selected for amplicons between 0.95kb and 2.5kb, cloned into the *SfiI* site in the MCS of pGADT7-RecAB, and transformed into DH5α *E. coli* for library amplification via Clontech.

Bait and prey co-transformation yielded 35.7 million colonies screened for an initial selection of 2705 positive colonies; these were independently screened via *lac-z*/β-galactosidase filter lift assay (Figure S1.1E-S1.1G) (Gietz et al., 1997). After selection, the 698 (25.8%) strongly positive colonies were further selected on SD-(L/W/H) + 50mM 3-AT for stringent selection (Figure S1.1H). A total of 574 (21.1%) colonies were retained as strong WUS PPIs for use in downstream applications (Table 1.1).

High – Throughput Sequencing Applied to Y2H is an Efficient Way to Identify Putative PPIs

Traditional Y2H screening approaches employ independent extraction and sequencing of each positive colony for PPI identification (Gietz et al., 1997, Brückner et al., 2009, Causier et al., 2012). However, the increased prevalence and reduced cost of high-throughput sequencing approaches provide an attractive alternative to traditional independent sequencing approaches. Prey library plasmids from the 574 PPI yeast colonies were extracted, pooled and PCR amplified via pGADT7-RecAB specific primers flanking the Multiple Cloning Site to enrich the prey sequences (Table S1.3). These products were fragmented via sonication for improved read coverage and extended with sequencing adapters. The resulting fragments were size selected between 100bp-500bp and checked to ensure high quality with an Agilent 2100 Bioanalyzer prior to sequencing via the Illumina Hi-seq2000 platform (Figure 1.1A).

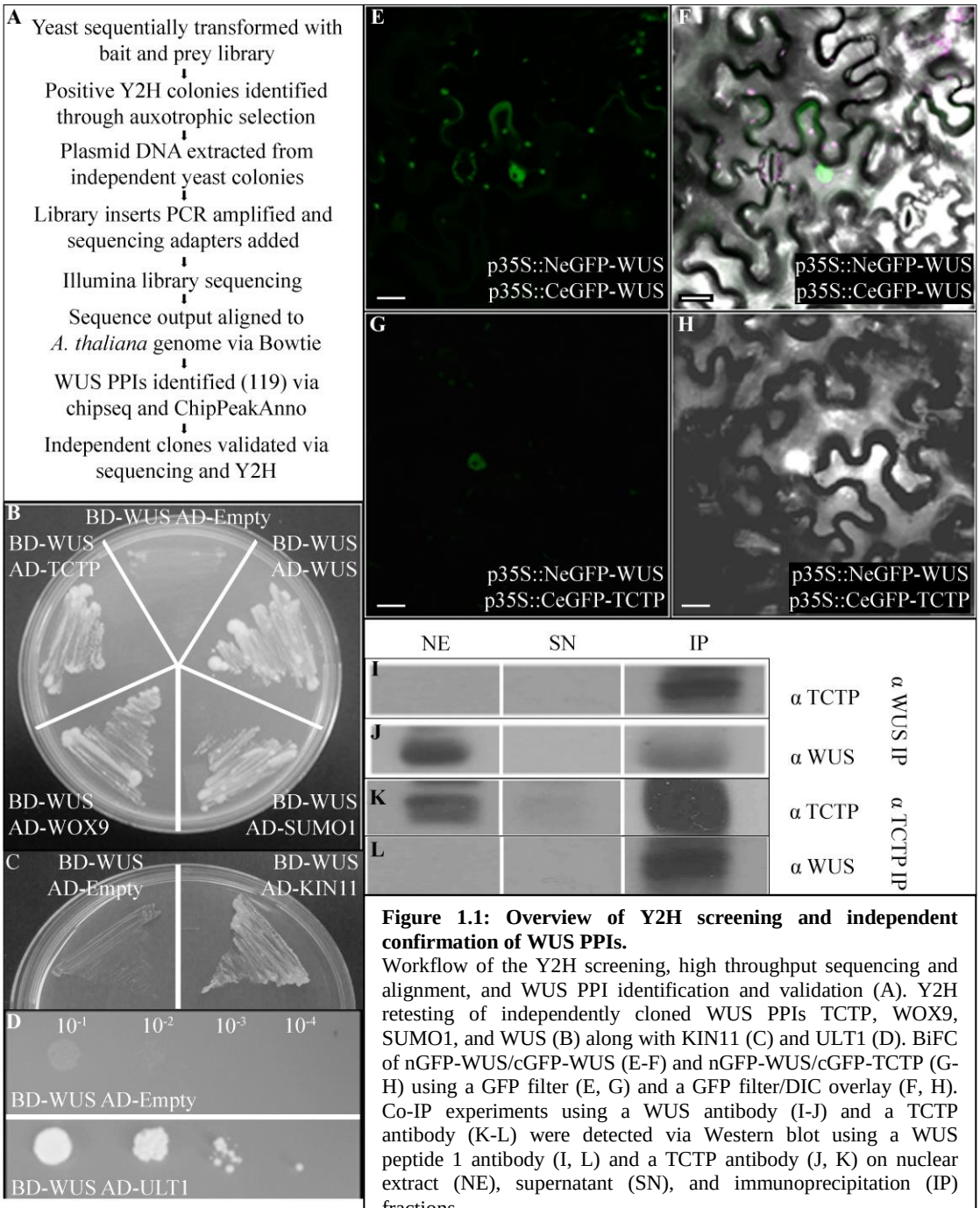

Figure 1.1: Overview of Y2H screening and independent confirmation of WUS PPIs.
Workflow of the Y2H screening, high throughput sequencing and alignment, and WUS PPI identification and validation (A). Y2H retesting of independently cloned WUS PPIs TCTP, WOX9, SUMO1, and WUS (B) along with KIN11 (C) and ULT1 (D). BiFC of nGFP-WUS/cGFP-WUS (E-F) and nGFP-WUS/cGFP-TCTP (G-H) using a GFP filter (E, G) and a GFP filter/DIC overlay (F, H). Co-IP experiments using a WUS antibody (I-J) and a TCTP antibody (K-L) were detected via Western blot using a WUS peptide 1 antibody (I, L) and a TCTP antibody (J, K) on nuclear extract (NE), supernatant (SN), and immunoprecipitation (IP) fractions.

The high-throughput sequencing yielded 30,588,252 total reads with 22,839,304 (74.7%) reads passing the Illumina chastity filter. From this set, a total of 3,506,325 (15.4%) reads were appropriately aligned to the TAIR9 genome using the Bowtie short read alignment program. The chipseq and ChipPeakAnno packages in R were used to identify gene IDs and their respective GO Terms, revealing 119 WUS PPIs (Figure 1.2A, Table S1.1) (Zhu et al., 2010, Zhu 2013, Sarkar et al., ver 1.20.0).

Independent Confirmation of a PPI Subset Reveals High Correlation of True Positives

Sequence alignment was initially vetted through observational analysis of piled reads on target gene exons using the Integrative Genomics Viewer (IGV) (Figure S1.2A-S1.2G) (Robinson et al., 2011 and Thorvaldsdóttir et al., 2013). AT4G15030, HB-1, AT5G02710, AP19, and AT1G17370 (5/7, 71%) were all confirmed as positive interactors via independent clone amplification and Sanger sequencing analysis (Figure S1.2H, Table S1.2). Additionally, a subset of identified genes were independently cloned and transformed for Y2H reconfirmation. Of these independent Y2H transformations, SUMO1, TCTP, WOX9, ULT1, KIN11 and WUS were all confirmed as positive interactors (75%), while AGO1 and its close family member AGO10 were false positives (25%) (Figure 1.1B-1.1D, Figure S1.1I-S1.1L). Interestingly, AGO1 and AGO10 each had a small number of read alignments localized to the 5’ and 3’ ends of their respective cDNAs (Figure S1.2F-S1.2G). As the size of both of these cDNAs is much larger than the size selection limit of 2.5kb, this suggests that partial clones of these and potentially other genes could be present in the library. However, all independent interactions were

confirmed with the full length CDS of each gene. Combining all methods of reconfirmation resulted in a true positive rate of 71-75%. The 95 WUS PPIs with cell type specific expression data (80%) are all present in at least one SAM cell type, and of those 79 (83%) are in all of the characterized cell types (Figure 1.2B) (Yadav et al., 2009).

An alternate method for confirmation of PPIs is BiFC, which excels in the ability to directly visualize PPIs using fluorescent protein reporters (Walter et al., 2004). We cloned the CDS of eGFP into two halves to generate NeGFP (AA 1-155) and CeGFP (AA 156-239), which were each cloned in frame to the N-terminus of the CDS of WUS and TCTP under control of a *2xCaMV 35S* promoter (*p2x35S*). Co-infiltration of appropriate NeGFP and CeGFP CDS fusion pairs in *N. benthamiana* leaves revealed positive interactions in the nucleus and cytosol of WUS-WUS, and WUS-TCTP with appropriate controls through confocal microscopy visualization (Figure 1.1E-1.1H, Figure S1.2I-S1.2L).

In addition to sequencing and Y2H confirmation, we needed to confirm that these interactions occur *in planta* to show functional significance of the WUS PPIs. To this end, we obtained antibodies for Translationally Controlled Tumor Protein (TCTP) in order to test the interaction with WUS *in planta* via Co-IP using previously described WUS antibodies (Berkowitz et al., 2008, van den Burg et al., 2010, Yadav et al., 2011). Nuclear proteins isolated from *clv3-2*, *pWUS::eGFP-WUS* SAMs were immunoprecipitated with TCTP antibodies, run on SDS-PAGE, and Western blotted with WUS antibodies to detect the PPIs. The WUS band was identified at 40kDa, while

control Western blot bands were identified at 19kDa for TCTP as expected (Figure 1.1I-1.1L). Additionally, immunoprecipitation was performed using a WUS-specific antibody, and WUS-TCTP interaction was analyzed by Western blot detection of TCTP in the WUS-IP fraction. WUS immunoprecipitation success was corroborated by WUS Western detection using a different WUS antibody in the immunoprecipitated fraction that the one used for immunoprecipitation.

GO Term and Cell Type Expression Analysis Reveals Potential Roles of New WUS PPIs

GO Term IDs for 119 WUS PPIs were identified and used to group the PPIs into the following categories for functional characterization: Cell Cycle Regulation (1), Cell-Cell Communication and Secretory Pathways (7), Defense (8), Cell Signaling (10), Chromatin Remodeling (10), Cell Metabolism (10), Nucleic Acid Metabolism (13), Transcription Factor (14), Protein Folding and Stability (19), and Unknown Protein (27) (Figure 1.2A). Furthermore, enrichment of GO Slim terms across the WUS PPIs was analyzed for GO Slim Cellular Component, GO Slim Molecular Function, and GO Biological Process (Figure 1.2C-1.2E, Figure S1.3A-S1.3B). Additionally, the WUS PPIs were analyzed using previously published cell type expression data to determine SAM expression patterns (Figure 1.2B) (Yadav et al., 2014).

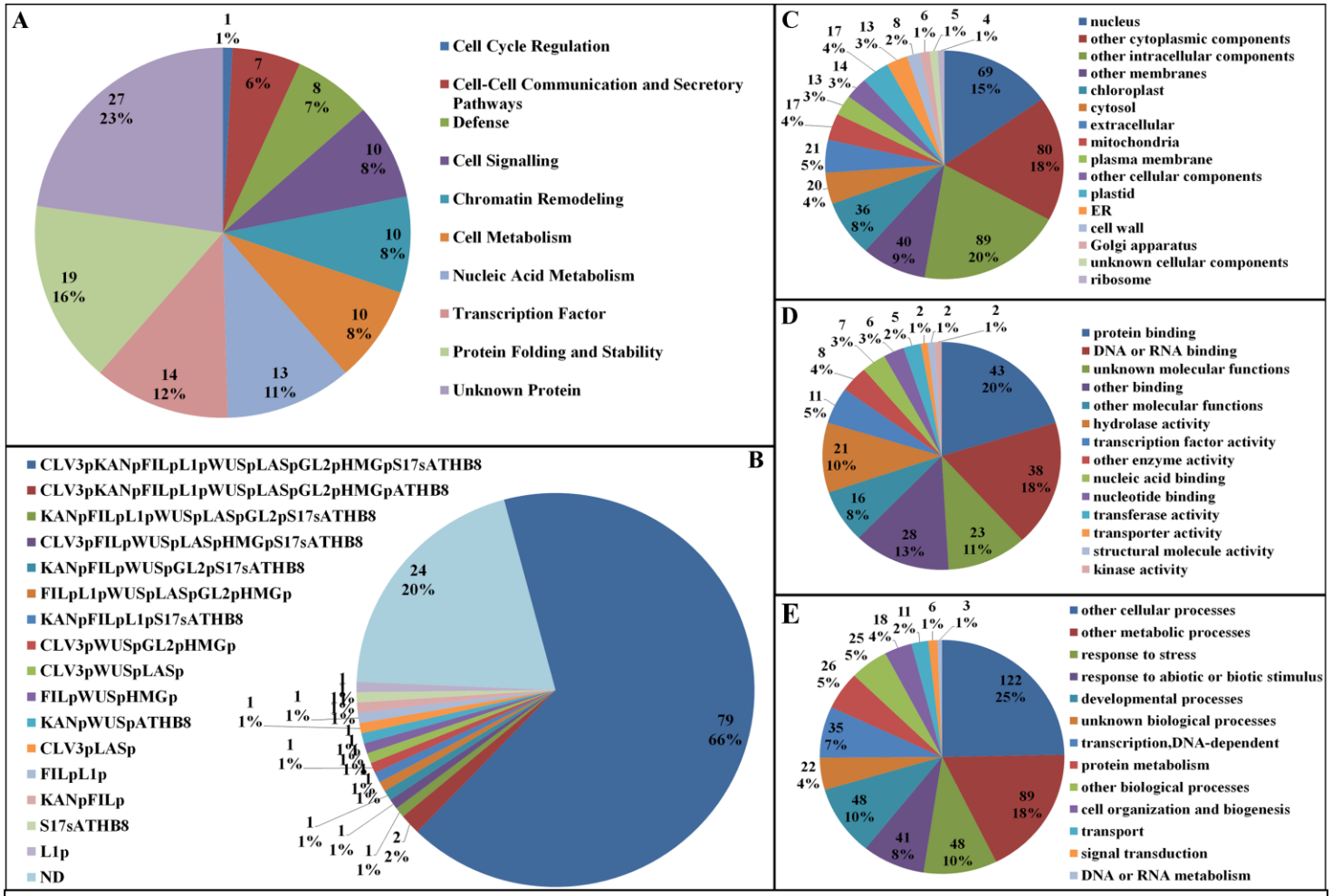

Figure 1.2: Analysis of WUS PPIs based on GO Slim and cell type expression data. All 119 WUS PPIs were categorized into functional groups based on GO Term representation (A). Cell type expression data of WUS PPIs based on SAM cell types were also identified (B). GO Slim representation of WUS PPIs in GO Cellular Component (C), GO Molecular Function (D), and GO Biological Function (E). ND represents no defined cell types.

Discussion

Even after its discovery almost 20 years ago, many factors regulating WUS function and regulation remain largely unknown (Laux et al., 1996). Much of the previous work on WUS function focused on characterizing the homeostatic feedback loop between WUS and CLV3 signaling, which is critical in the maintenance of stem cells in the SAM (Mayer et al., 1998, Brand et al., 2000, Schoof et al. 2000). Additional work has been performed to look at the transcriptional targets of WUS, and how WUS functions as both an activator of stem cell promoting factors and a repressor of differentiation promoting factors, a key aspect that is crucial in defining the spatial distribution of the stem cell pool (Ikeda et al., 2009 and Yadav et al., 2011). Still other work has focused on the interactions between WUS and hormones such as Auxin and Cytokinin in the role of SAM development (Leibfried et al., 2005, Gallois et al., 2004, Busch et al., 2010). Lastly, WUS also plays a prominent role in cell division rates, as the division rates in stem cells is much lower than that of the surrounding cells differentiating into the peripheral zone and into the organ primordia (Reddy and Meyerowitz 2005, Yadav et al., 2010). However, many of the co-regulators responsible for specifying WUS function in each of these varied roles have yet to be identified.

The cell type expression data of the WUS PPIs reveals that the PPIs with identified cell type expression patterns all are present in at least one cell type in the SAM (Figure 1.2B). This bolsters the reliability of the data, as it confirms that the WUS PPIs are all expressed in cell types that WUS can be present in, thus facilitating the opportunity for WUS PPIs to occur. While most of the WUS PPIs are present in a

majority of the cell types currently characterized in the SAM, there are 16 that are present in unique cell types and 8 that are expressed in three cell types or less (Table 1.2) (Yadav et al., 2009). Of particular note in this group are *WUS*, *YAB3*, and *AT2G25510*. WUS presence in limited cell types is expected from known expression data (Mayer et al., 1998, Reddy and Meyerowitz 2005). YAB3 is a differentiation promoting transcription factor typically expressed in the outer peripheral zone of the SAM along the border of the developing organ primordia (Goldshmidt et al., 2008, Yadav et al., 2014). *AT2G25510* is solely expressed in the L1 layer of the SAM, and could reveal a potential stem cell specific regulation of WUS. WUS protein mobility itself reveals a mechanism for direct interaction even when the expression zones do not overlap (Yadav et al., 2011, Yadav et al., 2014).

It is common for PPIs to modulate the function of a protein in a spatial or temporal manner to create complexes for specialized tasks. Previously identified PPIs with WUS include WUS, HAM1/2/4, and TPL/TPR4; to date these have been only considered as cofactors for WUS transcription except in the case of WUS-WUS homodimers, which have been implemented in WUS protein movement (Kieffer et al., 2006, Daum et al., 2014, Zhou et al., 2015). However, HAM1/HAM2/HAM4 and TPL/TPR4 were not identified in the screen presented in this work. One possibility is due to the size selection parameters of 0.95kb-2.5kb for cDNAs cloned into the prey library. The cDNAs of TPL/TPR4 are larger than 2.5kb, and as such were excluded from the prey library pool even though they have been previously confirmed independently as Y2H targets. HAM1/HAM2/HAM4 may have been outcompeted by other WUS PPIs or

underrepresented in the PCR amplification steps used to generate the sequencing library. WUS itself was identified as its own PPI, and here we provide an enlarged WUS PPI network that provides insight into the multi-faceted functions of WUS in development.

GO term enrichment and putative function was used to categorize each of the 119 PPIs into functional groupings (Figure 1.2A). The groups consisting of Cell Cycle Regulation (1) and Cell Metabolism (10) are factors that could be relevant to WUS mediated regulation of cell division. TCTP, the sole member of the Cell Cycle Regulation group has been previously described in *A. thaliana* and *D. melanogaster* to participate in mitotic cell cycle control and regulation of cell size (Berkowitz et al., 2008 and Brioudes et al., 2010). Members of the Cell Metabolism group, such as CAT2, and MS1 participate in catabolic and redox processes, which have been shown to regulate cell cycle progression (Queval et al., 2007, Zdarska et al., 2013). The function of these PPIs could be further analyzed with regards to WUS in characterizing the mechanisms responsible for delaying the cell cycle progression of stem cells, and how normal progression is restored as differentiated cells are displaced to the periphery and primordia of the SAM.

Furthermore, the categories of Chromatin Remodeling (10), Nucleic Acid Metabolism (13), and Transcription Factor (14) are likely factors affecting WUS transcription specificity and efficiency. WUS, FLK, ULT1, SAP18, and others in these groups have all been shown to regulate transcription either through direct binding to DNA or as cofactors (Yadav et al., 2013, Mockler et al., 2004, Pires et al., 2014, Liu et al., 2009). In particular, FLK, ULT1, and SAP18 are all involved in the floral transition and development of floral organs, and the stem cell termination that results from this

transition is driven through interactions with Polycomb Group proteins, of which ULT1 is a member (Liu et al., 2009). Chromatin mediated regulation of WUS expression through WUS PPIs could reveal spatial-temporal regulation of WUS essential to the proper termination of stem cell maintenance in proper floral development. In addition, less characterized members of these groups include proteins with zinc finger, basic helix-loop-helix, and homeobox motifs, all of which are well characterized DNA binding motifs. Many of these factors could further specify WUS function through specialization of WUS DNA binding motif recognition across the 2361 genes that it differentially regulates, and could function as spatial-temporal specific regulators of WUS target modulation (Yadav et al., 2009).

The understanding of the role of WUS in Cell-Cell Communication (7), Cell Signaling (10) and Defense (8) is more limited in scope, yet these PPIs provide new avenues for analysis of WUS function. AP19 and several microtubule motor proteins could assist in WUS movement within the cell (Maldonado-Mendoza and Nessler, 1997). The protein kinase KIN11 plays multiple roles, both as a protein kinase signaling molecule and as a potential protein stability factor due to its interaction with the proteasome via direct binding to the SKP1/ASK1 and 20S proteasome PAD1 subunits (Farras et al., 2001, Baena-Gonzalez et al., 2007). In relation to these potential mechanisms, the Protein Folding and Stability group (19) contains ASK2, PAD1, and several polyubiquitin family members, all of which strengthen the link to a mechanism where WUS stability is regulated through PPIs (Liu et al., 2004). Additionally SUMO1,

protein modifier of transcriptional function, subcellular localization, and protein stability is present (Miura and Hasegawa, 2010 and van den Burg et al., 2010).

Finally, there is a large group of WUS PPIs without a known function (27). This perhaps contains the most potential for discovery, as the continued identification of new proteins will perhaps link WUS to as of yet uncovered pathways. The prospect of defining completely novel pathways for WUS function is exciting not just in the context of stem cell maintenance, but also in the relation of core developmental pathways to other plant functions.

In summary, we present a new WUS PPI network that provides new avenues for analysis of WUS mediated mechanisms of stem cell maintenance. In total, 119 WUS PPIs have been identified in this screen, and subset validation via independent sequencing, Y2H, BiFC and Co-IP revealed a 71-75% true positive rate. We propose that WUS PPIs identified in this screen diversify WUS function by manipulating WUS target gene regulation, WUS mediated cell division control, WUS stability in the SAM, and perhaps most intriguingly by affecting a currently unidentified mechanism of WUS function. These WUS PPIs provide new avenues for analysis of WUS function, and will hopefully further our understanding of the mechanisms of stem cell maintenance in a more general fashion.

Methods

Generation of Bait and Prey DNA for Y2H Screening

The full length WUS coding sequence was cloned into the pGBKT7 MCS via the *Nde*I/*Eco*RI sites and sequenced via Sanger sequencing to generate pGBKT7 WUS.

cDNA generated from SAM tissue of *ap1-1 cal-1* plants was size selected for fragments between 0.95kb-2.5kb via gel extraction, cloned into the *SfiI* site of pGADT7-RecAB, and transformed into DH5α via Clonetech to create prey library glycerol stock. Prey library DH5α glycerol stock was diluted from 1mL into 21mL with MQ H_2O (sterile). Diluted stock culture was plated on 50 x 150mm diameter plates of lysogeny broth (LB) media containing 50µg/mL ampicillin and grown for 18hrs at 37^{o}C for colony selection. 10mL of LB media was added to each plate, resuspended via a sterile spreader, and drained into a sterile 1L beaker. pGADT7-RecAB prey library was isolated from the DH5α suspension via Midiprep (Life Technologies, K2100-04).

Y2H Bait Transformation and Transactivation Assay

All Y2H transformation procedures were adapted from (Geitz et al 1997) and performed under sterile conditions. All yeast cultures were grown at 30^{o}C and liquid cultures were shaken at 200rpm; centrifugation was performed at 3,000rpm. AH109 yeast (Clontech) was streaked on yeast extract peptone dextrose (YPD) media under sterile conditions and grown for 48hrs. A pinhead sized blob of yeast was resuspended in 1mL 0.1M lithium acetated (LiAC). This yeast was pelleted via centrifugation for 30sec, the supernatant was removed, and the pellet was resuspended again in 1mL 0.1M LiAC. The previous step was repeated; however the pellet was resuspended after the addition of the following reagents in order: 240µL of 50% polyethylene glycol (PEG) 3350, 36µL of 1M LiAC, 50µL 2.5uM DNA-salmon sperm, 5µL of pGBKT7 WUS plasmid, and 29µL of sterile MQ H_2O. After resuspension, the yeast transformation mixture was heat shocked in a 42^{o}C water bath for 45min. Transformed yeast cells were then pelleted via

centrifugation for 30sec, and the supernatant removed. The yeast pellet was resuspended in 500uL of sterile MQ H_2O and 100uL each of this mixture was plated on synthetic defined (SD)-W plates, sealed with parafilm, and grown for 2-4d until colonies formed.

AH109 yeast transformed with pGBKT7 WUS were plated on SD-W, SD-(W/L), and SD-(W/L/H) dropout plates with 3-Amino-1,2,4-triazole (3AT) at 0mM, 5mM, 10mM, and 25mM concentrations and grown for 3-5d until colonies formed.

Y2H Prey Library Transformation

AH109 yeast previously transformed with pGBKT7 WUS on SD-W plates were used to inoculate a 50mL 2xYPD culture that was incubated 18hrs in a 250mL flask. Two 250mL 2xYPD cultures were inoculated with 1.5mL each of the saturated overnight yeast culture and incubated 18 hours. Both cultures were transferred to a sterile 4L baffled flask, and 500mL of additional SD-(W/L) media was added to this flask. This culture was then incubated for 2-3hrs and the cells collected by centrifugation for 5min. Pellets were resuspended in a total volume of 25mL 0.1M LiAC and homogenized. This mix was incubated for 15min, and during incubation the DNA salmon-sperm stock aliquot was boiled at 100^{o}C for 5min. After incubation, the yeast suspension was centrifuged for 5min and the supernatant decanted. The following mixture was added to the pellet: 14.40mL of 50% polyethylene glycol (PEG) 3350, 2.16mL of 1M LiAC, 1.25mL 2.5µM DNA-salmon sperm, 1mL of pGADT7 library plasmid, 0.79mL of sterile MQ H_2O, and 2mL of DMSO. This mixture was resuspended to ensure complete homogenization. The suspension was then incubated at 50rpm for 30min at a 45^{o} angle and then transferred to a 42^{o}C water bath and incubated for 1hr, with gentle mixing every 10min. The mix was

centrifuged for 5min, the supernatant decanted and the pellet resuspended in 14mL sterile MQ H2O; this was diluted by a factor of 1/10, and 150uL was plated onto each of 90 SD-(W/L/H) plates. Additionally, four plates of SD-(W/L) plates were plated with a dilution factor of 1/100 to determine transformation efficiency as described below. All plates were incubated for 3d until colonies formed. Colonies were counted and transformation efficiency calculated from SD-(W/L) plates.

Transformation Efficiency (TE) = [colony number (cfu)*suspension volume (mL)]/(plating volume (mL)*DNA added (µg)].

TE = [2400cfu*14mL]/[0.6mL*0.8ug] = 7 x 10^4 cfu/µg

Y2H Selection and lacZ Screening

Colonies from plates containing double transformed yeast were independently streaked onto grid marked SD-(W/L/H) + 10mM 3AT plates and grown for 4d to make master plates. Stocks of Z-buffer (60mM Na_2HPO_4, 40mM $NaH_2PO_4{\cdot}H_2O$, 10mM KCl, 1mM $MgSO_4{\cdot}7H_2O$, 39mM 2-β-mercaptoethanol, pH to 7.0) and 100mg/mL 5-bromo-4-chloro-3-indolyl-β-D-galactopyranoside (X-gal) in dimethlyformamide (DMF) were made into a working Z buffer + 1mg/mL X-gal solution for the filter lift assay. Sterile Whatman paper was cut into circles and soaked with working Z buffer + 1mg/mL X-gal solution. Soaked filter paper was flattened on the grid marked master plates. After 1min incubation, the Whatman paper and plate were marked at the same location for alignment and colony identification. The Whatman paper was then removed from the yeast master plate, submerged in liquid N_2 for 15s, and then incubated in a petri dish at 30^{o}C for 16-18hrs. This was repeated for all library master plates, and the positive colonies were

identified as strong, weak, or negative. Strong colonies were used to generate master plates on SD-(W/L/H) + 50mM 3AT. These stringent master plates were grown at 30^{o}C for 4d and identified as strong, weak or negative colonies based on yeast growth. Strong colonies were selected for isolation of DNA and clone identification described below.

Extraction of DNA from Yeast Colonies

Colonies from above were processed using a CTAB DNA extraction protocol for isolation of plasmid DNA. Enough CTAB buffer was measured to add 600µL per yeast sample. The CTAB buffer was mixed with 1µL 2-β-mercaptoethanol per 1mL of CTAB in the fume hood. Yeast from master plates was mixed in 600µL CTAB/2-β-mercaptoethanol until homogenous. All samples were flash frozen, thawed, and then sonicated for 20s each. Samples were incubated at 65^{o}C for 20min, and then 600µL of phenolchloroform was added and thoroughly mixed. Samples were centrifuged at 13,000rpm for 5min, and the supernatant transferred to 1.5mL sterile tube. Isopropanol was added to each sample at a 0.7 volume ratio, mixed thoroughly, and centrifuged at 13,000rpm for 5min. The supernatant was discarded, the pellet washed with 500µL of 70% ethanol, and centrifuged at 13,000rpm for 5min. The supernatant was decanted and air dried, then pellets were resuspended in 100µL of sterile MQ H_2O, vortexed, and incubated at 65^{o}C for 20min. All samples were stored at -20^{o}C.

Generation of Sequencing Library

Isolated plasmids were pooled and amplified via pGADT7-RecAB specific PCR primers, then sonicated to shorten the amplicons for addition of Illumina Hi-Seq2000

sequencing adapters. Pooled adapter modified DNA was PCR amplified for enrichment and size selected for fragments between 100bp and 500bp.

Sequencing Library Quality Check, High Throughput Sequencing Alignment, and Independent Y2H Reconfirmation

All DNA quality analysis and sequencing was performed at the Institute for Integrative Genome Biology (IIGB) at UCR. Library samples were analyzed via the Agilent 2100 Bioanalyzer for DNA quality check prior to sequencing via the Illumina HiSeq2000 platform. Sequence alignment was performed using Bowtie and R at the Bioinformatics Core at IIGB. The sequencing output file was aligned to the TAIR 9 *A. thaliana* reference genome (Langmead et al., 2009). Read extension, peak calling, annotation, sequence identification, and GO Term enrichment was performed using the chipseq and ChiPpeakAnno packages in R. All network maps were generated with Cytoscape software (www.cytoscape.org) (Zhu et al., 2010, Zhu 2013, Sarkar et al., ver 1.20.0, Shannon et al., 2003).

CDS based on the TAIR 9 *A. thaliana* reference genome were used generate clones from the positive interactors for insertion into the MCS of pGADT7 backbone. Using the previously described transformation protocol, these targets were independently tested for interaction with WUS.

Co-Immunoprecipitation in *A. thaliana*

Nuclear protein extracts were isolated from *clv3-2* pWUS::eGFP-WUS SAMs and immunoprecipitated with a TCTP antibody according to previous methods (Berkowitz et al., 2008, van den Burg et al., 2010). The protein complex was run on a 12.5% SDS-

PAGE gel and Western blots against WUS peptide antibodies (1:1000) along with SUMO1 (1:1000) and TCTP (1:5000) control antibodies were performed. An antibody made against a peptide containing the amino-acids 92 to 106 of WUS was used to corroborate the specificity of WUS inmunoprecipitation (Yadav et al., 2011).

Bimolecular Fluorescence Complementation in *N. benthamiana*

CDS of the N-terminus of eGFP (AA 1-155, NeGFP) and the C-terminus of eGFP (AA 156-239, CeGFP) were cloned in frame to the N-terminus of WUS and TCTP to generate fusion proteins for transient expression under control of the *2xCaMV 35S* promoter. These constructs along with negative controls were transiently syringe infiltrated into 3-4 week old *N. benthamiana* leaves and incubated for 2d in a continuous light growth chamber according to previous work (Walter et al., 2004). Leaf sections were cut and placed onto slides with 10% glycerol, imaged via the Leica SP5 Confocal microscope, and analyzed via ImageJ. Excitation was at 488nm and emission was captured from at 500nm-525nm using a 40x water objective at 1.5x magnification.

Supplemental Figures

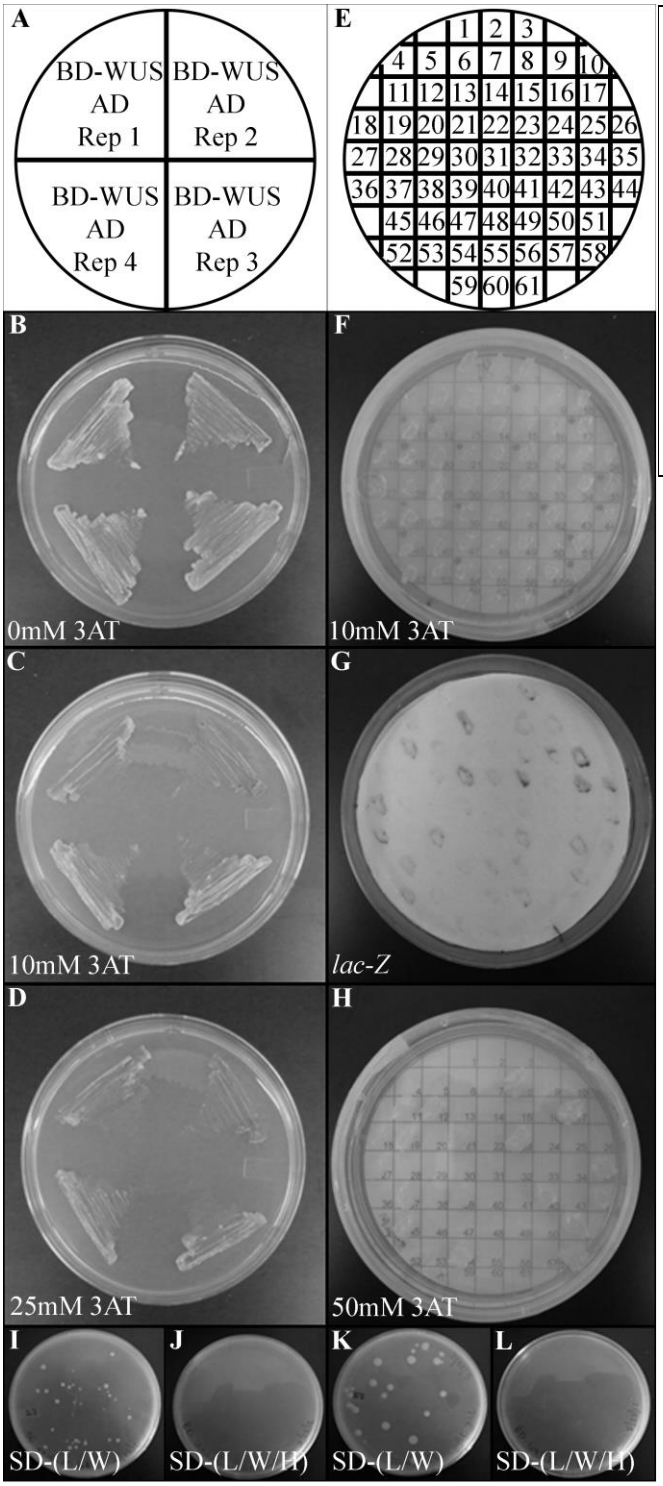

Figure S1.1: Y2H transactivation assay, library screening, and negative WUS PPIs. A map of the 4 replicates of BD-WUS transformed alone into AH109 yeast (A) and tested for transactivation growth on SD-(L/W/H) plates containing 0mM 3AT (B), 10mM 3AT (C), and 25 mM 3AT (D). A grid map of the Y2H library master plates (E) and a representative Y2H master plate on SD-(L/W/H) and 10mM 3AT (F), lac-Z selection (G), and 50mM 3AT (H). BD-WUS/AD-AGO1 co-transformed yeast on non-selective SD-(L/W) (I) and selective SD-(L/W/H) (J) plates, and BD-WUS/AD-AGO10 on non-selective SD-(L/W) (K) and selective SD-(L/W/H) (L).

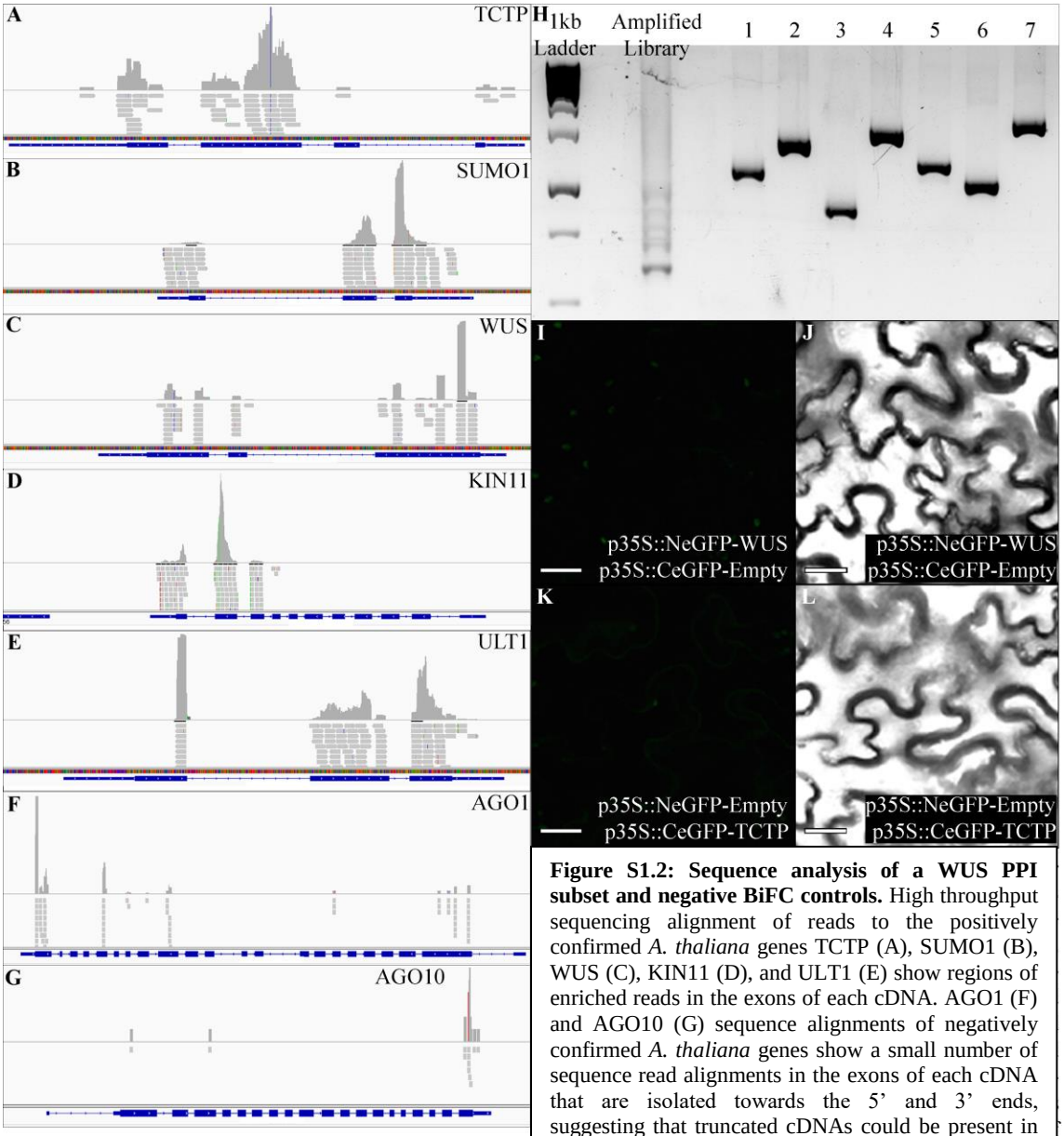

Figure S1.2: Sequence analysis of a WUS PPI subset and negative BiFC controls. High throughput sequencing alignment of reads to the positively confirmed *A. thaliana* genes TCTP (A), SUMO1 (B), WUS (C), KIN11 (D), and ULT1 (E) show regions of enriched reads in the exons of each cDNA. AGO1 (F) and AGO10 (G) sequence alignments of negatively confirmed *A. thaliana* genes show a small number of sequence read alignments in the exons of each cDNA that are isolated towards the 5' and 3' ends, suggesting that truncated cDNAs could be present in the library. PCR amplified products of the AD-Library and 7 independently sequenced WUS PPIs were run on a DNA agarose gel (H). Negative BiFC controls for nGFP-WUS/cGFP-Empty and nGFP-Empty/cGFP-TCTP using a GFP filter (I, J) and a GFP filter/DIC overlay (K, L).

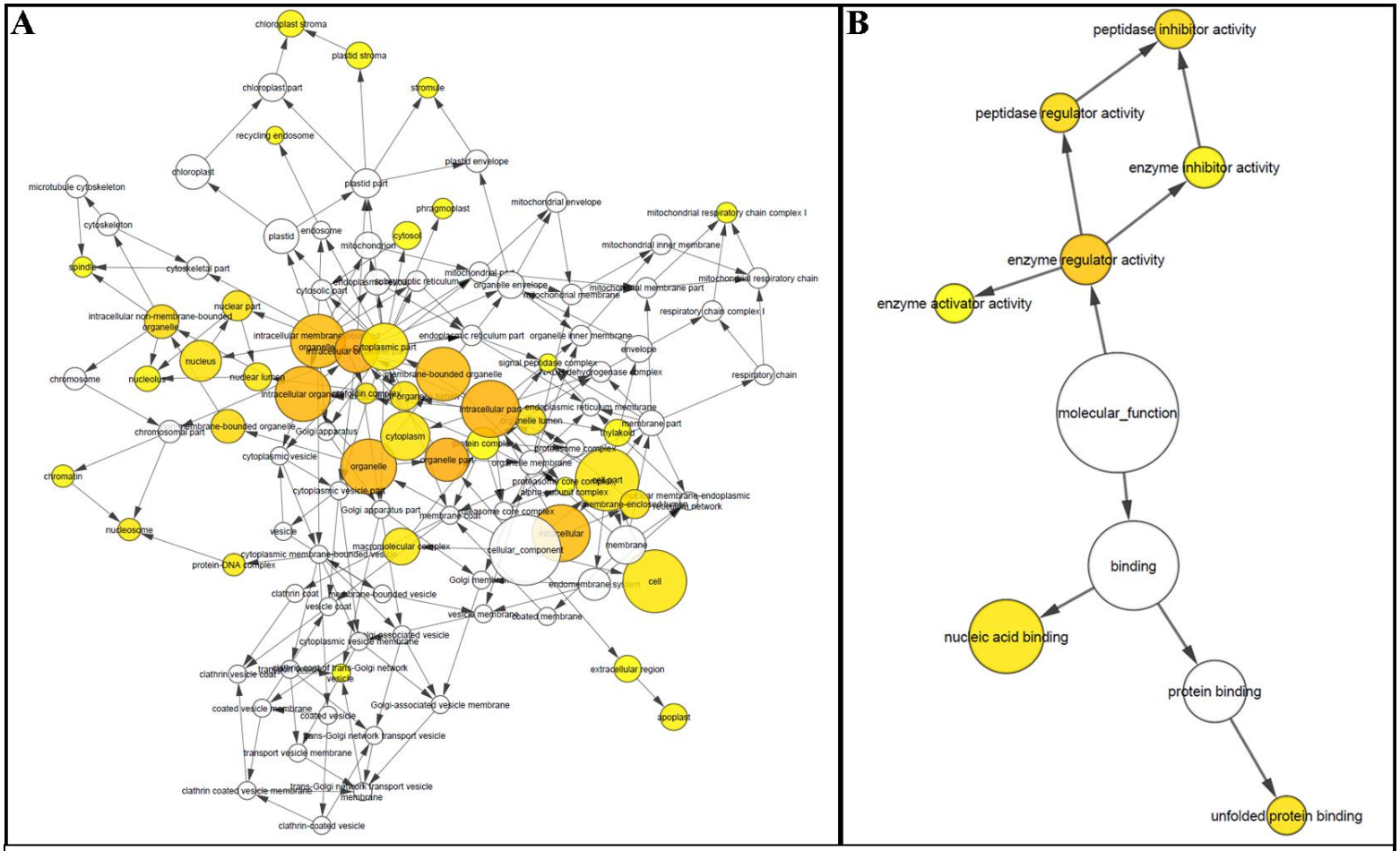

Figure S1.3: Network of WUS PPIs. WUS PPIs were integrated into a network based on GO Terms Cell Component (A) and Molecular function (B). Orange and yellow nodes are significantly enriched GO Terms (P<0.05).

Tables

Table 1.1: Selection Data for Y2H Screen

	10mM 3AT	β - Gal Assay	50mM 3AT
Call Type	**Call Count**	**Call Type**	**Call Count**
Yes	2676	698	574
No	29	2007	123
Total	2705	2705	697
% Yes	99	26	82
% No	1	74	18

Table 1.2: List of WUS PPIs with Unique Cell Type Localization

AGI ID	Annotation	Cell Type	GO Term Function	Subcellular Localization
AT1G69600	ATHB29__ZFHD1 (ZINC FINGER HOMEODOMAIN 1); DNA binding / transcription activator/ transcription factor	CLV3pKANpFILpL1 pWUSpLASpGL2pH MGpATHB8	Transcription Factor	nucleus
AT4G35090	CAT2 (CATALASE 2); catalase	CLV3pKANpFILpL1 pWUSpLASpGL2pH MGpATHB8	Cell Metabolism	extracellular, mitochondria, peroxisome, plastid
AT1G21830	unknown protein	KANpFILpL1pWUSp LASpGL2pS17sATH B8	Unknown Protein	cytosol, mitochondria, nucleus, plastid
AT1G28520	ATVOZ1__VOZ1 (VASCULAR PLANT ONE ZINC FINGER PROTEIN);	CLV3pFILpWUSpLA SpHMGpS17sATHB8	Transcription Factor	mitochondria, nucleus

	transcription activator			
AT2G02130	PDF2.3__LCR68 (LOW-MOLECULAR-WEIGHT CYSTEINE-RICH 68); peptidase inhibitor, defense	KANpFILpWUSpGL2pS17sATHB8	Defense	ER, extracellular, nucleus
AT1G18680	HNH endonuclease domain-containing protein	FILpL1pWUSpLASpGL2pHMGp	Nucleic Acid Metabolism	extracellular, mitochondria, plastid
AT1G54040	ESR_TASTY__ESP (EPITHIOSPECIFIER PROTEIN); enzyme regulator	KANpFILpL1pS17sATHB8	Cell Signaling	cytosol, extracellular, mitochondria, peroxisome
AT5G59860	RNA recognition motif (RRM)-containing protein	CLV3pWUSpGL2pHMGp	Nucleic Acid Metabolism	cytosol, mitochondria, nucleus
AT2G17950	PGA6_WUS1__WUS (WUSCHEL); DNA binding / protein binding / transcription factor/ transcription regulator	CLV3pWUSpLASp	Transcription Factor	nucleus
AT5G48500	unknown protein	FILpWUSpHMGp	Unknown Protein	cytosol, extracellular, plastid
AT1G17860	trypsin and protease inhibitor family protein / Kunitz family protein	KANpWUSpATHB8	Protein Folding and Stability	cytosol, ER, extracellular
AT1G67035	unknown protein, 190AA	CLV3pLASp	Unknown Protein	mitochondria, nucleus
AT4G00180	YAB3 (YABBY3); protein binding / transcription factor	FILpL1p	Transcription Factor	mitochondria, nucleus, plastid
AT1G73620	thaumatin-like protein, putative / pathogenesis-related protein, putative	KANpFILp	Defense	ER, extracellular, mitochondria
AT3G10870	ATMES17__MES17 (METHYL ESTERASE 17); hydrolase/ hydrolase, acting	S17sATHB8	Cell Signaling	golgi, nucleus, plastid

	on ester bonds / methyl indole-3-acetate esterase, Signaling (methyl IAA)			
AT2G25510	unknown protein	L1p	Unknown Protein	ER, extracellular, mitochondria, nucleus, plastid

Table S1.1: List of WUS PPIs with Their Cell Type, Functional Grouping, and Subcellular Localization

AGI ID	Annotation	Cell Type	GO Term Function	Subcellular Localization
AT3G16640	TCTP (TRANSLATIONALLY CONTROLLED TUMOR PROTEIN), auxin homeostasis, cell growth regulation	CLV3pKANpFILpL1 pWUSpLASpGL2pH MGpS17sATHB8	Cell Cycle Regulation	cytosol, nucleus, PM, plastid, vacuole
AT1G34245	EPF2__FUNCTIONS IN: molecular_function unknown; INVOLVED IN: biological_process unknown; LOCATED IN: endomembrane system; EXPRESSED IN: 13 plant structures; EXPRESSED DURING: 9 growth stages; BEST Arabidopsis thaliana protein match is: EPF1 (EPIDERMAL PATTERNING FACTOR 1) (TAIR:AT2G20875.1); Has 12 Blast hits to 12 proteins in 4 species: Archae - 0; Bacteria - 0; Metazoa - 0; Fungi - 0; Plants - 12; Viruses - 0; Other Eukaryotes - 0 (source: NCBI BLink).	ND	Cell-Cell Communication and Secretory Pathways	cytosol, ER, extracellular, plastid
AT2G17380	AP19; protein binding / protein transporter	CLV3pKANpFILpL1 pWUSpLASpGL2pH	Cell-Cell Communication and	cytosol, mitochondria, nucleus

		MGpS17sATHB8	Secretory Pathways	
AT2G20990	ATSYTA_NTMC2T1.1_NTMC2TYPE1.1_SYT1__SYTA (SYNAPTOTAGMIN A), secretory pathway	ND	Cell-Cell Communication and Secretory Pathways	cytosol, ER, extracellular, PM, plastid, vacuole
AT2G21010	C2 domain-containing protein, C2 membrane targeting protein domain	ND	Cell-Cell Communication and Secretory Pathways	cytosol, mitochondria
AT3G51590	LTP12 (LIPID TRANSFER PROTEIN 12); lipid binding	ND	Cell-Cell Communication and Secretory Pathways	cell wall, ER, golgi, nucleus, plastid
AT4G15030	unknown protein, similarity to kinesin motor family	CLV3pKANpFILpL1pWUSpLASpGL2pHMGpS17sATHB8	Cell-Cell Communication and Secretory Pathways	mitochondria, nucleus
AT4G15930	microtubule motor	CLV3pKANpFILpL1pWUSpLASpGL2pHMGpS17sATHB8	Cell-Cell Communication and Secretory Pathways	cytosol
AT1G08830	CSD1 (COPPER/ZINC SUPEROXIDE DISMUTASE 1); superoxide dismutase, defense	CLV3pKANpFILpL1pWUSpLASpGL2pHMGpS17sATHB8	Defense	cytosol
AT1G18250	ATLP-1, Thaumatin, pathogenesis-related:IPR001938(12)	CLV3pKANpFILpL1pWUSpLASpGL2pHMGpS17sATHB8	Defense	ER, extracellular, mitochondria, plastid
AT1G52600	signal peptidase, putative	CLV3pKANpFILpL1pWUSpLASpGL2pHMGpS17sATHB8	Defense	cytosol, ER, mitochondria, PM, plastid
AT1G73620	thaumatin-like protein, putative / pathogenesis-related protein, putative	KANpFILp	Defense	ER, extracellular, mitochondria

AT2G02120	LCR70__PDF2.1; peptidase inhibitor, defense	ND	Defense	ER, extracellular, mitochondria
AT2G02130	PDF2.3__LCR68 (LOW-MOLECULAR-WEIGHT CYSTEINE-RICH 68); peptidase inhibitor, defense	KANpFILpWUSpGL2pS17sATHB8	Defense	ER, extracellular, nucleus
AT2G22425	peptidase	CLV3pKANpFILpL1pWUSpLASpGL2pHMGpS17sATHB8	Defense	ER, extracellular, mitochondria, plastid
AT4G11320	cysteine proteinase, putative	ND	Defense	cytosol, ER, extracellular
AT1G13930	Involved in response to salt stress. Knockout mutants are hypersensitive to salt stress.	CLV3pKANpFILpL1pWUSpLASpGL2pHMGpS17sATHB8	Cell Signaling	nucleus, PM, plastid
AT1G30960	GTP-binding protein (ERG)	CLV3pKANpFILpL1pWUSpLASpGL2pHMGpS17sATHB8	Cell Signaling	cytosol, mitochondria, nucleus, plastid
AT1G54040	ESR_TASTY__ESP (EPITHIOSPECIFIER PROTEIN); enzyme regulator	KANpFILpL1pS17sATHB8	Cell Signaling	cytosol, extracellular, mitochondria, peroxisome
AT1G66410	ACAM-4__CAM4 (calmodulin 4); calcium ion binding / signal transducer	CLV3pKANpFILpL1pWUSpLASpGL2pHMGpS17sATHB8	Cell Signaling	cytosol, nucleus, PM
AT1G70490	ATARFA1D__ARFA1D; GTP binding / phospholipase activator/ protein binding	CLV3pKANpFILpL1pWUSpLASpGL2pHMGpS17sATHB8	Cell Signaling	cytosol, mitochondria, peroxisome, PM
AT3G10870	ATMES17__MES17 (METHYL ESTERASE 17); hydrolase/ hydrolase, acting on ester bonds / methyl indole-3-acetate esterase,	S17sATHB8	Cell Signaling	golgi, nucleus, plastid

	Signaling (methyl IAA)			
AT3G12145	FLOR1, leucine rich repeat, interacts directly with MADS domain transcription factor	ND	Cell Signaling	cytosol, nucleus, plastid
AT3G29160	ATKIN11_KIN11_SNRK1.2__AKIN11 (Arabidopsis SNF1 kinase homolog 11); protein binding / protein kinase	CLV3pKANpFILpL1pWUSpLASpGL2pHMGpS17sATHB8	Cell Signaling	cytosol, mitochondria, plastid
AT4G03520	ATHM2; enzyme activator	CLV3pKANpFILpL1pWUSpLASpGL2pHMGpS17sATHB8	Cell Signaling	mitochondria, nucleus, plastid
AT4G13520	SMAP1 (SMALL ACIDIC PROTEIN 1), auxin Signaling	CLV3pKANpFILpL1pWUSpLASpGL2pHMGpS17sATHB8	Cell Signaling	nucleus, plastid
AT1G06760	histone H1, putative	CLV3pKANpFILpL1pWUSpLASpGL2pHMGpS17sATHB8	Chromatin Remodeling	nucleus
AT1G51060	HTA10; DNA binding	CLV3pKANpFILpL1pWUSpLASpGL2pHMGpS17sATHB8	Chromatin Remodeling	mitochondria, nucleus
AT1G52740	HTA9 (HISTONE H2A PROTEIN 9); DNA binding	CLV3pKANpFILpL1pWUSpLASpGL2pHMGpS17sATHB8	Chromatin Remodeling	mitochondria, nucleus
AT2G38810	HTA8 (HISTONE H2A 8); DNA binding	CLV3pKANpFILpL1pWUSpLASpGL2pHMGpS17sATHB8	Chromatin Remodeling	mitochondria, nucleus, plastid
AT3G10770	nucleic acid binding	CLV3pKANpFILpL1pWUSpLASpGL2pHMGpS17sATHB8	Chromatin Remodeling	mitochondria, nucleus

AT4G28190	ULT1 (ULTRAPETALA1); DNA binding	CLV3pKANpFILpL1 pWUSpLASpGL2pH MGpS17sATHB8	Chromatin Remodeling	cytosol, mitochondria, nucleus, plastid
AT4G40030	histone H3.2	CLV3pKANpFILpL1 pWUSpLASpGL2pH MGpS17sATHB8	Chromatin Remodeling	mitochondria, nucleus, plastid
AT4G40040	histone H3.2	CLV3pKANpFILpL1 pWUSpLASpGL2pH MGpS17sATHB8	Chromatin Remodeling	mitochondria, nucleus, plastid
AT5G59690	histone H4	ND	Chromatin Remodeling	mitochondria, nucleus, plastid
AT5G59970	histone H4	ND	Chromatin Remodeling	mitochondria, nucleus
AT1G80230	cytochrome c oxidase family protein	CLV3pKANpFILpL1 pWUSpLASpGL2pH MGpS17sATHB8	Cell Metabolism	cytosol, mitochondria, plastid
AT2G16600	ROC3; peptidyl-prolyl cis-trans isomerase, secretory pathway	CLV3pKANpFILpL1 pWUSpLASpGL2pH MGpS17sATHB8	Cell Metabolism	cytosol, PM
AT3G01850	ribulose-phosphate 3-epimerase, cytosolic, putative / pentose-5-phosphate 3-epimerase, putative	CLV3pKANpFILpL1 pWUSpLASpGL2pH MGpS17sATHB8	Cell Metabolism	cytosol, extracellular, PM
AT3G02730	ATF1__TRXF1 (THIOREDOXIN F-TYPE 1); enzyme activator	CLV3pKANpFILpL1 pWUSpLASpGL2pH MGpS17sATHB8	Cell Metabolism	cytosol, plastid
AT3G09390	ATMT-1_ATMT-K__MT2A (METALLOTHIONEIN 2A); copper ion binding	CLV3pKANpFILpL1 pWUSpLASpGL2pH MGpS17sATHB8	Cell Metabolism	extracellular, nucleus, plastid
AT3G63080	MEE42__ATGPX5	CLV3pKANpFILpL1	Cell Metabolism	cytosol, mitochondria,

	(glutathione peroxidase 5); glutathione peroxidase	pWUSpLASpGL2pH MGpS17sATHB8		PM, plastid
AT4G35090	CAT2 (CATALASE 2); catalase	CLV3pKANpFILpL1 pWUSpLASpGL2pH MGpATHB8	Cell Metabolism	extracellular, mitochondria, peroxisome, plastid
AT5G02380	MT2B (METALLOTHIONEIN 2B); copper ion binding	CLV3pKANpFILpL1 pWUSpLASpGL2pH MGpS17sATHB8	Cell Metabolism	extracellular, plastid
AT5G04260	WCRKC2 (WCRKC THIOREDOXIN 2)	CLV3pKANpFILpL1 pWUSpLASpGL2pH MGpS17sATHB8	Cell Metabolism	mitochondria, plastid
AT5G17920	ATCIMS_ATMETS__ATMS 1; 5-methyltetrahydropteroyltriglutamate-homocysteine S-methyltransferase/ methionine synthase	ND	Cell Metabolism	cytosol, mitochondria, peroxisome, PM, vacuole
AT1G17370	UBP1B mRNA 3'-UTR binding	CLV3pKANpFILpL1 pWUSpLASpGL2pH MGpS17sATHB8	Nucleic Acid Metabolism	mitochondria, nucleus
AT1G18680	HNH endonuclease domain-containing protein	FILpL1pWUSpLASp GL2pHMGp	Nucleic Acid Metabolism	extracellular, mitochondria, plastid
AT1G48410	AGO1 (ARGONAUTE 1); endoribonuclease/ miRNA binding / protein binding / siRNA binding	CLV3pKANpFILpL1 pWUSpLASpGL2pH MGpS17sATHB8	Nucleic Acid Metabolism	cytosol, nucleus
AT2G23350	PABP4__PAB4 (POLY(A) BINDING PROTEIN 4); RNA binding / translation initiation factor	CLV3pKANpFILpL1 pWUSpLASpGL2pH MGpS17sATHB8	Nucleic Acid Metabolism	mitochondria, nucleus, plastid

AT2G26460	SMU2__RED family protein, nuclear RNA splicing	CLV3pKANpFILpL1 pWUSpLASpGL2pH MGpS17sATHB8	Nucleic Acid Metabolism	nucleus
AT3G04610	FLK (flowering locus KH domain); RNA binding / nucleic acid binding	CLV3pKANpFILpL1 pWUSpLASpGL2pH MGpS17sATHB8	Nucleic Acid Metabolism	cytosol, nucleus, plastid
AT3G47490	HNH endonuclease domain-containing protein	CLV3pKANpFILpL1 pWUSpLASpGL2pH MGpS17sATHB8	Nucleic Acid Metabolism	mitochondria, nucleus, plastid
AT4G24770	ATRBP31_ATRBP33_CP31__RBP31 (31-KDA RNA BINDING PROTEIN); RNA binding / poly(U) binding	CLV3pKANpFILpL1 pWUSpLASpGL2pH MGpS17sATHB8	Nucleic Acid Metabolism	mitochondria, nucleus, plastid
AT4G25630	ATFIB2__FIB2 (FIBRILLARIN 2); snoRNA binding	ND	Nucleic Acid Metabolism	mitochondria, nucleus, plastid
AT5G02530	RNA and export factor-binding protein, putative	CLV3pKANpFILpL1 pWUSpLASpGL2pH MGpS17sATHB8	Nucleic Acid Metabolism	cytosol, mitochondria, nucleus
AT5G08290	YLS8; catalytic, spliceosomal complex	CLV3pKANpFILpL1 pWUSpLASpGL2pH MGpS17sATHB8	Nucleic Acid Metabolism	cytosol, nucleus
AT5G47210	nuclear RNA-binding protein, putative	CLV3pKANpFILpL1 pWUSpLASpGL2pH MGpS17sATHB8	Nucleic Acid Metabolism	nucleus, PM
AT5G59860	RNA recognition motif (RRM)-containing protein	CLV3pWUSpGL2pH MGp	Nucleic Acid Metabolism	cytosol, mitochondria, nucleus
AT1G28420	Homeobox-1	CLV3pKANpFILpL1 pWUSpLASpGL2pH MGpS17sATHB8	Transcription Factor	nucleus

AT1G28520	ATVOZ1__VOZ1 (VASCULAR PLANT ONE ZINC FINGER PROTEIN); transcription activator	CLV3pFILpWUSpLASpHMGpS17sATHB8	Transcription Factor	mitochondria, nucleus
AT1G54830	NF-YC3 (NUCLEAR FACTOR Y, SUBUNIT C3); DNA binding / transcription factor	CLV3pKANpFILpL1pWUSpLASpGL2pHMGpS17sATHB8	Transcription Factor	nucleus, plastid
AT1G69600	ATHB29__ZFHD1 (ZINC FINGER HOMEODOMAIN 1); DNA binding / transcription activator/ transcription factor	CLV3pKANpFILpL1pWUSpLASpGL2pHMGpATHB8	Transcription Factor	nucleus
AT2G17950	PGA6_WUS1__WUS (WUSCHEL); DNA binding / protein binding / transcription factor/ transcription regulator	CLV3pWUSpLASp	Transcription Factor	nucleus
AT2G33880	WUSCHEL-RELATED HOMEOBOX 9 (WOX9), STIMPY		Transcription Factor	mitochondria, nucleus, plastid
AT2G38880	ATHAP3_ATNF-YB1_HAP3_HAP3A__NF-YB1 (NUCLEAR FACTOR Y, SUBUNIT B1); transcription factor	CLV3pKANpFILpL1pWUSpLASpGL2pHMGpS17sATHB8	Transcription Factor	nucleus
AT2G45640	ATSAP18__SAP18 (SIN3 ASSOCIATED POLYPEPTIDE P18); protein binding / transcription regulator	CLV3pKANpFILpL1pWUSpLASpGL2pHMGpS17sATHB8	Transcription Factor	mitochondria, nucleus, plastid

AT4G00180	YAB3 (YABBY3); protein binding / transcription factor	FILpL1p	Transcription Factor	mitochondria, nucleus, plastid
AT4G04780	MED21 (MEDIATOR 21), Encodes the med21 subunit of the mediator complex which is involved in transcriptional regulation	ND	Transcription Factor	cytosol, plastid
AT4G32730	ATMYB3R-1_ATMYB3R1_MYB3R-1_MYB3R1__PC-MYB1; DNA binding / transcription coactivator/ transcription factor	CLV3pKANpFILpL1 pWUSpLASpGL2pH MGpS17sATHB8	Transcription Factor	nucleus, peroxisome, PM
AT5G23090	NF-YB13 (NUCLEAR FACTOR Y, SUBUNIT B13); transcription factor	CLV3pKANpFILpL1 pWUSpLASpGL2pH MGpS17sATHB8	Transcription Factor	cytosol, nucleus, plastid
AT5G57150	basic helix-loop-helix (bHLH) family protein	CLV3pKANpFILpL1 pWUSpLASpGL2pH MGpS17sATHB8	Transcription Factor	nucleus
AT5G58850	ATMYB119__MYB119 (MYB DOMAIN PROTEIN 119); DNA binding / transcription factor	ND	Transcription Factor	nucleus
AT1G01230	ORMDL family protein, protein folding	CLV3pKANpFILpL1 pWUSpLASpGL2pH MGpS17sATHB8	Protein Folding and Stability	extracellular, mitochondria, PM
AT1G03680	ATM1_TRX-M1__ATHM1; enzyme activator	CLV3pKANpFILpL1 pWUSpLASpGL2pH MGpS17sATHB8	Protein Folding and Stability	extracellular, mitochondria, plastid
AT1G17860	trypsin and protease inhibitor	KANpWUSpATHB8	Protein Folding and	cytosol, ER, extracellular

	family protein / Kunitz family protein		Stability	
AT1G47128	RD21A__RD21 (responsive to dehydration 21); cysteine-type endopeptidase/ cysteine-type peptidase	CLV3pKANpFILpL1 pWUSpLASpGL2pH MGpS17sATHB8	Protein Folding and Stability	ER, extracellular, plastid, vacuole
AT2G02100	PDF2.2__LCR69 (LOW-MOLECULAR-WEIGHT CYSTEINE-RICH 69); peptidase inhibitor	CLV3pKANpFILpL1 pWUSpLASpGL2pH MGpS17sATHB8	Protein Folding and Stability	ER, extracellular, nucleus, PM
AT2G34860	EDA3 (embryo sac development arrest 3); heat shock protein binding / unfolded protein binding	CLV3pKANpFILpL1 pWUSpLASpGL2pH MGpS17sATHB8	Protein Folding and Stability	nucleus, plastid
AT2G36170	ubiquitin extension protein 2 (UBQ2) / 60S ribosomal protein L40 (RPL40A)	CLV3pKANpFILpL1 pWUSpLASpGL2pH MGpS17sATHB8	Protein Folding and Stability	cytosol, nucleus
AT3G51260	PAD1 (20s proteasome alpha subunit pad1); endopeptidase/ peptidase/ threonine-type endopeptidase	CLV3pKANpFILpL1 pWUSpLASpGL2pH MGpS17sATHB8	Protein Folding and Stability	cytoskeleton, cytosol, mitochondria, nucleus, plastid, vacuole
AT3G52590	EMB2167_ERD16_HAP4__ UBQ1 (UBIQUITIN EXTENSION PROTEIN 1); protein binding / structural constituent of ribosome	CLV3pKANpFILpL1 pWUSpLASpGL2pH MGpS17sATHB8	Protein Folding and Stability	cytosol, nucleus
AT3G62600	ERDJ3B__ATERDJ3B; heat shock protein binding / unfolded protein binding	CLV3pKANpFILpL1 pWUSpLASpGL2pH MGpS17sATHB8	Protein Folding and Stability	cytosol, ER, extracellular, mitochondria, PM
AT4G05320	UBQ10 (POLYUBIQUITIN	CLV3pKANpFILpL1	Protein Folding and	cytosol, mitochondria,

	10); protein binding	pWUSpLASpGL2pH MGpS17sATHB8	Stability	nucleus
AT4G26840	ATSUMO1_SUM1_SUMO 1__SUMO1 (SMALL UBIQUITIN-LIKE MODIFIER 1); protein binding / protein tag	CLV3pKANpFILpL1 pWUSpLASpGL2pH MGpS17sATHB8	Protein Folding and Stability	mitochondria, nucleus
AT5G09540	DNAJ heat shock domain containing protein, protein folding	CLV3pKANpFILpL1 pWUSpLASpGL2pH MGpS17sATHB8	Protein Folding and Stability	cytosol, extracellular, nucleus
AT5G23290	PFD5__PDF5 (PREFOLDIN 5); unfolded protein binding	CLV3pKANpFILpL1 pWUSpLASpGL2pH MGpS17sATHB8	Protein Folding and Stability	extracellular, plastid
AT5G38650	proteasome maturation factor UMP1 family protein	CLV3pKANpFILpL1 pWUSpLASpGL2pH MGpS17sATHB8	Protein Folding and Stability	cytosol, mitochondria, nucleus
AT5G42190	SKP1B__ASK2 (ARABIDOPSIS SKP1-LIKE 2); protein binding / ubiquitin-protein ligase	CLV3pKANpFILpL1 pWUSpLASpGL2pH MGpS17sATHB8	Protein Folding and Stability	cytosol
AT5G47590	heat shock protein related, proteolysis, 264AA	ND	Protein Folding and Stability	cytosol, plastid
AT5G49510	PFD3__PDF3 (PREFOLDIN 3); unfolded protein binding	CLV3pKANpFILpL1 pWUSpLASpGL2pH MGpS17sATHB8	Protein Folding and Stability	cytosol, nucleus
AT5G67360	ARA12; serine-type endopeptidase	CLV3pKANpFILpL1 pWUSpLASpGL2pH MGpS17sATHB8	Protein Folding and Stability	ER, extracellular, plastid
AT1G11120	unknown protein	CLV3pKANpFILpL1 pWUSpLASpGL2pH	Unknown Protein	mitochondria, nucleus, plastid

		MGpS17sATHB8		
AT1G21830	unknown protein	KANpFILpL1pWUSpLASpGL2pS17sATHB8	Unknown Protein	cytosol, mitochondria, nucleus, plastid
AT1G53280	DJ-1 family protein	CLV3pKANpFILpL1pWUSpLASpGL2pHMGpS17sATHB8	Unknown Protein	cytosol, mitochondria, plastid
AT1G67035	unknown protein, 190AA	CLV3pLASp	Unknown Protein	mitochondria, nucleus
AT2G01021	unknown protein, 33AA	ND	Unknown Protein	NA
AT2G20120	COV1 (CONTINUOUS VASCULAR RING), unknown function, 268AA	CLV3pKANpFILpL1pWUSpLASpGL2pHMGpS17sATHB8	Unknown Protein	extracellular, PM
AT2G25510	unknown protein	L1p	Unknown Protein	ER, extracellular, mitochondria, nucleus, plastid
AT2G33220	FUNCTIONS IN: molecular_function unknown; INVOLVED IN: photorespiration; LOCATED IN: mitochondrion, mitochondrial membrane, plastid, respiratory chain complex I; EXPRESSED IN: 25 plant structures; EXPRESSED DURING: 15 growth stages; CONTAINS InterPro DOMAIN/s: GRIM-19 (InterPro:IPR009346); BEST Arabidopsis thaliana protein match is: MEE4	ND	Unknown Protein	cytosol, mitochondria

	(maternal effect embryo arrest 4) (TAIR:AT1G04630.1); Has 226 Blast hits to 226 proteins in 98 species: Archae - 0; Bacteria - 0; Metazoa - 125; Fungi - 53; Plants - 38; Viruses - 0; Other Eukaryotes - 10 (source: NCBI BLink).			
AT3G07350	unknown protein	CLV3pKANpFILpL1 pWUSpLASpGL2pH MGpS17sATHB8	Unknown Protein	nucleus
AT3G10730	ATSUN2_SUN2__sad1/unc-84-like 2 family protein	CLV3pKANpFILpL1 pWUSpLASpGL2pH MGpS17sATHB8	Unknown Protein	cytoskeleton, ER, mitochondria, nucleus, plastid
AT3G12300	unknown protein, 190AA	CLV3pKANpFILpL1 pWUSpLASpGL2pH MGpS17sATHB8	Unknown Protein	extracellular, mitochondria, nucleus
AT3G15450	unknown protein	CLV3pKANpFILpL1 pWUSpLASpGL2pH MGpS17sATHB8	Unknown Protein	extracellular, mitochondria, nucleus, peroxisome
AT3G18215	unknown protein, 244AA	CLV3pKANpFILpL1 pWUSpLASpGL2pH MGpS17sATHB8	Unknown Protein	ER, extracellular, PM
AT3G50580	unknown protein	ND	Unknown Protein	ER, extracellular, nucleus
AT3G55770	LIM domain-containing protein, FUNCTIONS IN: zinc ion binding	CLV3pKANpFILpL1 pWUSpLASpGL2pH MGpS17sATHB8	Unknown Protein	mitochondria, nucleus
AT4G11211	unknown protein, 21AA	ND	Unknown Protein	mitochondria, plastid
AT4G17620	glycine-rich protein	CLV3pKANpFILpL1 pWUSpLASpGL2pH	Unknown Protein	mitochondria, nucleus, plastid

		MGpS17sATHB8		
AT4G20150	unknown protein	CLV3pKANpFILpL1 pWUSpLASpGL2pH MGpS17sATHB8	Unknown Protein	cytosol, ER, mitochondria, plastid, vacuole
AT5G02710	Unknown protein, Chromatin remodeling related	ND	Unknown Protein	mitochondria, nucleus, plastid
AT5G02720	unknown protein	ND	Unknown Protein	cytosol, mitochondria
AT5G08060	unknown protein	CLV3pKANpFILpL1 pWUSpLASpGL2pH MGpS17sATHB8	Unknown Protein	mitochondria, nucleus, plastid
AT5G14030	translocon-associated protein beta (TRAPB) family protein, 195AA	CLV3pKANpFILpL1 pWUSpLASpGL2pH MGpS17sATHB8	Unknown Protein	ER, extracellular, mitochondria, PM, vacuole
AT5G41980	unknown protein, 374AA	ND	Unknown Protein	cytosol
AT5G42530	unknown protein, 71AA	ND	Unknown Protein	ER, extracellular, nucleus
AT5G48480	unknown protein, 166AA	CLV3pKANpFILpL1 pWUSpLASpGL2pH MGpS17sATHB8	Unknown Protein	cytosol, plastid
AT5G48500	unknown protein	FILpWUSpHMGp	Unknown Protein	cytosol, extracellular, plastid
AT5G49440	unknown protein, 181AA	ND	Unknown Protein	nucleus

Table S1.2: WUS PPI Clones Verified via Independent Sanger Sequencing

AGI ID	Annotation	Cell Type	GO Term Function	Subcellular Localization
AT4G15030	unknown protein, similarity to kinesin motor family	CLV3pKANpFILpL1 pWUSpLASpGL2pH MGpS17sATHB8	Cell-Cell Communication and Secretory Pathways	mitochondria, nucleus
AT1G28420	Homeobox-1	CLV3pKANpFILpL1 pWUSpLASpGL2pH MGpS17sATHB8	Transcription Factor	nucleus
AT5G02710	Unknown protein, Chromatin remodeling related	ND	Unknown Protein	mitochondria, nucleus, plastid
AT2G17380	AP19; protein binding / protein transporter	CLV3pKANpFILpL1 pWUSpLASpGL2pH MGpS17sATHB8	Cell-Cell Communication and Secretory Pathways	cytosol, mitochondria, nucleus
AT1G17370	UBP1B mRNA 3'-UTR binding	CLV3pKANpFILpL1 pWUSpLASpGL2pH MGpS17sATHB8	Nucleic Acid Metabolism	mitochondria, nucleus

Table S1.3: Primers

Primer Name	Primer Sequence
WUS CDS Fwd NdeI	CATATGGAGCCGCCACAG
WUS CDS Rev EcoRI	GAATTCCTAGTTCAGACGTAG
Matchmaker 5’ AD LD-Insert Screening Amplifier	CTATTCGATGATGAAGATACCCCACCAAACCC
Matchmaker 3’ AD LD-Insert Screening Amplifier	GTGAACTTGCGGGGTTTTTCAGTATCTACGAT

Chapter 2: A Reverse Genetics Screen of WUS PPIs Reveals Factors with Possible Functional Roles in WUS Mediated SAM Maintenance

Introduction

The previously described Y2H screen yielded a large output of 119 putative WUS PPIs to analyze. While this provides many avenues for future research, the initial objective was to identify a PPI that could be characterized in depth through biochemical and genetic analyses in order to understand specific WUS-mediated mechanisms working on the protein level to regulate SAM maintenance and plant development. Such an endeavor is impractical on the scale of the entire PPI network, so the next objective was to select one of the most relevant PPI targets to further analyze. We decided to filter this dataset by identifying functionally relevant PPIs through a genetic screen in *A. thaliana*.

Genetic screens can be classified into two main groups: classical forward genetics and the more recently established reverse genetics (Alonso and Ecker, 2006). The forward genetics screen group includes experiments such as T-DNA and transposon insertion, EMS mutagenesis, and X-ray mutagenesis. T-DNA and transposon insertion screens rely on the disruption of gene products through the random insertion of DNA fragments into the genome that will infrequently displace the continuity of the transcribed genomic region, resulting in a nonfunctional mRNA that fails to produce a functional translation product (Krysan et al., 1999). EMS mutagenesis relies on chemical transformations of individual bases in a genome, and can result in many base changes in a single plant (Page and Grossniklaus, 2002). X-ray mutagenesis uses high energy disruption of the genome, and can yield many changes including DNA rearrangements,

sequence deletions, and breakages (Koornneef et al., 1982). The random nature of the DNA disruptions introduced in these types of screens prevents them from being used to identify gene function directly, rather they are used to generate novel and interesting phenotypes and then from those phenotypes identify the gene responsible for that particular phenotype (Alonso and Ecker, 2006). These types of approaches were widely used to develop an initial database of interesting genes and their functions early on in the adoption of *A. thaliana* as a model system, and can still be used in existing mutant backgrounds to identify suppressor or enhancer phenotypes that reveal additional genes relevant in the pathways of such a pre-existing mutant background.

Conversely, reverse genetics screens are used to identify the phenotypes resulting from the knockdown or overexpression of a specific known gene or set of genes (Alonso and Ecker, 2006). The ability to associate a phenotype to a specific genotype is critical in the initial characterization of unknown gene function. These screens quickly became prominent after the sequencing of the *A. thaliana* genome, which provided both a large set of previously uncharacterized genes and a template for cloning these genes (Kaul et al., 2000). The most common uses of reverse genetics employ the screening of random mutations within a gene and its surrounding region for knockout phenotypes, constitutive overexpression, or targeted knockdown of a specific gene or gene set (Alonso and Ecker 2006). Random mutation screens typically analyze collections of mutations across a gene or gene set to isolate particular mutations with phenotypic changes. Overexpression studies drive the expression of a gene or gene set in a constituent and ectopic manner such that an over accumulation of gene product is present in the plant and the resulting

phenotype is characterized (Bundock and Hooykaas, 2005, Kremer et al., 2013). Targeted gene knockdown screens may take advantage of RNAi or VIGS (Viral Induced Gene Silencing) systems to specifically knockdown the expression of a target gene or gene set and analyze the phenotype generated (Hilson et al., 2004, Robertson 2004, Ueno et al., 2007). Again, these screens can also be used to identify suppressor or enhancer phenotypes within a previously characterized mutant background.

In order to focus the analysis of the 119 PPIs, we isolated a subset of 62 PPIs based on the previous GO Term categorization and independent confirmations to further filter through phenotypic characterization *in planta*. We performed a functional reverse genetics suppressor screen in *clv3-2 pWUS::eGFP-WUS* plants using a constitutively active RNAi system to knockdown the expression of target genes present in the PPI network (Clark et al., 1995, Ueno et al., 2007, Yadav et al., 2011). Single mutant *clv3-2* plants have greatly enlarged stems and SAMs along with distinct club-like siliques with 3 fused carpels (Clark et al., 1995). Double mutant *wus-1 clv3-2* plants completely suppress the *clv3-2* single mutation and produce flat SAMs with few organs like the *wus-1* single mutant (Schoof et al., 2000). Therefore, PPIs with functional relevance in proper WUS function would likely inhibit WUS function and yield phenotypic suppression in the *clv3-2* background when knocked down via RNAi, resulting in populations that are easier to screen quickly for target identification. Additionally, these lines harbor the *pWUS::eGFP-WUS* construct that generate a functional and visibly trackable eGFP-WUS fusion protein to easily identify changes in WUS accumulation and mobility within the SAM via confocal microscopy.

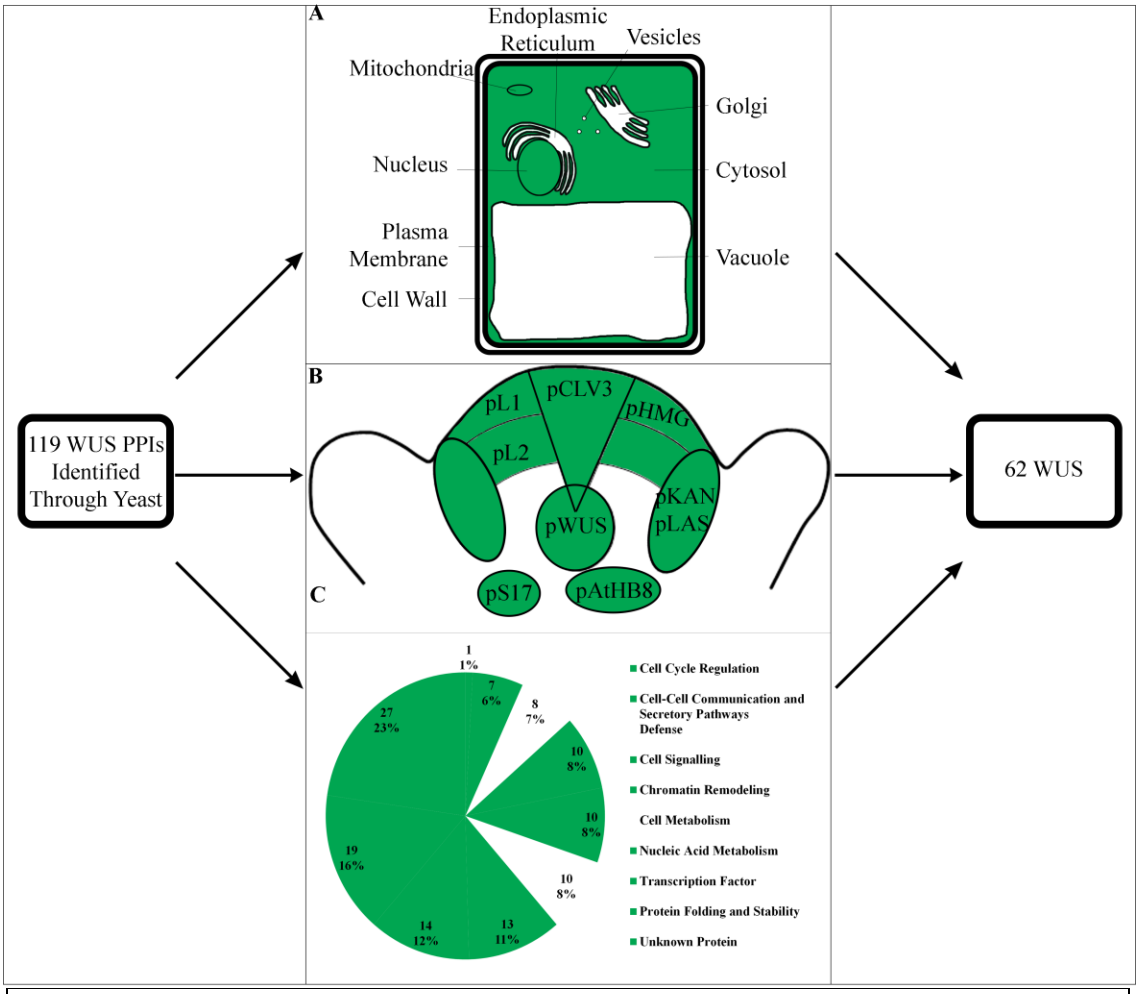

Figure 2.1: Filtering of 119 WUS PPIs Into a Subset of 62 for Screening with RNAi. Filtering by subcellular localization (A), cell type expression data (B) and GO Term category enrichment (C). Areas in green represent the regions and categories from which WUS PPIs were retained to result in the final 62 WUS PPIs used in RNAi screening.

Presented here is a reverse genetics screen using RNAi to functionally characterize a subset of the previously identified WUS PPI network. The original 119 WUS PPIs were filtered to 62 targets that were cloned into a constitutively active RNAi knockdown construct. These were introduced into *clv3-2 pWUS::eGFP-WUS* plants and screened for phenotypic suppression and effects on protein accumulation and movement in the SAM to identify those WUS PPIs with a relevant connection to WUS function in SAM maintenance.

Results

Bioinformatic Datasets Provide Tools for Further Enrichment of the WUS PPI Network

Initial Y2H screening led to a WUS PPI network of 119 proteins. However, there are several previously existing bioinformatics datasets that can be applied to this interactome to enrich those members that are likely to be the most relevant for affecting proper WUS function. The first of these is the SUBcellular location database for Arabidopsis proteins (SUBA), which contains localization data for over 6,700 Arabidopsis proteins (Heazlewood et al., 2007). Based on this dataset, WUS is enriched in the nucleus, cytosol, and mitochondria, and enrichment of WUS PPIs in these three subcellular locations was initially used to filter the data (Figure 2.1A). Then, the previously generated cell type expression dataset was used to filter out WUS PPIs that are ubiquitously expressed throughout the SAM and enrich those that are expressed in a more restricted pattern in the SAM (Figure 2.1B) (Yadav et al., 2014). While many of the WUS PPIs were expressed in all currently defined SAM cell types, focusing analysis on those with unique expression patterns could help refine the role of cell-type specific factors in WUS-mediated stem cell maintenance. Finally, the GO Term categorization was used to focus on interactors that are involved in known WUS processes, including Cell Cycle Regulation, Cell-Cell Communication and Signaling Pathways, Cell Signaling, Chromatin Remodeling, Nucleic Acid Metabolism, Transcription Factor, Protein Folding and Stability, and Unknown Proteins (Figure 2.1C). After all of these

filtering mechanisms were applied, a total of 62 remaining WUS PPIs from the original 119 were used for the functional characterization screening.

Generation and Screening of the pYU501 RNAi Library Reveal a Small Subset of Functionally Relevant WUS PPI Targets

The cDNA of each of the remaining 62 WUS PPIs was used to develop individual primers that amplify the region contained within each target's coding sequence (CDS). Using the SAM cDNA library as a template, each WUS PPI was amplified and sequentially cloned into the pYU501 binary destination vector through the intermediate pENTR Gateway entry vector (Ueno et al., 2007). The pYU501 vector contains two tandem inverted Gateway cloning sites surrounding a WRKY33 intron along with a *35SCaMV* promoter to drive ectopic expression of the RNAi hairpin fragment (Ueno et al., 2007). After recombination of each clone into the pYU501 destination vector, site-specific PCR primers for each of the cloning sites were used to PCR amplify and confirm the insertion into both sites (Table S2.2). Final constructs were then transformed into *A. tumefaciens* for floral dip into *clv3-2 pWUS::eGFP-WUS* plants. For each construct, approximately 20,000 of T_0 seeds per line were screened via hygromycin selection to obtain positive T_1 plants for phenotypic suppression analysis. Partial suppressor lines were identified as those with reduced SAM size, reduced stem size, and reduced apical dominance (Clark et al., 1995, Yu et al., 2000). Of the 62 initial lines, the four partial *clv3-2* suppressors identified and maintained for further characterization were TCTP, FLORAL TRANSITION AT THE MERISTEM4 (FLOR1), AT3G12300, and AT1G67035 (Figure 2.2A-2.2J).

Figure 2.2: Phenotypes of RNAi Partial *clv3-2* Suppressor Lines. Phenotypes of *clv3-2* (A-B), RNAi TCTP (C-D), RNAi FLOR1 (E-F), RNAi AT3G12300 (G-H), and RNAi AT1G67035 (I-J). RNAi lines have smaller SAMs and reduced apical dominance compared to *clv3-2*. (Scale bars = 10mm)

Fluorescent Confocal Imaging Reveals a Subset of WUS PPIs with Potential Effects on WUS Accumulation and SAM Size

Axillary SAMs from each T_2 line and *clv3-2* controls were imaged via fluorescent confocal microscopy to visualize any effects on the eGFP-WUS fusion protein accumulation and movement, along with any changes in SAM size and structure as measured by the membrane bound FM4-64x dye (Figure 2.3A-2.3O). Confocal image data was processed in a semi-quantitative manner within independent cell layers to determine the average relative fluorescence of eGFP-WUS across the nuclei of cells in each independent cell layer and compared to the *clv3-2 pWUS::eGFP-WUS* control (n=3) (Figure S2.1A-S2.1T). RNAi lines for *AT3G12300* and *AT1G67035* had lower eGFP-WUS signal than *clv3-2* across all 4 cell layers (Figure 2.4A). RNAi lines for *TCTP* had lower eGFP-WUS signal than *clv3-2* in the L1 and L4 layers, but slightly higher signal in L2 and L3 layers (Figure 2.4A). Interestingly, RNAi *FLOR1* lines maintained elevated eGFP-WUS signal compared to *clv3-2* across all layers, with almost double the signal in L2 and L3 layers (Figure 2.4A).

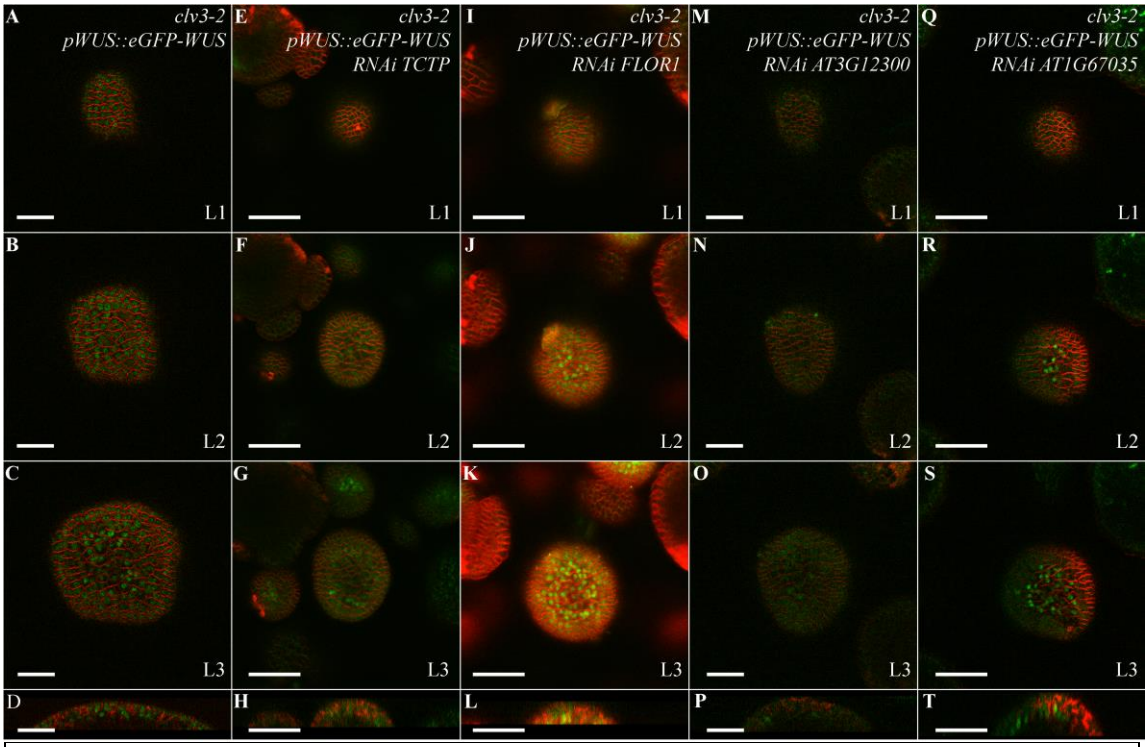

Figure 2.3: Confocal Images of pYU501 Lines with clv3-2 Suppression Phenotypes. Inflorescence SAMs of clv3-2 (A-D), RNAi TCTP (E-H), RNAi FLOR1 (I-L), RNAi AT3G12300 (M-P), and RNAi AT1G67035 (Q-T). SAM layers are respresented by L1 (A, E, I, M, Q), L2 (B, F, J, N, R), and L3 (C, G, K, O, S), along with longitudinal sections (D, H, L, P, T) . Green signal is eGFP-WUS, red signal is FM4-64X plasma membrane bound dye. (Scale bars=50µm, n=3)

Additionally, the area of each SAM measured at each cell layer was calculated to determine the relative SAM size of each line and show partial suppression of the *clv3-2* enlarged SAM phenotype (Figure S2.1A-S2.1T) (Yu et al., 2000). Compared to the *clv3-2* controls, analysis of three independent lines for all four knockdown constructs resulted in smaller SAMs across all layers (Figure 2.4B). RNAi *AT3G12300* lines were the largest SAMs, with each cell layer between 64-70% of the area of *clv3-2* SAMs. The next closest line in area across all layers was RNAi *AT1G67035*, which maintained a layer area 41-43% of the *clv3-2* SAMs. RNAi *FLOR1* lines were 50% of the *clv3-2* area in L1, but decreased in relative size to 41% in L2, 37% in L3, and 33% in L4. Finally, RNAi *TCTP* lines showed the strongest decrease in SAM size, with the L1 layer only 18% of the *clv3-*

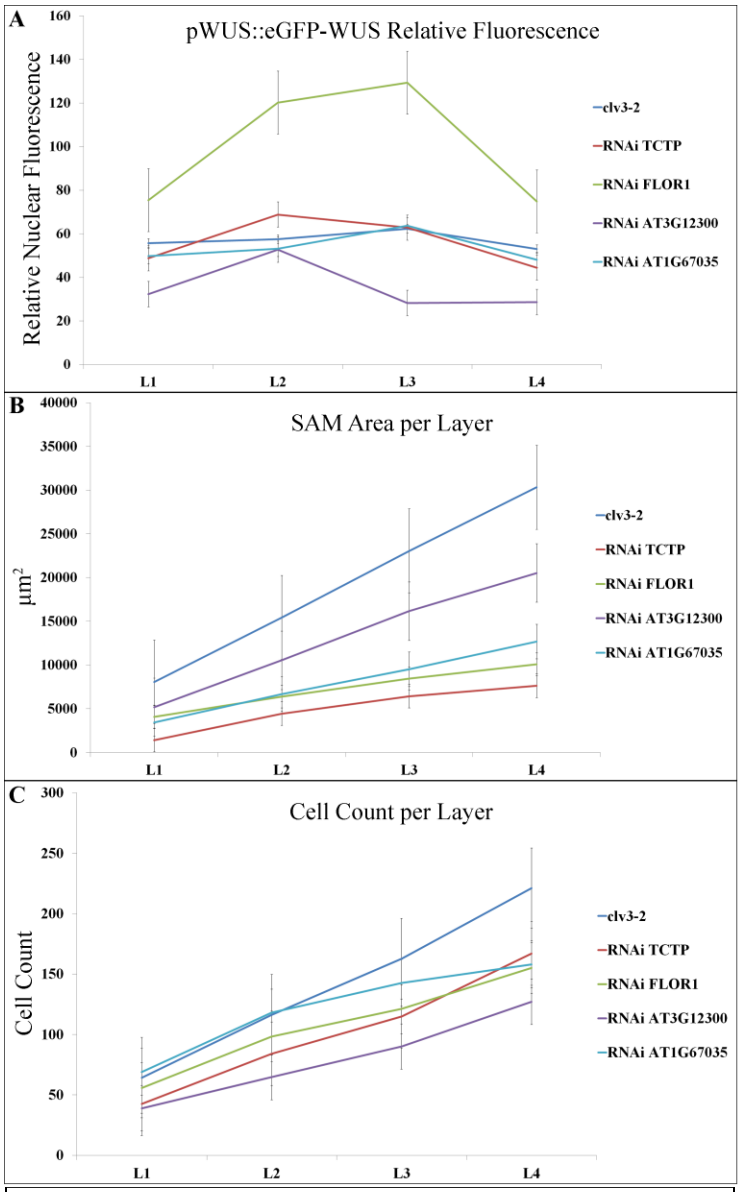

Figure 2.4: Semi-quantitative Analysis of eGFP-WUS Accumulation and SAM Size in RNAi Partial *clv3-2* Suppressor Phenotypes. The average nuclear accumulation of eGFP-WUS relative fluorescence in each cell layer was measured (A). The area of each transversal cross section was measured at each cell layer depth to provide SAM size comparisons (B). The number of cells present in each layer was measured (C). Error bars represent standard error. (n=3).

2 area in L1, increasing to a maximum of 29% in L2 and decreasing again to 28% in L3 and 25% in L4. The reduction in SAM size for each RNAi line across all SAM cell layers is consistent with partial suppression of the *clv3-2* phenotype.

The size of a plant organ is typically controlled by a combination of how many cells are present and how large those cells are (Beemster et al., 2005, Kalve et al., 2014). In order to elucidate the source of the reduced SAM size in each partial *clv3-2* suppressor line, the number of cells per SAM layer was counted to see if the size difference was due to cell number or cell size. RNAi *TCTP*, *FLOR1*, and *AT3G12300* all had lower cell counts per layer than *clv3-2*,

suggesting that the difference in SAM size is likely due to the number of cells present. However, RNAi *AT1G67035* had a similar cell number to *clv3-2* in the L1 and L2 layers with a reduction in cell number only in the L3 and L4 layers, suggesting that cell size in at least the L1 and L2 layers for these lines are due to a reduction in cell size.

Discussion

The identification of novel WUS PPIs with functional relevance to SAM maintenance is an important facet of understanding the complex nature of plant development. The previous tandem Y2H and high throughput sequencing analysis yielded a diverse array of putative WUS PPIs, some of which were confirmed via independent retesting using several approaches. Indeed, uncovering the functional relevance of these WUS PPIs is a more critical experiment in determining the network of regulators that are necessary to function in concert with WUS in maintaining the SAM. A reverse genetics screen using RNAi knockdown is an excellent way to characterize the functional relevance of the target WUS PPIs in SAM maintenance; however the initial dataset was quite large at 119 putative WUS PPIs. The time required for independently cloning, creating transgenic lines, and screening the entirety of these lines would have been prohibitive, especially when there are relevant informatics resources to refine the WUS PPIs and identify those with a higher likelihood of functional relevance in SAM regulation (Heazlewood et al., 2007, Yadav et al., 2014, unpublished data). To this end, the SUBA localization database was used as the initial tool to enrich the WUS PPI dataset, using the simple concept that spatial proximity of a functionally relevant WUS PPI should occur in the same subcellular compartments of the nucleus, cytosol, and

mitochondria in which WUS is enriched (Figure 2.1A) (Heazlewood et al., 2007). Next, we incorporated previously annotated cell type specific expression data to ensure that any putative WUS PPIs with a restricted cell type expression pattern was retained for the functional screen (Yadav et al., 2014). This ensured that any WUS PPI with a potential for cell type specific WUS-mediated function in the SAM could be characterized to expand the currently limited knowledge of WUS function in specific SAM cell types (Yadav et al., 2014). Finally, the GO Term enrichment had previously been used to broadly categorize WUS PPIs into groupings with a similar functional role. This provided another simple filter to eliminate the 18 members in the categories of Defense and Cell Metabolism. While these WUS PPIs could very well provide a crucial role in SAM maintenance, the potential for WUS-mediated relevance is less direct than those present in the categories of Cell Cycle Regulation, Cell-Cell Communication and Secretory Pathways, Chromatin Remodeling, Nucleic Acid Metabolism, Transcription Factor, Protein Folding and Stability, and Unknown Proteins (Figure 2.1C).

Based on the RNAi knockdown screen to identify suppressors of the *clv3-2* phenotype, a total of four genes that were partial suppressors with reduced stem size, reduced apical dominance, and smaller SAMs were identified: *TCTP*, *FLOR1*, *AT3G12300*, and *AT1G67035* (Berkowitz et al., 2008, Brioudes et al., 2010, Acevedo et al., 2004, Torti et al., 2012). *TCTP* is a critical gene found across the eukaryotic taxa with several characterized roles in the regulation of cell division, cell growth, and cell morphology (Bommer and Thiele, 2004, Berkowitz et al., 2008, Brioudes et al., 2010). More recent work with *AtTCTP* has shown that it has a conserved function in mitotic cell

division, yet lacks the additional regulation of cell morphology and size performed by the mammalian homologues (Brioudes et al., 2010). WUS itself is also responsible for maintaining the proper cell division rates of the SAM, a complex process which involves spatial regulation of WUS accumulation and long distance signaling to the distal cells of the SAM periphery and organ boundary (Reddy and Meyerowitz, 2005, Yadav et al., 2010). The RNAi *TCTP* lines show a reduced accumulation of eGFP-WUS in the L1 and L4 layers, and an increased accumulation in the L2 layer. This fluctuation in eGFP-WUS accumulation resulted in the smallest SAM size based on transversal layer sections, and the second smallest cell count per layer, suggesting that the RNAi *TCTP* may result in a reduction of cell division that leads to partial *clv3-2* suppression (Figures 2.4A-2.4C, S2.1A-S2.1H).

FLOR1 is a plant specific protein that in concert with AGAMOUS (AG) is responsible for the initiation of floral development (Acevedo et al., 2004, Torti et al., 2012). This makes its potential interaction with WUS more relevant, as WUS directly activates *AG* (Ikeda et al., 2009). The interaction of WUS and FLOR1 could be a precursor complex that when formed signals the start of the floral transition through the activation of *AG*. Additionally, after its activation AG directly represses the expression of WUS through the recruitment of PcG proteins in order to terminate the floral meristem (Liu et al., 2011). The lack of FLOR1 in these RNAi lines results in a much higher level of eGFP-WUS accumulation across all cell layers and more than double that of *clv3-2* in the L2 and L3 layers (Figure 2.4A). However, the size and cell numbers of RNAi *FLOR1* SAMs are still lower than *clv3-2*, and combined with the partial *clv3-2* suppression

phenotypes suggest that this enrichment of eGFP-WUS may also come at some negative consequence to the ability of WUS to repress differentiation factors in the stem cell domain.

AT3G12300 and *AT1G67035* encode two proteins of unknown function, and as such their discussion is more limited to the partial *clv3-2* suppression shown in this screen. Knockdown of each of these targets resulted in a reduced accumulation of eGFP-WUS in the *clv3-2* background (Figure 2.4A). This could be due to several factors such as a reduction of WUS stability in the SAM, a reduction of WUS transcriptional activity, or a reduction of the size of the RM. Additionally, RNAi *AT3G12300* lines exhibited a reduction of SAM size and cell number as expected with the partial *clv3-2* suppression phenotype (Figures 2.4B-2.4C, S2.1M-S2.1P). While RNAi *AT1G67035* lines also had a reduced SAM size compared to *clv3-2*, they interestingly had a similar number of cells in the L1 and L2 layers (Figure 2.4B-2.4C). This suggests that in these layers the size difference of the SAM is likely due to the size of the cells in each layer. While further characterization of this process is needed, this initial evidence points to AT1G67035 involvement in cell cycle regulation, which is interesting given the role of WUS in regulating cell division patterns in the SAM (Reddy and Meyerowitz, 2005, Yadav et al., 2010).

While this RNAi reverse genetics screen revealed a small subset of WUS PPIs with potential functional relevance in WUS-mediated SAM maintenance, there are some limitations inherent to the screening process. First, there were no complete suppressors of *clv3-2* identified as all lines maintained the club-like siliques with three fused carpels

characteristic of *clv3-2* (Figure 2.2A-2.2J) (Clark et al., 1995). This suggests that none of the WUS PPIs screened are completely responsible for WUS function in SAM maintenance, which is highly plausible given the diverse functions and properties of WUS including regulation of stem cell maintenance, cell division, and protein mobility (Mayer et al., 1998, Leibfried et al., 2005, Reddy and Meyerowitz, 2005, Yadav et al., 2011). Also, there is a small potential that functionally relevant WUS PPIs could have been filtered out prior to the RNAi screen due to the bioinformatics datasets used to enrich the final 62 WUS PPIs used in the screen. The likelihood of this is small given the variety of datasets used to filter this information; however it cannot be completely ignored (Figure 2.1A-2.1C). Finally, there are some targets in the screening process that may have not shown strong phenotypes due to the complementarity of other members in the same protein family. Interesting candidates such as ULTRAPETALA1 (ULT1), SNF-1 KINASE HOMOLOG 11 (KIN11), ARABIDOPSIS SKP1 HOMOLOGUE 1 (ASK1) and SUMO1 are members of larger protein families. ULT1 has been shown to regulate the termination of floral meristems and regulate the expression domain of WUS (Fletcher 2001, Carles et al., 2005). KIN11 is a member of a protein family involved in signaling kinase pathways, along with ASK1 and its family members also regulate functionality of the proteasome, which has profound effects on protein stability (Farras et al., 2001, Fordham-Skelton et al., 2002). In *A. thaliana* SUMO1 is part of a three member family that has involvement in many plant functions, including subcellular localization, post-translational modification, and transcriptional regulation (Saracco et al., 2007, Miller et al., 2010, van den Burg et al., 2010). It is likely that homologous protein family members

could complement the RNAi used and therefore dampen or eliminate any phenotypic effects that resulted. In fact, further analysis of SUMO1 that will follow in the next chapter will demonstrate its functional relevance in WUS-mediated SAM maintenance.

In conclusion, the enrichment of the WUS PPIs using informatics datasets was essential for generating the final set of 62 WUS PPIs from the original 119 of the initial Y2H screen. The reverse genetics RNAi screen of these 62 WUS PPIs presented here was used to identify TCTP, FLOR1, AT3G12300, and AT1G67035 as four WUS PPIs with partial suppression of the *clv3-2* phenotype. Further analysis revealed that FLOR1 had the largest effect on eGFP-WUS accumulation in the SAM with a near two-fold increase in accumulation in the L2 and L3 layers. All four identified lines showed a reduction in SAM size, with *RNAi TCTP* lines containing the smallest SAMs. Finally, all of the lines except *RNAi AT1G67035* showed a decrease in cell number corresponding to the decrease in SAM size; *RNAi AT1G67305* had a similar number of cells as *clv3-2* in the L1 and L2 layers. These targets provide interesting bases for further study of the specific mechanisms involved in WUS mediated SAM maintenance and the expanding WUS network.

Methods

Enrichment of the WUS PPI Network for Functional Characterization

All 119 WUS PPI network members were annotated with publicly available GO Term associations, subcellular localization data, and cell type expression patterns based on datasets from the Gene Ontology (www.geneontology.org) GO Term database, SUBA (http://suba3.plantenergy.uwa.edu.au) database, and SAM enriched cell sorting datasets

respectively (Yadav et al., 2014). GO Terms were used to select PPIs previously isolated into the following groups: Cell Cycle Regulation, Cell-Cell Communication and Signaling Pathways, Cell Signaling, Chromatin Remodeling, Nucleic Acid Metabolism, Transcription Factor, Protein Folding and Stability, and Unknown Proteins. SUBA subcellular localization data was used to select PPIs enriched in at least one of the subcellular compartments shared by WUS: nucleus, cytosol, and mitochondria (Heazlewood et al., 2007). Cell sorting gene expression was used to ensure all PPIs with any cell type specific expression patterns in the SAM (i.e. not expressed ectopically across all cell types) were included for functional analysis. Final selection yielded 62 WUS PPIs in the WUS PPI Enriched Network for downstream characterization analysis.

Cloning of the 62 WUS PPI Enriched Network into an Ectopic RNAi Plant Expression Vector

Primers for each of the 62 WUS PPI Enriched Network targets were designed based on the 5' and 3' ends of the coding sequence (CDS) for each target. A Gateway (GW) compatible "CACC" adapter sequence was added to the 5' end of the forward 5' primer to facilitate recombination into the pYU501 plant expression vector. AD library cDNA was used as a template for Phusion PCR amplification of each target. PCR products were isolated and inserted into the pENTR GW compatible entry vector, then recombined into the pYU501 plant expression vector. The pYU501 T-DNA region has a 35SCaMV promoter, two inverted GW compatible recombination sites surrounding a nested WRKY33 intron, a NOS-terminator sequence, and a hygromycin resistance gene for plant selection (Ueno et al., 2007). The proper insertion of the targets into both sites

of each of the final constructs was confirmed using plasmid specific primers unique to each recombination site (Table S2.2).

Transformation of *clv3-2 pWUS::eGFP-WUS* Plants and Screening

clv3-2 pWUS::eGFP-WUS plants were grown for 3-4 weeks on potting media in continuous light. Final pYU501 clones were transformed into *A. tumefaciens GV3101* and grown at 30^{o}C for 2d. Several small colonies were used to inoculate a 5mL LB culture grown at 250rpm for 1d. This culture was used to inoculate large 250mL LB cultures grown at 250rpm for 1-2d. These cultures were centrifuged in sterile 250mL bottles at 3,500rpm for 15min. The supernatant was decanted and the pellet resuspended in 5% sucrose on ice with gentle mixing. After complete resuspension of the pellet, 0.0075% Silwet-77 was added with 8-10 vigorous shakes to ensure complete mixing. This mixture was poured into sterile boxes, and the flowers of 30-35 plants were submerged into the mixture with gentle shaking for 30s and covered in the dark for 1d. This was repeated for all lines analyzed. Plants were then returned to continuous light growth conditions for 4 weeks until silique dehiscence. Seeds were collected, dried, sterilized via NaOCl and selected on 0.5% MS plates containing 25µg/mL hygromycin in continuous light for 12d (Murashige and Skoog, 1962). At least ten positive T_1 plants per construct were then transferred to potting media and phenotypically scored after bolting. Seeds were collected, and 5 T_2 plants from each T_1 parent were phenotypically scored and those with suppression or enhancer phenotypes were imaged via fluorescent confocal microscopy.

Sample Preparation and Fluorescent Confocal Imaging of Plants

Sterile plastic boxes were filled with 30-40mL of 1% MS media. Axillary stems were clipped with sharp forceps about 20mm below the tip of the apex. Floral buds were removed with sharp forceps from the stem and tissue surrounding the apical meristem as close to the stem/pedicel junction as possible. The 6-8 stems were inserted vertically into each MS media box and stabilized by pipetting 200-300µL of 35-40^{o}C 2% agarose around the base of each stem. Stems were then completely submerged in DI H_2O and precise removal of the remaining floral buds excepting the closest 3-5 was performed under a stereoscopic dissecting microscope. The H_2O was decanted and the plant apices dried via capillary action of Kimwipes placed just below the apex.

A working solution of 10% w/v FM4-64x, 2% TE buffer, and 2% Silwet-77 was made for staining the apices. For each apex, 1-2µL of FM4-64x working solution was applied and incubated for 10-15min, ensuring that no drying out occurred. Apices were then scanned using a Zeiss 510 confocal microscope using the LSM 510 imaging software. Fluorescence of eGFP excited at 488nm was captured from 500-530nm, while fluorescence of FM4-64x excited at 545nm was captured from 565-615nm via a 63x water immersion lens. Confocal image stacks were analyzed via the Zeiss LSM Image Browser and ImageJ.

Supplemental Figure

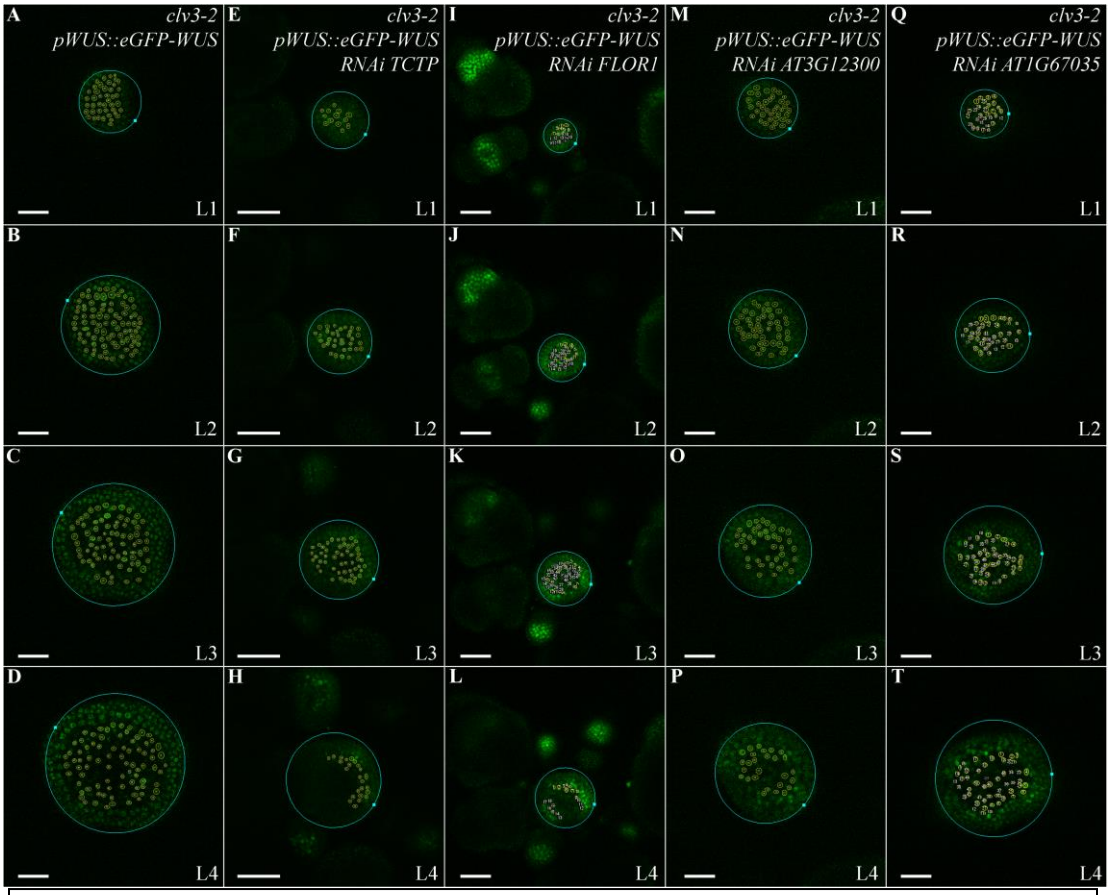

Figure S2.1: Semi-quantitative Analysis of eGFP-WUS and SAM Size in RNAi Lines. Semi-quantitative measurements of eGFP-WUS and SAM size by layer area in clv3-2 (A-D), RNAi TCTP (E-H), RNAi FLOR1 (I-L), RNAi AT3G12300 (M-P), and RNAi AT1G67035 (Q-T). Yellow circles with ROIs represent enclosed nuclei from which relative fluorescence signal was obtained from each SAM layer (L1, L2, L3, and L4), and blue circles represent the enclosed area used to calculate SAM area for each layer (Scale bars=50μm, n=3).

Supplemental Tables

Table S2.1: WUS PPIs Used in RNAi Knockdown Reverse Genetics Screen

AGI ID	Annotation	Cell Type	GO Term Function	Subcellular Localization
AT2G17380	AP19; protein binding / protein transporter	CLV3pKANpFILpL1pWUSpLASpGL2pHMGpS17sATHB8	Cell-Cell Communication and Secretory Pathways	cytosol, mitochondria, nucleus
AT2G20990	ATSYTA_NTMC2T1.1_NTMC2TYPE1.1_SYT1__SYTA (SYNAPTOTAGMIN A), secretory pathway	ND	Cell-Cell Communication and Secretory Pathways	cytosol, ER, extracellular, PM, plastid, vacuole
AT4G28190	ULT1 (ULTRAPETALA1); DNA binding	CLV3pKANpFILpL1pWUSpLASpGL2pHMGpS17sATHB8	Chromatin Remodeling	cytosol, mitochondria, nucleus, plastid
AT5G02710	Unknown protein, Chromatin remodeling related	ND	Unknown Protein	mitochondria, nucleus, plastid
AT2G45640	ATSAP18__SAP18 (SIN3 ASSOCIATED	CLV3pKANpFILpL1pWUSpLASpGL2pHMGpS17sATHB8	Transcription Factor	mitochondria, nucleus, plastid

	POLYPEPTIDE P18); protein binding / transcription regulator			
AT4G26840	ATSUMO1_SUM1_SUMO1__SUMO1 (SMALL UBIQUITIN-LIKE MODIFIER 1); protein binding / protein tag	CLV3pKANpFILpL1pWUSpLASpGL2pHMGpS17sATHB8	Protein Folding and Stability	mitochondria, nucleus
AT3G16640	TCTP (TRANSLATIONALLY CONTROLLED TUMOR PROTEIN), auxin homeostasis, cell growth regulation	CLV3pKANpFILpL1pWUSpLASpGL2pHMGpS17sATHB8	Cell Cycle Regulation	cytosol, nucleus, PM, plastid, vacuole
AT2G16600	ROC3; peptidyl-prolyl cis-trans isomerase,	CLV3pKANpFILpL1pWUSpLASpGL2pHMGpS17sATHB8	Cell Metabolism	cytosol, PM

	secretory pathway			
AT3G29160	ATKIN11_KIN11_SNRK1.2__AKIN11 (Arabidopsis SNF1 kinase homolog 11); protein binding / protein kinase	CLV3pKANpFILpL1pWUSpLASpGL2pHMGpS17sATHB8	Cell Signalling	cytosol, mitochondria, plastid
AT1G70490	ATARFA1D__ARFA1D; GTP binding / phospholipase activator/ protein binding	CLV3pKANpFILpL1pWUSpLASpGL2pHMGpS17sATHB8	Cell Signalling	cytosol, mitochondria, peroxisome, PM
AT4G13520	SMAP1 (SMALL ACIDIC PROTEIN 1), auxin signalling	CLV3pKANpFILpL1pWUSpLASpGL2pHMGpS17sATHB8	Cell Signalling	nucleus, plastid
AT1G13930	Involved in response to salt stress. Knockout mutants are hypersensitive to salt stress.	CLV3pKANpFILpL1pWUSpLASpGL2pHMGpS17sATHB8	Cell Signalling	nucleus, PM, plastid

AT1G66410	ACAM-4__CAM4 (calmodulin 4); calcium ion binding / signal transducer	CLV3pKANpFILpL1pWUSpLASpGL2pHMGpS17sATHB8	Cell Signalling	cytosol, nucleus, PM
AT1G30960	GTP-binding protein (ERG)	CLV3pKANpFILpL1pWUSpLASpGL2pHMGpS17sATHB8	Cell Signalling	cytosol, mitochondria, nucleus, plastid
AT3G12145	FLOR1, leucine rich repeat, interacts directly with MADS domain transcription factor	ND	Cell Signalling	cytosol, nucleus, plastid
AT3G10870	ATMES17__MES17 (METHYL ESTERASE 17); hydrolase/ hydrolase, acting on ester bonds / methyl indole-3-acetate	S17sATHB8	Cell Signalling	golgi, nucleus, plastid

	esterase, signalling (methyl IAA)			
AT4G15030	unknown protein, similarity to kinesin motor family	CLV3pKANpFILpL1pWUSpLASpGL2pHMGpS17sATHB8	Cell-Cell Communication and Secretory Pathways	mitochondria, nucleus
AT4G15930	microtubule motor	CLV3pKANpFILpL1pWUSpLASpGL2pHMGpS17sATHB8	Cell-Cell Communication and Secretory Pathways	cytosol
AT2G21010	C2 domain-containing protein, C2 membrane targeting protein domain	ND	Cell-Cell Communication and Secretory Pathways	cytosol, mitochondria
AT1G34245	EPF2__FUNCTIONS IN: molecular_function unknown; INVOLVED IN: biological_process unknown; LOCATED IN: endomembran	ND	Cell-Cell Communication and Secretory Pathways	cytosol, ER, extracellular, plastid

	e system; EXPRESSED IN: 13 plant structures; EXPRESSED DURING: 9 growth stages; BEST Arabidopsis thaliana protein match is: EPF1 (EPIDERMAL PATTERNING FACTOR 1) (TAIR:AT2G20875.1); Has 12 Blast hits to 12 proteins in 4 species: Archae - 0; Bacteria - 0; Metazoa - 0; Fungi - 0; Plants - 12; Viruses - 0; Other Eukaryotes - 0 (source:			

	NCBI BLink).			
AT1G18250	ATLP-1, Thaumatin, pathogenesis-related:IPR001938(12)	CLV3pKANpFILpL1pWUSpLASpGL2pHMGpS17sATHB8	Defense	ER, extracellular, mitochondria, plastid
AT1G52600	signal peptidase, putative	CLV3pKANpFILpL1pWUSpLASpGL2pHMGpS17sATHB8	Defense	cytosol, ER, mitochondria, PM, plastid
AT1G73620	thaumatin-like protein, putative / pathogenesis-related protein, putative	KANpFILp	Defense	ER, extracellular, mitochondria
AT3G62600	ERDJ3B__ATERDJ3B; heat shock protein binding / unfolded protein binding	CLV3pKANpFILpL1pWUSpLASpGL2pHMGpS17sATHB8	Protein Folding and Stability	cytosol, ER, extracellular, mitochondria, PM
AT5G23290	PFD5__PDF5 (PREFOLDIN 5); unfolded protein binding	CLV3pKANpFILpL1pWUSpLASpGL2pHMGpS17sATHB8	Protein Folding and Stability	extracellular, plastid
AT4G05320	UBQ10	CLV3pKANpFILpL1p	Protein Folding and Stability	cytosol, mitochondria,

	(POLYUBIQUITIN 10); protein binding	WUSpLASpGL2pHMGpS17sATHB8		nucleus
AT5G42190	SKP1B__ASK2 (ARABIDOPSIS SKP1-LIKE 2); protein binding / ubiquitin-protein ligase	CLV3pKANpFILpL1pWUSpLASpGL2pHMGpS17sATHB8	Protein Folding and Stability	cytosol
AT5G49510	PFD3__PDF3 (PREFOLDIN 3); unfolded protein binding	CLV3pKANpFILpL1pWUSpLASpGL2pHMGpS17sATHB8	Protein Folding and Stability	cytosol, nucleus
AT1G01230	ORMDL family protein, protein folding	CLV3pKANpFILpL1pWUSpLASpGL2pHMGpS17sATHB8	Protein Folding and Stability	extracellular, mitochondria, PM
AT2G34860	EDA3 (embryo sac development arrest 3); heat shock protein binding / unfolded protein	CLV3pKANpFILpL1pWUSpLASpGL2pHMGpS17sATHB8	Protein Folding and Stability	nucleus, plastid

	binding			
AT1G17860	trypsin and protease inhibitor family protein / Kunitz family protein	KANpWUSpATHB8	Protein Folding and Stability	cytosol, ER, extracellular
AT5G47590	heat shock protein related, proteolysis, 264AA	ND	Protein Folding and Stability	cytosol, plastid
AT3G04610	FLK (flowering locus KH domain); RNA binding / nucleic acid binding	CLV3pKANpFILpL1pWUSpLASpGL2pHMGpS17sATHB8	RNA Metabolism	cytosol, nucleus, plastid
AT5G02530	RNA and export factor-binding protein, putative	CLV3pKANpFILpL1pWUSpLASpGL2pHMGpS17sATHB8	RNA Metabolism	cytosol, mitochondria, nucleus
AT2G23350	PABP4__PAB4 (POLY(A) BINDING PROTEIN 4); RNA binding / translation initiation	CLV3pKANpFILpL1pWUSpLASpGL2pHMGpS17sATHB8	RNA Metabolism	mitochondria, nucleus, plastid

	factor			
AT1G48410	AGO1 (ARGONAUTE 1); endoribonuclease/ miRNA binding / protein binding / siRNA binding	CLV3pKANpFILpL1pWUSpLASpGL2pHMGpS17sATHB8	RNA Metabolism	cytosol, nucleus
AT2G26460	SMU2__RED family protein, nuclear RNA splicing	CLV3pKANpFILpL1pWUSpLASpGL2pHMGpS17sATHB8	RNA Metabolism	nucleus
AT5G47210	nuclear RNA-binding protein, putative	CLV3pKANpFILpL1pWUSpLASpGL2pHMGpS17sATHB8	RNA Metabolism	nucleus, PM
AT1G17370	UBP1B mRNA 3'-UTR binding	CLV3pKANpFILpL1pWUSpLASpGL2pHMGpS17sATHB8	RNA Metabolism	mitochondria, nucleus
AT4G32730	ATMYB3R-1_ATMYB3R1_MYB3R-1_MYB3R1__PC-MYB1; DNA binding / transcription coactivator/	CLV3pKANpFILpL1pWUSpLASpGL2pHMGpS17sATHB8	Transcription Factor	nucleus, peroxisome, PM

	transcription factor			
AT4G04780	MED21 (MEDIATOR 21), Encodes the med21 subunit of the mediator complex which is involved in transcriptional regulation	ND	Transcription Factor	cytosol, plastid
AT3G55770	LIM domain-containing protein, FUNCTIONS IN: zinc ion binding	CLV3pKANpFILpL1pWUSpLASpGL2pHMGpS17sATHB8	Unknown Protein	mitochondria, nucleus
AT3G10730	ATSUN2_SUN2__sad1/unc-84-like 2 family protein	CLV3pKANpFILpL1pWUSpLASpGL2pHMGpS17sATHB8	Unknown Protein	cytoskeleton, ER, mitochondria, nucleus, plastid
AT3G18215	unknown protein, 244AA	CLV3pKANpFILpL1pWUSpLASpGL2pHMGpS17sATHB8	Unknown Protein	ER, extracellular, PM
AT5G14030	translocon-associated protein beta (TRAPB) family	CLV3pKANpFILpL1pWUSpLASpGL2pHMGpS17sATHB8	Unknown Protein	ER, extracellular, mitochondria, PM, vacuole

	protein, 195AA			
AT3G12300	unknown protein, 190AA	CLV3pKANpFILpL1pWUSpLASpGL2pHMGpS17sATHB8	Unknown Protein	extracellular, mitochondria, nucleus
AT5G08060	unknown protein	CLV3pKANpFILpL1pWUSpLASpGL2pHMGpS17sATHB8	Unknown Protein	mitochondria, nucleus, plastid
AT1G11120	unknown protein	CLV3pKANpFILpL1pWUSpLASpGL2pHMGpS17sATHB8	Unknown Protein	mitochondria, nucleus, plastid
AT3G07350	unknown protein	CLV3pKANpFILpL1pWUSpLASpGL2pHMGpS17sATHB8	Unknown Protein	nucleus
AT3G15450	unknown protein	CLV3pKANpFILpL1pWUSpLASpGL2pHMGpS17sATHB8	Unknown Protein	extracellular, mitochondria, nucleus, peroxisome
AT1G67035	unknown protein, 190AA	CLV3pLASp	Unknown Protein	mitochondria, nucleus
AT5G48500	unknown protein	FILpWUSpHMGp	Unknown Protein	cytosol, extracellular, plastid
AT1G21830	unknown protein	KANpFILpL1pWUSpLASpGL2pS17sATHB8	Unknown Protein	cytosol, mitochondria, nucleus, plastid
AT2G25510	unknown protein	L1p	Unknown Protein	ER, extracellular, mitochondria, nucleus, plastid
AT3G50580	unknown protein	ND	Unknown Protein	ER, extracellular, nucleus

AT5G41980	unknown protein, 374AA	ND	Unknown Protein	cytosol
AT3G51590	LTP12 (LIPID TRANSFER PROTEIN 12); lipid binding	ND	Cell-Cell Communication and Secretory Pathways	cell wall, ER, golgi, nucleus, plastid
AT2G33880	WUSCHEL-RELATED HOMEOBOX 9 (WOX9), STIMPY		Transcription Factor	mitochondria, nucleus, plastid
AT4G00180	YAB3 (YABBY3); protein binding / transcription factor	FILpL1p	Transcription Factor	mitochondria, nucleus, plastid
AT2G38880	ATHAP3_ATNF-YB1_HAP3_HAP3A__NF-YB1 (NUCLEAR FACTOR Y, SUBUNIT B1); transcription factor	CLV3pKANpFILpL1pWUSpLASpGL2pHMGpS17sATHB8	Transcription Factor	nucleus

AT5G23090	NF-YB13 (NUCLEAR FACTOR Y, SUBUNIT B13); transcription factor	CLV3pKANpFILpL1pWUSpLASpGL2pHMGpS17sATHB8	Transcription Factor	cytosol, nucleus, plastid
AT1G54830	NF-YC3 (NUCLEAR FACTOR Y, SUBUNIT C3); DNA binding / transcription factor	CLV3pKANpFILpL1pWUSpLASpGL2pHMGpS17sATHB8	Transcription Factor	nucleus, plastid

Table S2.2: Primers

Primer Name	Primer Sequence
pU104 35S	CTATCCTTCGCAAGACCCTTCC
pU517-WRKYi-down	TCGGAAGTGATAAAGTTATGGGTCAACGGT
pU518-WRKYi-up	ACCGTTGACCCATAACTTTATCACTTCCGA
Rv59 M13reverse	CAGGAAACAGCTATGACCATGATTAC
AT2G16600GATE-F	CACCATGGCAACAAACCCTAAAGTCTAC
AT2G16600GATE-R	CTAAGAAATCTGACCACAATCAG
AT3G29160GATE-F	CACCATGGATCATTCATCAAATAGATTTG
AT3G29160GATE-R	TCAGATCACACGAAGCTCTGTAAG
AT1G70490GATE-F	CACCATGGGGTTGAGTTTCGCCAAGC
AT1G70490GATE-R	TCATGCCTTGCCAGCGATGTTG
AT4G13520GATE-F	CACCATGAGGCCGATGCAGCTGG
AT4G13520GATE-R	TTAGTTGATATCGGTGTCATC
AT1G13930GATE-F	CACCATGAATTTCATCTCCGATCAGG
AT1G13930GATE-R	TCACTTCAAGAAACCTTGAGCC
AT1G66410GATE-F	CACCATGGCGGATCAGCTAACTGATG
AT1G66410GATE-R	TCACTTAGCCATCATAATCTTGAC
AT1G30960GATE-F	CACCATGAAAGCTTTTAGATCTCTACG
AT1G30960GATE-R	TCACTTGAGCTTAACCTGGAGAATG
AT3G12145GATE-F	CACCATGAAGCTCTTTGTTCATCTC
AT3G12145GATE-R	TTAACAAGCCTTAAGGGGAGTTCC
AT3G10870GATE-F	CACCATGGCGGAGGAGAATCAAGAAG
AT3G10870GATE-R	TTAGATAGAACCGACGGAAACG
AT4G15030GATE-F	CACCATGACTTCTTCGGCGGCGATC
AT4G15030GATE-R	TCACCCATTACCCGGGAACATCC
AT4G15930GATE-2F	CACCATGAGTGACGGGAGGAGGAAG
AT4G15930GATE-2R	TTAACCCGACTTGAAGAGCAGCAC
AT2G21010GATE-F	CACCATGGGCATGATAAATCCATACG
AT2G21010GATE-R	TCAAAAGGCAGTTTGCCAGTCAAGC
AT1G34245GATE-F	CACCATGACGAAGTTTGTACGCAAG
AT1G34245GATE-R	TCAAGCTCTAGATGGCACGTG
AT1G18250GATE-F	CACCATGGCTTCAATCAACCTCTTCC
AT1G18250GATE-R	TTAATGGCGATGATGAGGGCAAAAG
AT1G52600GATE-F	CACCATGGGTTGGATCGGAGAAACTG
AT1G52600GATE-R	TCAATCCTTTGACGTTATAACG

AT1G73620GATE-F	CACCATGACCAATGAGAAATGTGAAG
AT1G73620GATE-R	TCAACGGCCGCGGTGAGGGC
AT3G62600GATE-F	CACCATGGCGATTCGGTGGTCGGAGCTG
AT3G62600GATE-R	CTAAGCAAAGACTTCTTTAATCTTC
AT5G23290GATE-F	CACCATGGCGTCGTCATCATCGAGAG
AT5G23290GATE-R	TCACGACGTGGTTGCAGCTGTTAAC
AT4G05320GATE-F	CACCATGCAGATCTTTGTTAAGACTC
AT4G05320GATE-R	TTAGAAACCACCACGAAGACGCAG
AT5G42190GATE-F	CACCATGTCGACGGTGAGAAAAATCAC
AT5G42190GATE-R	TCATTCAAACGCCCACTGATTCTCAC
AT5G49510GATE-F	CACCATGTCGTCGTCTTCTCCGAGTG
AT5G49510GATE-R	TCATGAATCTGCAACAGCAATAG
AT1G01230GATE-F	CACCATGGCGAATCTGTATGTGAAAGC
AT1G01230GATE-R	TTATTTATCACCATTGATACCAAAG
AT2G34860GATE-F	CACCATGGCGGCATCATCATCTCATCTC
AT2G34860GATE-R	TCATGAATCAGGAAGAAGCCGAC
AT1G17860 5’ CDS Gateway	CACCATGTCATCACTTCTCTATATCTTC
AT1G17860 3’ CDS	CTAGTATGCTCTTTTGAACATAAC
AT5G47590 5’ CDS Gateway	CACCATGGGTGAGACAAAGGCAGATTTC
AT5G47590 3’ CDS	TCATTCAATAGGGTTTCTTTTGTTGTTGATG
AT3G04610 5’ CDS Gateway	CACCATGGCTGAAGCTGAAGATCAGC
AT3G04610 3’ CDS	TCAGTAACCGTAGCCTGAGCTG
AT5G02530 5’ CDS Gateway	CACCATGTCAGGTGGCTTAGATATGTC
AT5G02530 3’ CDS	CTAACTTGTTTCCATTGCCTCTTTG
AT2G23350 5’ CDS Gateway	CACCATGGCTCAGGTTCAAGCTCCTTC
AT2G23350 3’ CDS	TCATAAATGATCATTGATGGAAAG
AT1G48410 5’ CDS Gateway	CACCATGGTGAGAAAGAGAAGAACGG
AT1G48410 3’ CDS	TCAGCAGTAGAACATGACACGC
AT2G26460 5’ CDS Gateway	CACCATGAAACCTTCAAAATCGCATC
AT2G26460 3’ CDS	TCAATGCTTGGATCTCTTAGGAG
AT5G47210 5’ CDS Gateway	CACCATGGCGTCTTTGAACCCTTTCG
AT5G47210 3’ CDS	CTAGCCCAACGAAGGGAACTGAG
AT1G17370 5’ CDS Gateway	CACCATGCAGAGGTTGAAGCAGCAGC

AT1G17370 3’ CDS	TTACTGGTAGTACATGAGCTGC
AT4G32730 5’ CDS Gateway	CACCATGAAGCGTGAGATGAAAGCAC
AT4G32730 3’ CDS	CTATCTGCAACTCTTCAAAAGG
AT4G04780 5’ CDS Gateway	CACCATGGATATAATCTCACAGTTGC
AT4G04780 3’ CDS	TCATTCAGGTTTCTTCATGTTCAGG
AT3G55770 5’ CDS Gateway	CACCATGTCTTTTACAGGAACTCAAC
AT3G55770 3’ CDS	TTAAGATTCAGGAACGGAGGCTG
AT3G10730 5’ CDS Gateway	CACCATGTCGGCGTCAACGGTGTCAATC
AT3G10730 3’ CDS	TCAAGCATGAGCAACAGAGACTG
AT3G18215 5’ CDS Gateway	CACCATGTGGACGGAGGAATCTTTGG
AT3G18215 3’ CDS	CTACAGAGTATGAACAGCTGATTC
AT5G14030 5’ CDS Gateway	CACCATGGCCGTCGCTGTAGCTAAGC
AT5G14030 3’ CDS	TTAACGCTTCTTCTTGCTGCTTGCC
AT3G12300 5’ CDS Gateway	CACCATGTTCAAGAACACGTTTCAATC
AT3G12300 3’ CDS	TCATGCTTTCTGCACTGGGAGATAC
AT5G08060 5’ CDS Gateway	CACCATGGCGAAATCAGTGTCGACGG
AT5G08060 3’ CDS	TTATTTCTCGTAGCCTCCACCAC
AT1G11120 5’ CDS Gateway	CACCATGAGAGACCTTGAGCACTTAAAG
AT1G11120 3’ CDS	TCAACATTCTTGAATGGAGTTTGAGC
AT3G07350 5’ CDS Gateway	CACCATGGGTTTCTCTAGAGCAAAAC
AT3G07350 3’ CDS	TTATCGTGTTCGCACAAATAGAC
AT3G15450 5’ CDS Gateway	CACCATGTTGGCAATATTTCAGAAAG
AT3G15450 3’ CDS	TCAACGAGAATTAGCCAGCGCC
AT1G67035 5’ CDS Gateway	CACCATGAAGGATACAATCTCAAACC
AT1G67035 3’ CDS	TCAATAAATTTGTCTGTAACCTAG
AT5G48500 5’ CDS Gateway	CACCATGGACTACGAATACGGAGGAG
AT5G48500 3’ CDS	TCAAAGCACCCGTGTTGGCAAAAAAC
AT1G21830 5’ CDS Gateway	CACCATGGATATGTACAAAGATGATAG

AT1G21830 3’ CDS	TCAACTTTTACTTTTCCTGGATTTTTTTC
AT2G25510 5’ CDS Gateway	CACCATGATGCACGCTTTACTATTCC
AT2G25510 3’ CDS	TTATTTATTATAGCGGCCGTTCGAC
AT3G50580 5’ CDS Gateway	CACCATGAAAACCTCCATCGTGCTTG
AT3G50580 3’ CDS	CTAGCAGGTGACATGGCAAGTG
AT5G41980 5’ CDS Gateway	CACCATGGAGATCTCCGGCGAAGAAG
AT5G41980 3’ CDS	TTAGAAGGTTGACATATTTTGGAC
AT3G51590 5’ CDS Gateway	CACCATGGCGTTTACTCCGAAGATCATC
AT3G51590 3’ CDS	TCACACGGCAGTCGATATACTG
AT1G54830-GATE-F	CACCATGGATCAACAAGGACAATCATC
AT1G54830-GATE-R	CTAATTGTCAGGATCCTGCTGCTCAGG
AT2G33880-GATE-F	CACCATGGCTTCTTCGAATAGACACTG
AT2G33880-GATE-R	CTAGATCAGATAGTACGAGGCTCC
AT2G38880-GATE-F	CACCATGGCGGATACGCCTTCGAGCCC
AT2G38880-GATE-R	TTACCAGCTCGGCATTTCTTCACCAG
AT4G00180-GATE-F	CACCATGTCGAGCATGTCCATGTCGTCC
AT4G00180-GATE-R	CTAGTTATGGGCCACCCCAACGTTGGC
AT5G23090-GATE-F	CACCATGGATCCAATGGATATAGTCGGC
AT5G23090-GATE-R	TTAGCTTTGCGGACTTCTCTGGTCAG
AP19 Gateway 5' CDS	CACCATGATACATTTCGTGTTACT
AP19 REV XMA1	CCCGGGCTTGGTAGCCTGAGCAATT
P2:18 Gateway 5' CDS	CACCATGGATATGTCGCTTGCGTT
P2:18 REV XMA1	CCCGGGACTCGAGCTCGGATTACT
SAP18 Gateway 5' CDS	CACCATGGCTGAAGCAGCGAGAAG
SAP18 REV XMA1	CCCGGGGTAAATTGCCACATCCAG
SUMO Gateway 5' CDS	CACCATGTCTGCAAACCAGGAGG
SUMO REV XMA1	CCCGGGGGCCGTAGCACCACCAC
SYT1 Gateway 5' CDS	CACCATGGGCTTTTTCAGTACGAT
SYT1 REV XMA1	CCCGGGAGAGGCAGTTCGCCACTCGAGC
TCTP Gateway 5' CDS	CACCATGTTGGTGTACCAAGATC
TCTP REV XMA1	CCCGGGGCACTTGACCTCCTTCAA
ULT1 Gateway 5' CDS	CACCATGGCGAACAATGAGGGAG
ULT1 REV XMA1	CCCGGGAGCTTTGACATTGCTGG

Chapter 3: Biochemical and Genetic Analysis of the WUS-SUMO1/SUMO2 Interaction Reveals a Role for SUMO1/SUMO2 in WUS-Mediated SAM Maintenance

Introduction

The identification of functionally relevant WUS PPIs from the reverse genetics screen provided targets such as TCTP, FLOR1, AT3G12300, and AT1G67035 to focus future research on. However, the previously discussed likelihood of false negatives from the screen due to incomplete knockdown of targets and redundancy of protein family members still leaves some interesting targets that were not identified as having strong phenotypic effects. Many of these uncharacterized targets have been previously shown to regulate transcriptional activity, subcellular localization, protein stability, and protein complex assembly through post-translational mechanisms. One such WUS PPI target that encompasses all of these relevant functions is SUMO1, a small 100AA protein that is present in all eukaryotic organisms (Saracco et al., 2007).

SUMO1 is a member of an eight gene family in *A. thaliana*, of which seven are expressed in various cell types throughout the plant (Kurepa et al., 2003, Okada et al., 2009). Prior analysis of SUMO proteins has revealed two main mechanisms of action, the first of which consists of covalent conjugation to a lysine (K) residue on the target protein in a process known as SUMOylation (Rodriguez et al., 2001, Kurepa et al., 2003, Miura et al., 2007, Saracco et al., 2007). This process is similar to the ubiquitin conjugation system in that an E1/E2/E3 enzyme relay is required for covalent attachment of SUMO to the target protein (Kurepa et al., 2003). In *A. thaliana*, the three E1 ligases SUMO-

ACTIVATING ENZYME (SAE1a/SAE1b/SAE2) form a complex to link the mature SUMO with an exposed C-terminal diglycine [GG] motif to a cysteine [C] residue on the E1 (Kurepa et al., 2003, Saracco et al., 2007). Then SUMO is transferred to a cysteine [C] on the SUMO-CONJUGATING ENZYME1 (SCE1) E2 ligase through a transesterification reaction (Miura et al., 2007, Saracco et al., 2007). Finally, the SUMO is transferred via the E3 ligases SAP and MIZ (SIZ1)/HIGH PLOIDY2 (HPY2) to a target lysine [K] in the consensus Ψ-K-X-[E/D] motif, where Ψ is a large hydrophobic residue and X is any residue (Rodriguez et al., 2001, Muira et al., 2007a, Saracco et al., 2007, Huang et al., 2009, Ishida et al., 2009).

The second and much less characterized mechanism for SUMO function is through traditional non-covalent protein-protein interactions (Hecker et al., 2006, Elrouby et al., 2013). Several SUMO Interacting Motifs (SIMs) have been identified, including [V/I]-X-[V/I]-[V/I] in human RanBP2/Nup358, I-I-V-L-S-D-S-D in human Daxx, an S-X-S motif with a N-terminal stretch of hydrophobic residues and a C-terminal stretch of acidic residues, and a K-$X_{(3-5)}$-[I/V]-[I/L]-[I/L]-X_3-[D/E/Q/N]-[D/E]-[D/E] motif (Minty et al., 2000, Song et al., 2004, Hannich et al., 2005, Hecker et al., 2006, Elrouby et al., 2013). While these identified motifs have large variations in structure and length, the overall consensus of these motifs consists of a stretch of hydrophobic residues followed by a stretch of acidic residues.

The combination of these two mechanisms to drive SUMO-mediated post-translational regulation of target protein function facilitates a diverse set of niches for SUMO to occupy. Regulation of a target protein's transcriptional ability is a significant

role of SUMO that is of obvious relevance to WUS as a stem cell maintaining transcription factor (Mayer et al., 1998, Chupreta et al., 2005, Miura et al., 2007, Bauer et al., 2010, Miller et al., 2010, Mazur and van den Burg, 2012). A subset of six histone and DNA methyltransferases have also been shown to interact with SUMO, suggesting a link between SUMO and chromatin remodeling (Elrouby et al., 2013). Another important function of SUMO is the regulation of subcellular localization, particularly nuclear import and accumulation (Saracco et al., 2007, Mazur and van den Burg, 2012). A potentially relevant function of SUMO also includes the regulation of cytokinin signaling, which is suppressed in null mutants of the HPY2 E3 ligase (Huang et al., 2009). Other SUMO functions with less direct significance to WUS-mediated SAM maintenance include plant defense and stress processes (van den Burg et al., 2010, Marzur and van den Burg 2012).

While the diversity of SUMO family member functions suggest that they are an important factor in plant development and vitality, the only known phenotype for a single allele was a short day late flowering phenotype that was identified in *sumo3-1* null allele *A. thaliana* (Saracco et al., 2007, van den Burg et al., 2010). However, the presence of either SUMO1/SUMO2 is essential for plant development as the *sumo1-1, sumo2-1* null allele double mutant is embryonic lethal (Saracco et al., 2007, van den Burg et al., 2010). This suggests a functional redundancy between SUMO1/SUMO2, which is further supported by their overlapping expression domains (van den Burg et al., 2010). To subvert this problem and analyze the effects of SUMO1/SUMO2 on plant development, a plant with the *sumo1-1* null allele was transformed with a *p35S::amiRSUMO2* construct

to generate a knockdown line for both SUMO1/SUMO2 (*sumo1/2*) that produced viable plants (van den Burg et al., 2010). These plants showed pleiotropic effects, exhibiting partial sterility, phyllotaxy defects, loss of apical dominance, severe dwarfism, early senescence, and rosette leaf curling (van den Burg et al., 2010). Many of these effects are highly correlated to stem cell maintenance in the SAM, and along with the identification of SUMO1 as a WUS PPI provide a clear basis for determining the role of SUMO1/SUMO2 in WUS-mediate SAM maintenance.

The following work presents an analysis of SUMO1/SUMO2 effects on WUS accumulation and spread in the SAM. The region of SUMO1/SUMO2 interaction on the WUS protein is mapped via Y2H experiments, and the subcellular localization of these interactions is demonstrated using BiFC and Co-IP experiments. Finally, analysis of the WUS-mediated regulation of *CLV3* reveals a SUMO1/SUMO2 dependent mechanism involved in the perception and transcriptional regulation of *CLV3* by WUS.

Results

WUS Interacts with Both SUMO1/SUMO2 Across a Stretch of Residues Including the Acidic Motif and WUS-Box

SUMO1/SUMO2 have many diverse functions and are present across all eukaryotic taxa, therefore it is important to understand their relevance in WUS-mediated SAM maintenance (Kurepa et al., 2003, Dohmen 2004, Geiss-Friedlander and Melchior, 2007). The initial step in this analysis was determining the critical motifs on WUS that are necessary for SUMO1/SUMO2 interaction. WUS is made up of many motifs that regulate its many functions. Moving from the WUS N-terminus to the C-terminus, the

first critical domain is the DNA-binding homeodomain located between AA34 and AA102, which is essential for DNA binding and WUS transcription factor activity (Figure 3.1A) (Mayer et al., 1998, Ikeda et al., 2009, Busch et al., 2010, Yadav et al., 2011). The next important motif is the WUS homodimerization motif between AA134 and AA208, which is important for the modulation of WUS mobility in the SAM and formation of homodimeric complexes (Figure 3.1A) (Daum et al., 2014, unpublished data). The next motif between AA234 and AA246 is the Acidic motif, a less well characterized motif that nonetheless is important for modulating WUS transcriptional activity and the function of the C-terminal motifs that follow (Figure 3.1A) (Ikeda et al., 2009). The WUS-Box motif is a short stretch between AA253 and AA261 that in tandem with the EAR-Like motif between AA285 and AA292 is critical in regulating transcriptional repression activity for WUS target genes (Figure 3.1A) (Ikeda et al., 2009). Interestingly, analysis of WUS accumulation patterns with mutations in the WUS-Box and EAR-Like motifs reveal that they are also responsible for nuclear retention and nuclear export, respectively (unpublished data).

Using SUMOylation and SIM sequence prediction software GPS-SUMO 1.0, no strong SUMOylation sites were found in WUS, and only one predicted SIM sequence was identified from WUS46-50 (Table S3.1) (Ren et al., 2009, Zhao et al., 2014). Reducing the stringency of the software to pick up all potential sites reveals 13 putative weak SUMOylation sites and two additional weak SIM sites at WUS143-147 and WUS287-291 (Table S3.1) (Ren et al., 2009, Zhao et al., 2014).

In order to understand the relevance of the WUS-SUMO1/SUMO2 interaction, we created a series of deletions and mutations within WUS that allowed us to map the interactions and determine the critical regions for WUS-SUMO1/SUMO2 interaction. The interaction of each of these WUS variants with SUMO1/SUMO2 was determined through Y2H serial dilutions of 1x, 10^{-1}x, 10^{-2}x, and 10^{-3}x in order to compare the relative strength of interaction and identify the most critical WUS domains for WUS-SUMO1/SUMO2 interaction (Figure 3.1A) (Fields and Song, 1989, Gietz et al., 1997). All interactions were plated on SD-(L/W) yeast nutrient media lacking the essential amino acids L and W after an OD_{600} measurement of 0.4 to ensure that the basal growth was equal (Figure S3.1A-S3.1D) (Gietz et al., 1997). These same initial and serial dilutions were used for the selective experiment on SD-(L/W/H/A) yeast nutrient media lacking the essential amino acids L, W, H, and A to analyze each interaction, which was graded as either negative or Level 1-4 based on the number of serial dilutions for which positive growth was observed (Hirst et al., 2001).

In the negative control interaction with AD Empty, level 1 transactivation was seen in WUS1-253 and WUS1-292 Acidic Motif Mutation (AMM) (Figure 3.1B). Level 3 transactivation was seen in WUS1-292 WUS-Box Mutation (WBM), and level 4 transactivation was seen in WUS134-292, WUS1-292 EAR-Like Motif Mutation (EARM), WUS134-292 WBM, and WUS134-292 EARM (Figure 3.1B). For the interaction analysis with SUMO1, level 1 interaction was shown for WUS250-285, WUS1-292 WBM, and WUS134-292 AMM (Figure 3.1C). Level 3 interaction was

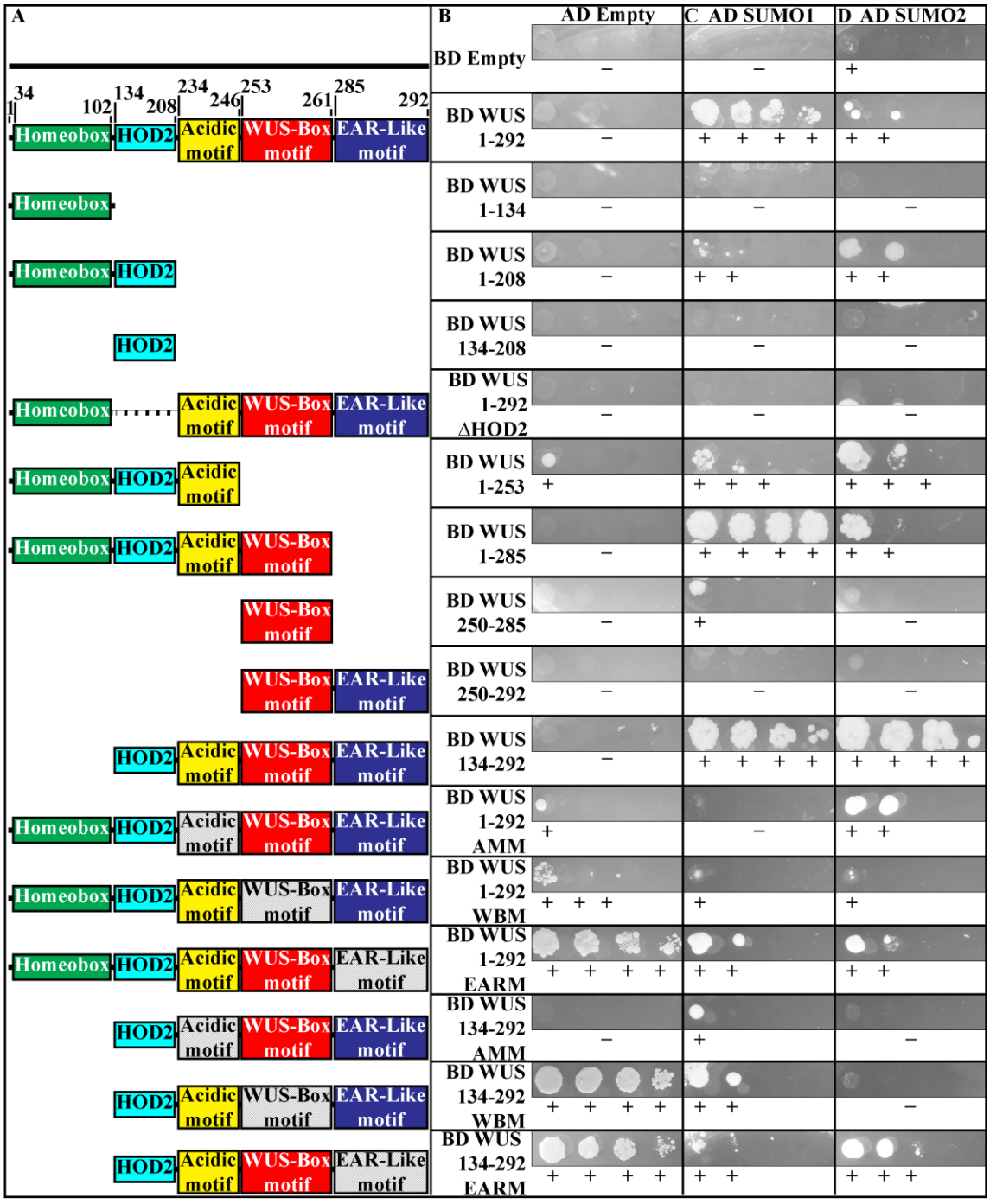
A
34
102
134
208
234
246
253
261
285
292
Homeobox
HOD2
Acidic motif
WUS-Box motif
EAR-Like motif
B
AD Empty
C AD SUMO1
D AD SUMO2
BD Empty
BD WUS 1-292
BD WUS 1-134
BD WUS 1-208
BD WUS 134-208
BD WUS 1-292 ΔHOD2
BD WUS 1-253
BD WUS 1-285
BD WUS 250-285
BD WUS 250-292
BD WUS 134-292
BD WUS 1-292 AMM
BD WUS 1-292 WBM
BD WUS 1-292 EARM
BD WUS 134-292 AMM
BD WUS 134-292 WBM
BD WUS 134-292 EARM

Figure 3.1: Selective Mapping the Interaction Region of WUS and SUMO1/SUMO2. Each of the WUS truncation and mutation constructs is diagramed (A) with including the amino acid boundaries of the following domains: Homeobox, HOD2 homodimerization domain, Acidic motif, WUS-Box motif, and EAR-Like motif. Mutated domains are marked with grey hashed boxes and annotated as AMM (Acidic motif mutant), WBM (WUS-Box mutant), and EARM (EAR-Like motif mutant). Yeast two-hybrid 10-fold serial dilution analysis of each WUS truncation and mutation construct interaction with and empty control vector (B), SUMO1 (C), and SUMO2 (D). Plus signs show the strength of interaction based on the number of serial dilutions for which positive interaction growth is present, while minus signs represent no positive interaction.

shown for WUS1-253, and level 4 interaction was shown for WUS1-292, WUS1-285, and WUS134-292 (Figure 3.1C). For the interaction analysis with SUMO2, level 1 interaction was shown for BD Empty and WUS1-292 WBM (Figure 3.1D). Level 2 interaction was shown for WUS1-292, WUS1-208, WUS1-285, WUS1-292 AMM, and WUS1-292 EARM (Figure 3.1D). Level 3 interaction was shown for WUS1-253 and WUS134-292 EARM, and level 4 interaction was shown for WUS134-292 (Figure 3.1D). Nearly all interactions present in the WUS-SUMO1 were also present in WUS-SUMO2, however the majority of these shared interactions were weaker or absent in SUMO2. The only interaction shared between these two groups that was stronger in WUS-SUMO2 was the WUS1-292 AMM interaction (Figure 3.1D). Comparative analysis of these interaction levels revealed that the region from WUS134-253 containing the WUS Homodimerization Motif and the Acidic Motif is critical for SUMO1/SUMO2 interaction. This interaction was enhanced in SUMO1 with the inclusion of the region between AA253 and AA285 containing the WUS-Box motif (Figure 3.1A-3.1D).

WUS Interacts with Both SUMO1/SUMO2 in the Nuclei and Cytosol of *N. benthamiana* Epidermal Cells and in the Nuclei of *A. thaliana* SAM Cells

The next step in analysis of the WUS-SUMO1/SUMO2 interaction was to demonstrate the presence of this interaction *in planta*. First, eGFP fusions to WUS, SUMO1, and SUMO2 were expressed in *N. benthamiana* epidermal cells under control of the *2xCaMV 35S* promoter (*p2x35S*) (Walter et al., 2004, Kerppola, 2008). This resulted in nuclear and cytosolic accumulation for all three constructs, although the levels of eGFP-SUMO1/eGFP-SUMO2 accumulation were much higher than that of eGFP-

WUS (Figure 3.2A-3.2F). Next, the N-terminal eGFP translational fusion with WUS (NeGFP-WUS) as used in Chapter 1 was co-expressed with C-terminal eGFP translational fusions with SUMO1/SUMO2 to visualize the WUS-SUMO1/SUMO2 interactions via BiFC (Figure 3.2G-3.2L). Interactions with NeGFP-WUS/CeGFP-WUS, NeGFP-WUS/CeGFP-SUMO1, and NeGFP-WUS/CeGFP-SUMO2 were all most strongly present in the nuclei, however weak signal in the cytosol suggested that some minimal amount of interaction was present there.

Another method to show *in planta* interaction in addition to BiFC is Co-IP (Isono and Schwechheimer, 2010). Using isolated nuclei from *clv3-2 pWUS::eGFP-WUS* SAMs and WUS antibodies as demonstrated previously, a commercial SUMO1/SUMO2 antibody was used for immunoprecipitation (Yadav et al., 2011). The isolated proteins were fractionated and detected by Western blotting, using both SUMO1/SUMO2 and WUS antibodies, with SUMO1/SUMO2 detected in all fractions and WUS detected in the immunoprecipitation fraction (Figure 3.2M-3.2N). This method also confirms that the interaction of WUS and SUMO1/SUMO2 occurs in SAM tissue.

sumo1/2 Knockdown Lines Result in Reduced WUS Accumulation in Distal Layers of the SAM and Increased Accumulation in the RM

After the WUS interaction region with SUMO1/SUMO2 was mapped and the interaction shown to occur *in planta*, the next step was to characterize the phenotypic effects of SUMO1/SUMO2 on WUS in order to understand their significance in WUS-mediated SAM maintenance. The previously generated *sumo1/2* knockdown lines result in many pleiotropic developmental defects, including improper phyllotaxy, loss of apical

dominance, partial sterility, curled leaves, and early senescence; they also provide an excellent background to analyze WUS without functional SUMO1/SUMO2 (Figure 3.3A-3.3D) (van den Burg et al., 2010).

The first step in this genetic analysis was to understand the effects of SUMO1/SUMO2 on WUS itself. To facilitate this effort, a series of previously generated WUS mutations and deletions translationally fused to eGFP were used to characterize the effects of *sumo1/2* on WUS accumulation in the SAM (unpublished data). To control for potential *sumo1/2* interference on general protein mobility and nuclear accumulation in the SAM, controls of *pWUS::eGFP* and a nuclear localization signal (NLS) tagged *pWUS::NLS-eGFP* were imaged in *Wt* and *sumo1/2* lines (Figure S3.3A-S3.3P). These accumulated eGFP throughout the SAM and showed no discernable effect on the mobility and nuclear accumulation of eGFP, thus demonstrating that any changes in WUS mobility or subcellular distribution in the SAM of *sumo1/2* plants are specific to WUS. The following constructs were introduced into *sumo1/2* lines and analyzed for changes in WUS mobility and accumulation: *pWUS::eGFP-WUS*, *pWUS::eGFP-WUS WBM*, *pWUS::eGFP-WUS EARM*, *pWUS::eGFP-WUS WBM/EARM*, and *pWUS::eGFP-WUS229-292* (Figures S3.3Q-S3.3FF, 3.4A-3.4X) (unpublished data).

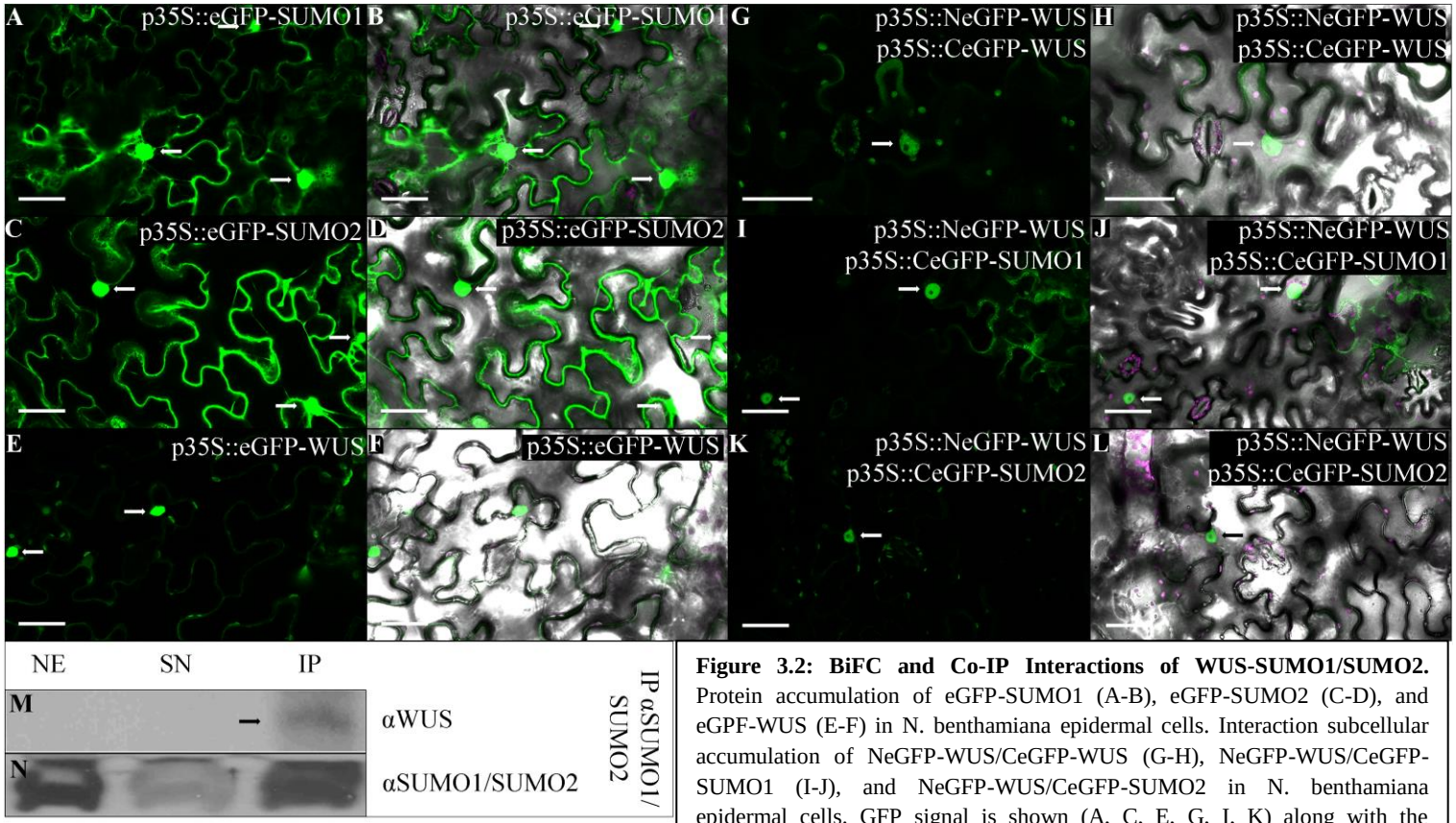

Figure 3.2: BiFC and Co-IP Interactions of WUS-SUMO1/SUMO2. Protein accumulation of eGFP-SUMO1 (A-B), eGFP-SUMO2 (C-D), and eGPF-WUS (E-F) in N. benthamiana epidermal cells. Interaction subcellular accumulation of NeGFP-WUS/CeGFP-WUS (G-H), NeGFP-WUS/CeGFP-SUMO1 (I-J), and NeGFP-WUS/CeGFP-SUMO2 in N. benthamiana epidermal cells. GFP signal is shown (A, C, E, G, I, K) along with the GFP/DIC overlay (B, D, F, H, J, L). Arrows show nuclear accumulation of the protein and interaction complexes. The Co-IP experiment using proteins immunoprecipitated with αSUMO1/SUMO2 from *clv3-2 pWUS::eGFP-WUS* SAMs and Western blot detection of αWUS (M) and αSUMO1/SUMO2 (N) in nuclear extract (NE), supernatant (SN), and immunoprecipitation fractions (IP). Arrow in (M) shows αWUS detection in the IP fraction. (Scale bars=50μm).

The *sumo1/2* lines with *pWUS::eGFP-WUS WBM* showed no perceptible change in WUS accumulation and spread; the WUS WBM cytosolic accumulation and further spread throughout the SAM was observed in both *Wt* and *sumo1/2* lines (Figure S3.3Q-S3.3U). Additionally, the *sumo1/2* lines with *pWUS::eGFP-WUS WBM/EARM* were nuclear enriched with some cytosolic accumulation in all layers, with higher accumulation in the RM of SAMs in both *Wt* and *sumo1/2* lines (Figure S3.3Y-S3.3FF). The *sumo1/2* lines with *pWUS::eGFP-WUS* in both inflorescence and vegetative phases retained the enriched nuclear accumulation as in *Wt* yet showed a strong change in the levels of WUS accumulation in each layer of the SAM ranging from a close to three-fold drop in relative accumulation in the L1 all the way to a four-fold drop in the L3 layer (Figures 3.4A-3.4H, 3.5A-3.5E). The *Wt* and *sumo1/2* lines with *pWUS::eGFP-WUS229-292* retained

Figure 3.3: Phenotypes of *sumo1/2* Plants. *Wt Col* plants have normal phylotaxy and fully developed siliques (A-B). *sumo1/2* plants are smaller, have irregular phylotaxy (white arrows), exhibit partial sterility (black arrows) and early senecence (C-D). (Scale bars=5mm).

low relative accumulation across all layers, however the nuclear accumulation was slightly enriched in *Wt* lines (Figures 3.4I-3.4P, 3.5E). Finally, the *Wt pWUS::eGFP-WUS EARM* lines retained nuclear accumulation and accumulation across all levels with higher relative accumulation in the SAM, while *sumo1/2* lines had reduced nuclear accumulation across the L1, L2, and L4 layers, with slightly higher relative accumulation in the L3 layer (Figures 3.4Q-3.4X, 3.5E). To demonstrate that these effects on WUS accumulation were on the protein and not the transcript, semi-quantitative RT-PCR was used to examine WUS transcript accumulation. No significant difference in *WUS* accumulation between *Wt* and *sumo1/2* SAMs relative to the *TUB2* housekeeping gene was observed (Figure S3.4A). Additionally, the area of each layer in the SAM was reduced in *sumo1/2* lines in comparison to the *Wt* (Figures 3.5F, S3.5A-S3.5X).

In all, this information shows that all variants with WBM present are not sensitive to *sumo1/2*, while other WUS variants result in reduced WUS accumulation in the SAMs of *sumo1/2* lines. Taken together with the WUS-SUMO1/SUMO2 Y2H mapping data, the significance of WUS-SUMO1/SUMO2 interaction over the WBM is represented by reduced WUS accumulation in the SAM.

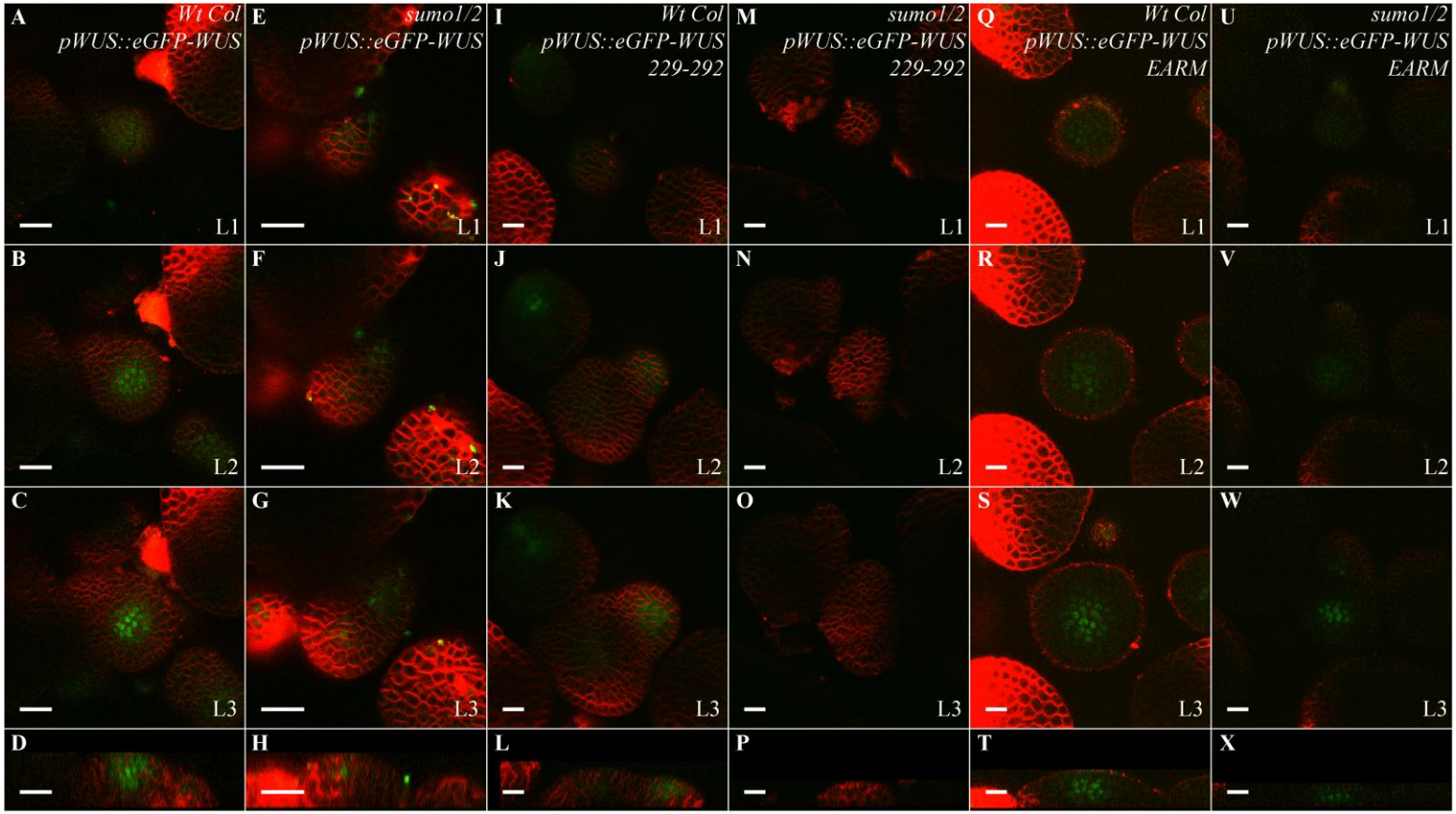

Figure 3.4: Accumulation of WUS and WUS Mutant Variants in *sumo1/2*. *Wt Col pWUS::eGFP-WUS* (A-D) has higher WUS accumulation across all SAM layers than *sumo1/2 pWUS::eGFP-WUS* (E-H). *Wt Col pWUS::eGFP-WUS229-292* (I-L) has low WUS accumulation in the SAM and higher WUS accumulation in floral primordia, whereas *sumo1/2 pWUS::eGFP-WUS229-292* (M-P) showed no WUS accumulation. *Wt Col pWUS::eGFP-WUS EARM* (Q-T) had close to *Wt* WUS accumulation and distribution, while *sumo1/2 pWUS::eGFP-WUS EARM* (U-X) had reduced WUS accumulation that was only highly enriched in a few cells of the L3. Green signal is eGFP-WUS, red signal is FM4-64X plasma membrane bound dye. (Scale bars=20μm).

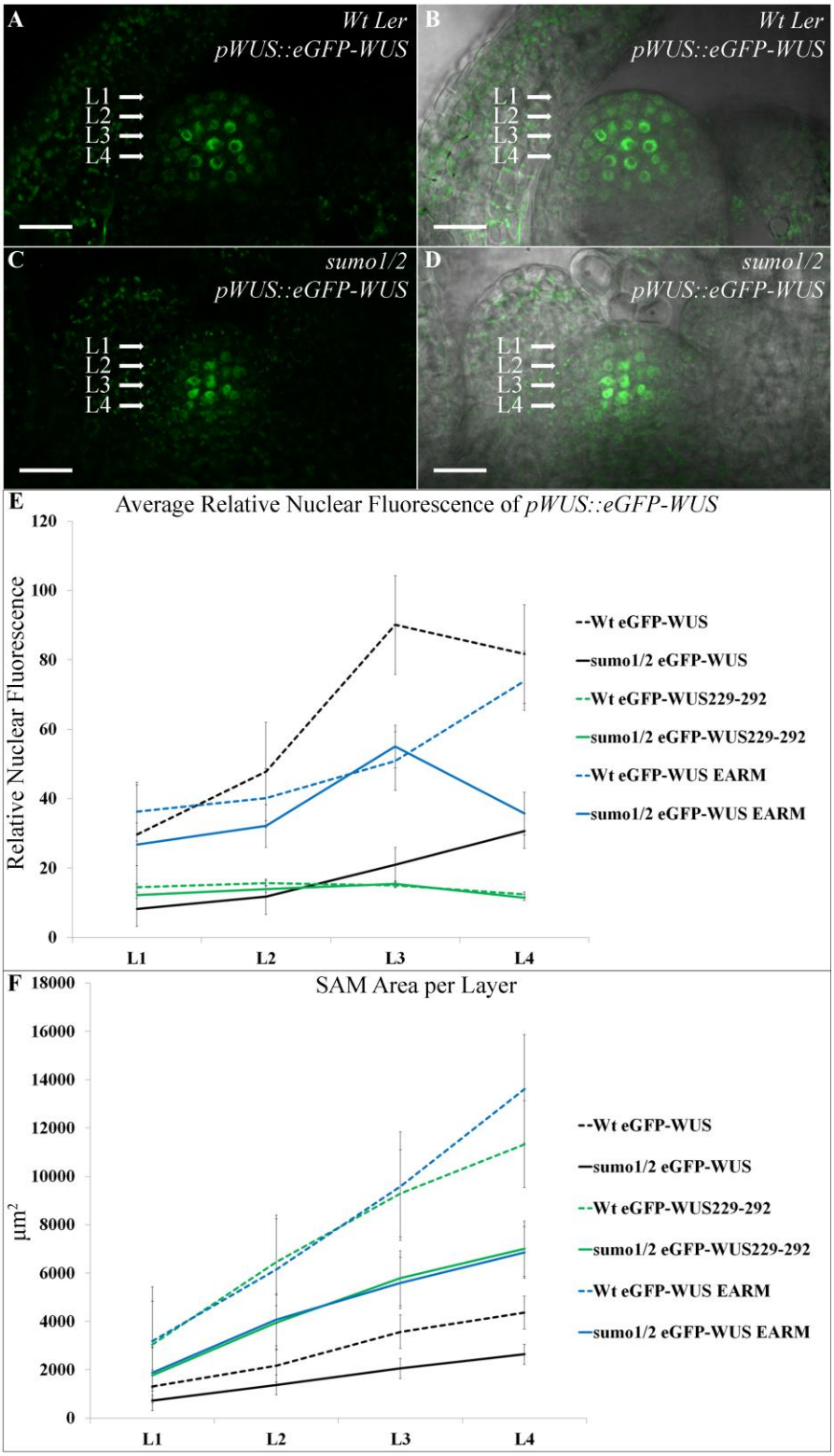
A
Wt Ler
pWUS::eGFP-WUS
L1
L2
L3
L4
B
Wt Ler
pWUS::eGFP-WUS
L1
L2
L3
L4
C
sumo1/2
pWUS::eGFP-WUS
L1
L2
L3
L4
D
sumo1/2
pWUS::eGFP-WUS
L1
L2
L3
L4
E
Average Relative Nuclear Fluorescence of pWUS::eGFP-WUS
Relative Nuclear Fluorescence
120
100
80
60
40
20
0
L1
L2
L3
L4
--Wt eGFP-WUS
—sumo1/2 eGFP-WUS
--Wt eGFP-WUS229-292
—sumo1/2 eGFP-WUS229-292
--Wt eGFP-WUS EARM
—sumo1/2 eGFP-WUS EARM
F
SAM Area per Layer
µm²
18000
16000
14000
12000
10000
8000
6000
4000
2000
0
L1
L2
L3
L4
--Wt eGFP-WUS
—sumo1/2 eGFP-WUS
--Wt eGFP-WUS229-292
—sumo1/2 eGFP-WUS229-292
--Wt eGFP-WUS EARM
—sumo1/2 eGFP-WUS EARM

Figure 3.5: Quantification of *pWUS::eGFP-WUS* in *Wt* and *sumo1/2* lines. Transverse sections of 9 day old seedlings of *Wt Ler pWUS::eGFP-WUS* (A-B) and *sumo1/2 pWUS::eGFP-WUS lines* (C-D). The average relative nuclear fluorescence of cells in the L1-L4 layers was measured in *Wt* and *sumo1/2* lines (E). The SAM area for each of the L1-L4 layers was measured in *Wt* and *sumo1/2* lines (F). Error bars represent standard error. (Scale bars=20µm, n=3).

sumo1/2 Knockdown Lines Reveal Increased Basal *pCLV3* Expression and Reduced *pCLV3* Sensitivity to WUS Levels

The next objective was to ascertain the functional significance of the *sumo1/2* effects on WUS function. The many aspects of WUS regulation of the stem cell population and maintenance of the SAM can be linked to the function of WUS as a transcription factor that both activates genes necessary for stem cell maintenance and represses genes responsible for cellular differentiation (Kieffer et al., 2006, Ikeda et al., 2009, Yadav et al., 2010, Yadav et al., 2011). While many questions still remain in understanding the underlying mechanisms involved in WUS-mediated *CLV3* expression, it is one of the most well characterized targets of WUS regulation to date (Schoof et al., 2000, Brand et al., 2002, Gordon et al., 2007, Yadav et al., 2011). Specifically, the manipulation of WUS levels through a Dexamethasone (Dex) inducible WUS-GR construct has been shown to expand the expression zone of *CLV3* in a temporal dependent manner (Yadav et al., 2010).

To understand the potential role of SUMO1/SUMO2 in the WUS-mediated regulation of *CLV3*, the constructs *p35S::WUS-GR* and *pCLV3::H2B-YFP* were introduced into both *Wt* and *sumo1/2* lines. Transversal sections of seedlings at seven days post germination were analyzed to determine the basal effects of WUS levels on *pCLV3::H2B-YFP* expression (Figure 3.6A-3.6D). At seven days, seedlings were transferred under sterile conditions to MS+10μM Dex or MS+Mock plates and returned to the growth chamber for two days of additional growth. After two days of Mock treatment, *sumo1/2* had a slightly increased number of *pCLV3::H2B-YFP* expressing

cells per layer and a higher relative nuclear fluorescence than *Wt* (Figure 3.6E-3.6H, 3.6M-3.6N). However, after two days of Dex treatment, the *Wt* had a significant increase in the number of *pCLV3::H2B-YFP* expressing cells and a significantly higher relative nuclear fluorescence in each layer in comparison to *sumo1/2* (Figures 3.6I-3.6N, S3.4B). This analysis reveals that SUMO1/SUMO2 activity is necessary for proper WUS-mediated regulation of *CLV3* transcription.

Discussion

SUMO1/SUMO2 are members of a diverse yet essential protein family that perform many necessary functions across eukaryotic taxa (Geiss-Friedlander and Melchior, 2007). Previous mouse studies have begun to link SUMO function to the equally essential function of stem cell development and maintenance. In mice, ubiquitin conjugating enzyme E2I (UBE2I) is essential for maintaining the sumoylation of the embryonic stem cell (ESC) factors POU domain class 5 transcription factor 1 (Oct4), SRY [sex determining region Y]-box 2 (Sox2), and Kruppel-like factor 4 (KLF4) (Tahmasebi et al., 2013). SUMOylation of Sox2 has been directly shown to inhibit its transcriptional activity through reducing DNA binding (Tsuruzoe et al., 2006). SUMOylation of Kruppel-like factor 5 (KLF5), a cell division regulator, is also essential for its nuclear import and subsequent potential to regulate gene expression (Du et al., 2008). SUMOylation of the nuclear receptor subfamily 2 group C member 1 (Tr2) also inhibits the activation of downstream essential ESC factors such as Oct4 (Park et al., 2007). Additionally, a bioinformatics analysis in *D. melanogaster* reveals that many of the bi-functional transcription factors important for developmental regulation, such as

Hunchback (Hb), Giant (Gt), and Kruppel (Kr) contain at least one SUMOylation site (Bauer et al., 2010). The consensus of these studies suggests a critical role for SUMO in the regulation of developmental processes and maintenance of stem cells. Combined with the previously discussed importance of SUMO function in essential plant processes provides a strong case for in depth analysis of the WUS-SUMO1/SUMO2 interaction and its role in stem cell maintenance in *A. thaliana*.

The first objective in characterization of the WUS-SUMO1/SUMO2 interaction was the identification of the mechanism by which SUMO1/SUMO2 interact with WUS. SUMOylation is by far the most prolifically analyzed mechanism of SUMO function and analysis of the relevance of SIMs and non-covalent SUMO interactions lags much farther behind (Minty et al., 2000, Song et al., 2004, Hecker et al., 2006, Elrouby et al., 2013). The initial GPS-SUMO 1.0 sequence analysis only revealed weak putative SUMOylation sequences and three SIM sequences at WUS46-50, WUS143-147, and WUS287-291. The deletion series used in this study revealed that the essential interaction sequence for WUS-SUMO1/SUMO2 existed from WUS134-253, with WUS253-285 enhancing the interaction specifically for SUMO1 (Figure 3.2A-3.2D). This essential sequence contains the SIM at WUS143-147 and three of the weak SUMOylation sites (Table S3.1). However, neither the SUMOylation sites nor the SIM site was sufficient to maintain the interaction alone, suggesting that an additional as of yet uncharacterized site is essential for the interaction.

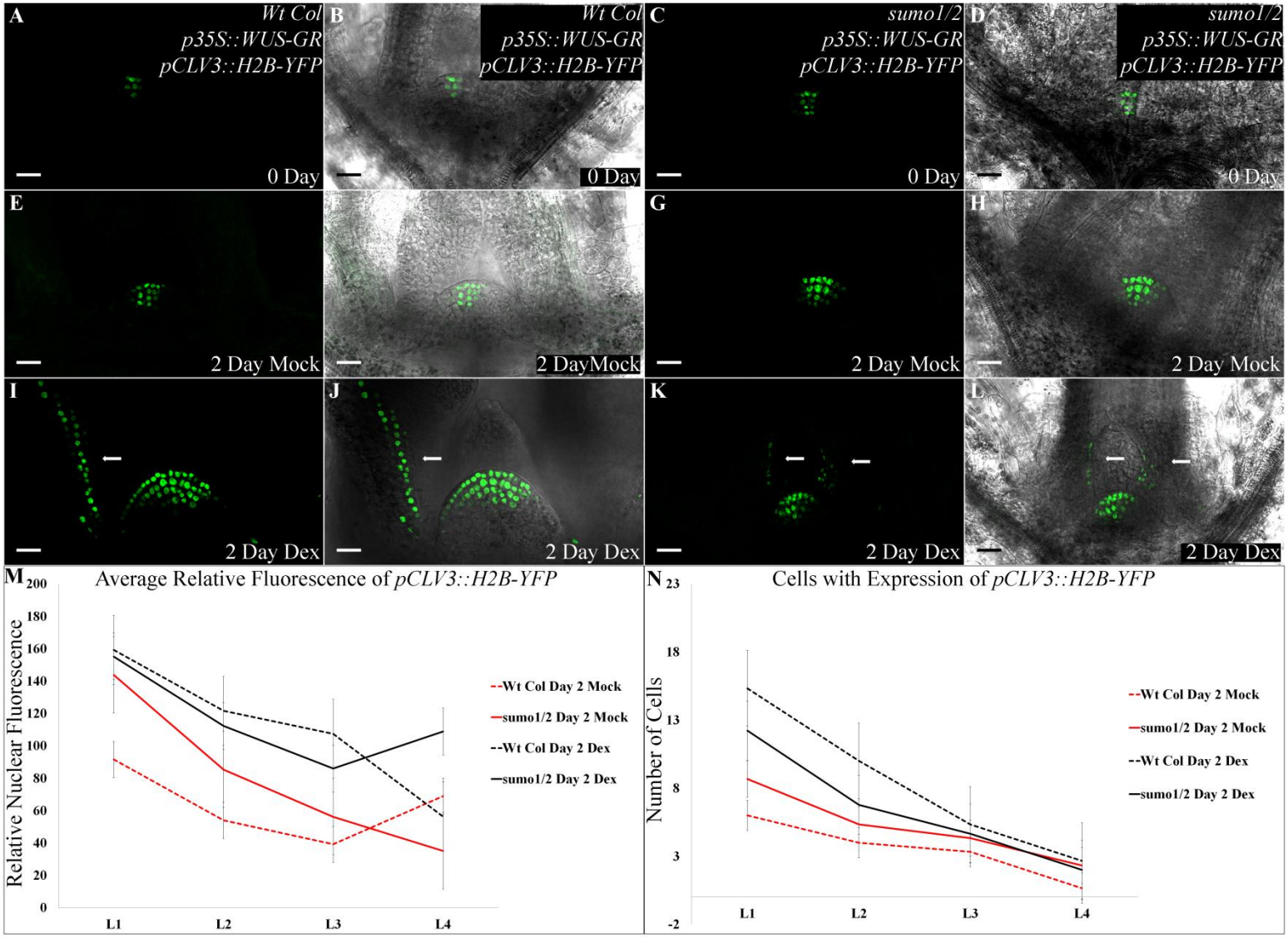
A
Wt Col
p35S::WUS-GR
pCLV3::H2B-YFP
0 Day
B
Wt Col
p35S::WUS-GR
pCLV3::H2B-YFP
0 Day
C
sumo1/2
p35S::WUS-GR
pCLV3::H2B-YFP
0 Day
D
sumo1/2
p35S::WUS-GR
pCLV3::H2B-YFP
0 Day
E
2 Day Mock
2 DayMock
G
2 Day Mock
H
2 Day Mock
I
2 Day Dex
J
2 Day Dex
K
2 Day Dex
L
2 Day Dex
M
Average Relative Fluorescence of pCLV3::H2B-YFP
Relative Nuclear Fluorescence
200
180
160
140
120
100
80
60
40
20
0
L1
L2
L3
L4
Wt Col Day 2 Mock
sumo1/2 Day 2 Mock
Wt Col Day 2 Dex
sumo1/2 Day 2 Dex
N
Cells with Expression of pCLV3::H2B-YFP
Number of Cells
23
18
13
8
3
-2
L1
L2
L3
L4
Wt Col Day 2 Mock
sumo1/2 Day 2 Mock
Wt Col Day 2 Dex
sumo1/2 Day 2 Dex

Figure 3.6: Response of *CLV3* Expression to Manipulation of WUS Levels in *sumo1/2*. Vegetative transverse sections of *Wt Col, p35S::WUS-GR, pCLV3::H2B-YFP* (A-B, E-F, I-J) *and sumo1/2 p35S::WUS-GR, pCLV3::H2B-YFP* (C-D, G-H, K-L) seedlings after 0 Days (A-D), 2 Days Mock treatment (E-H), and 2 Days Dex treatment (I-L). YFP signal is shown in (A, C, E, G, I, K) and YFP/DIC overlay is shown in (B, D, F, H, J, L). Arrows show ectopic *pCLV3::H2B-YFP* expression outside of the SAM after Dex treatment. Relative YFP fluorescence for each time point is shown in (M) across the most central four cells in each of the L1-L4 layers. The change of expression in *Wt* lines is nearly 200% between Mock/Dex treatments in the L1, while the change of expression in *sumo1/2* lines in the L1 is only about 15%. The number of SAM cells with *pCLV3::H2B-YFP* expression in each line is shown in (N). The change in the number of cells expressing *pCLV3::H2B-YFP* in *Wt* between Mock/Dex is about 300% in the L1, while the change in number of expressing cells in the L1 of *sumo1/2* is about 20%. Each subsequent layer has lower changes in expression, yet maintain the pattern of larger change in the *Wt* lines than in the *sumo1/2* lines except for the *Wt* accumulation of *pCLV3::H2B-YFP* in the L4 layer between Mock/Dex. Error bars represent standard error. (Scale bars=20µm, n=3).

The WUS Acidic Motif shares similar properties to that of the predicted SIM sites, and indeed the WUS AMM construct completely eliminated the WUS-SUMO1 interaction, while the WUS-SUMO2 interaction remained stable (Figure 3.2A-3.2D) (Minty et al., 2000, Song et al., 2004, Hannich et al., 2005, Hecker et al., 2006, Elrouby et al., 2013). Taken together, this suggests the presence of several sites is necessary for the WUS-SUMO1 interaction, which also enhances the likelihood that this interaction is a result of a SIM instead of SUMOylation of a target lysine. Also, the differential interaction between WUS-SUMO1 and WUS-SUMO2 across the WUS Acidic Motif, the identification of SUMO1 and not SUMO2 in the initial Y2H screen, along with the overall reduction in interaction strength between all WUS variants and SUMO2 suggests a preferential interaction between WUS-SUMO1.

The next experiments were designed to demonstrate the occurrence of the WUS-SUMO1/SUMO2 interaction in *A. thaliana* SAMs and demonstrate that this interaction occurs in the nucleus where WUS functions (Mayer et al., 1998). The SUMO antibody used cannot distinguish between SUMO1/SUMO2, so this Co-IP can only verify the interaction of at least one of these proteins occurs in the SAMs of *A. thaliana*. SUMO1/SUMO2 was detected in all fractions; however WUS was only detected in the Co-IP fraction despite its prominent accumulation in the nucleus. This is likely due to the low overall levels of WUS in the SAM in comparison to other proteins, since the RM expression region of the SAM is only consists of a few cells (Schoof et al., 2000). Regardless, the clear detection of WUS in the Co-IP fraction provides strong evidence that this interaction does indeed occur in SAM cells.

Additionally, the BiFC experiments show that while expression of WUS, SUMO1/SUMO2 individually results in nuclear and cytosolic accumulation of each protein, the interactions between WUS-SUMO1 and WUS-SUMO2 occur most strongly in the nucleus, with minor cytosolic accumulation. This is congruous with the fact that WUS accumulates much more strongly in the nucleus and the necessity for WUS to be nuclear localized to function as a transcription factor and regulate gene expression (Mayer et al., 1998).

Confirming the interaction between WUS-SUMO1/SUMO2 provided a strong basis to further pursue analysis of the function of SUMO1/SUMO2 in WUS-mediated stem cell maintenance. The first objective was to understand the effects of SUMO1/SUMO2 on WUS itself, since SUMO1/SUMO2 regulate many functions that are essential to WUS function such as protein stability, subcellular localization, mobility across cells, and transcriptional activity (Miura and Hasegawa, 2010, Mazur and van den Burg, 2012). WUS accumulation patterns outside of the RM are critical for its function, and initial analysis sought to understand potential SUMO1/SUMO2 effects on this phenomenon (Yadav et al., 2011). Control lines of eGFP and NLS-eGFP were expressed under the control of *pWUS* to ensure that general protein mobility and nuclear accumulation were unaffected in the SAMs of *sumo1/2* lines. A series of WUS mutations was used to characterize the effects of *sumo1/2* on WUS accumulation and determine the significance of existing WUS motifs on these resulting effects (Ikeda et al., 2009, unpublished data). Use of *sumo1/2* lines introduced with the eGFP-WUS fusion construct under its native promoter revealed a reduction in WUS accumulation in each layer in

comparison to *Wt*, ranging from 30% relative accumulation in the L1 layer to just under 20% relative accumulation in the L3 layer. Analysis of eGFP-WUS229-292 and eGFP-WUS EARM constructs both revealed a relative reduction in all layers of the *sumo1/2* lines except for the L3 layer, which was slightly elevated in *sumo1/2* lines. Finally, constructs of eGFP-WUS WBM and eGFP-WUS WBM/EARM showed no strong differences in WUS accumulation.

Analysis of all lines reveal that the *sumo1/2* knockdown lines only have a strong effect on WUS constructs retaining a functional WUS-Box Motif (Ikeda et al., 2009). This suggests that the WUS-Box Motif is able to interact with SUMO1/SUMO2 to affect the accumulation of WUS in the SAM. This would also mean that WUS constructs with the WBM that inhibit WUS-Box Motif function should not respond significantly to the knockdown of SUMO1/SUMO2 present in *sumo1/2* lines. WUS accumulation changes are not demonstrated in the eGFP-WUS WBM and eGFP-WUS WBM/EARM constructs used here, which combined with the earlier Y2H interaction mapping analysis, suggests that the WUS-Box Motif could enrich the WUS-SUMO1 interaction in order to ensure the proper distribution of WUS in the SAM. While this is an important step in understanding the functional relevance of the WUS-Box Motif in regulating the WUS-SUMO1/SUMO2 interaction, there are still many unanswered questions. Further characterization of SUMO1/SUMO2 alteration of WUS stability in addition to identification of tertiary co-factors that could require interaction with a WUS-SUMO1/SUMO2 complex to function are potential avenues of study that could reveal more insight to the mechanisms and significance of this regulation.

The next objective was to determine any effects that SUMO1/SUMO2 might have in WUS function, specifically as a transcription factor regulating target genes essential for SAM maintenance. WUS-mediated regulation of *CLV3* expression is one of the better characterized examples of WUS regulation, and was therefore used to understand these SUMO1/SUMO2 effects (Schoof et al., 2000, Brand et al., 2002, Gordon et al., 2007, Yadav et al., 2011). The inducible *p35S::WUS-GR* construct was introduced in tandem with the *pCLV3::H2B-YFP* construct to visualize the expression pattern of *CLV3*. The first significant change in the *pCLV3::H2B-YFP* expression is present even in *sumo1/2* Mock treated lines, which show relative expression levels closer to *Wt* Dex treated samples than *Wt* Mock samples and a slight increase in the number of *pCLV3::H2B-YFP* expressing cells in the SAM (Figure 3.6E-3.6J, 3.6M-3.6N). Lower levels of WUS accumulation have actually been shown to increase the expression of *CLV3* in the SAM, which is congruous with the reduced WUS accumulation that leads to higher levels of CLV3 expression in these lines (unpublished data). After Dex treatments, the difference between *Wt* lines and *sumo1/2* lines is more drastic, as the clear increase in relative expression levels in L1-L3 and more than doubled number of *pCLV3::H2B-YFP* expressing cells in the L1 and L2 layers are not present in *sumo1/2* lines (Figure 3.6I-3.6N). However, the response of *pCLV3::H2B-YFP* relative accumulation in the inner L4 layer of the SAM in which *WUS* is expressed is reversed in *Wt* and *sumo1/2* lines. Whereas in *Wt* lines *pCLV3::H2B-YFP* expression in the L4 layer is reduced after Dex treatment, *sumo1/2* lines show an increase in *pCLV3::H2B-YFP* L4 layer expression (Figure 3.6M). This suggests a differential regulation of SUMO1/SUMO2-mediated

effects on WUS transcriptional regulation of *CLV3* expression in the L4 layer in comparison to the L1-L3 layers. Analysis of cell type specific regulation of SUMO1/SUMO2 function with respect to WUS transcriptional ability would be necessary to tease out the nuances of this complex system.

While there are still many unanswered questions regarding mechanisms and importance of SUMO1/SUMO2 on WUS-mediated stem cell regulation, results from this study along with previously published data can begin to shed some light on the potential roles and functions of the WUS-SUMO1/SUMO2 interactions. SUMOylation and SIMs are both responsible for regulating the specificity and formation of heterodimeric complexes (Miura and Hasegawa, 2010, Mazur and van den Burg, 2012). WUS PPIs, including the previously studied TPL and SAP18 identified in this study are targets of SUMOylation (Miller et al., 2010, Lamoliatte et al., 2014). TPL is a strong transcriptional co-repressor, and its interaction with WUS across the transcriptionally relevant WUS-Box and EAR-Like Motifs have been linked to target gene repression (Kieffer et al., 2006, Long et al., 2006, Causier et al., 2012). SAP18 is a member of the SWI-independent 3 (SIN3) histone deacetylase complex that is SUMOylated and participates in epigenetic chromatin-remodeling regulated gene silencing (Golebiowski et al., 2009, Liu et al., 2009). SUMOylation of these targets may provide a mechanism to stabilize their binding with WUS using both the WUS-SUMO1/SUMO2 interaction and the basal interaction across the EAR Motif that these proteins normally recognize to function as co-repressors (Mazur and van den Burg, 2012). The necessity for SUMO1/SUMO2 in the formation of WUS co-repressor complexes could lead to reduction in WUS repressive

capability, which would also explain the elevated basal levels of *CLV3* expression in *sumo1/2* lines. However, a more comprehensive analysis of the requirement of SUMO for direct formation of WUS co-repressor complexes would need to be performed to confirm these potential roles.

These analyses demonstrate that WUS interacts with SUMO1/SUMO2 across an essential domain from WUS134-253, with the region between WUS253-WUS285 enhancing the interaction between WUS-SUMO1 specifically. Additionally, these interactions occur in the nucleus of plant cells and in SAM tissue. Interaction of SUMO1/SUMO2 across the WUS-Box Motif is essential in maintaining a proper distribution of WUS accumulation in the SAM. Finally, SUMO1/SUMO2 are required for proper *CLV3* expression with respect to WUS levels in the SAM.

Methods

Interaction Characterization Between SUMO1/SUMO2 and WUS

Primers based on the 5' and 3' ends of the SUMO1 and SUMO2 CDS were designed for amplification from a cDNA template to clone into pGADT7. A WUS deletion series based on the following AAs were generated to clone into pGBKT7: 1-134, 1-208, 134-208, 1-134Δ208-292, 1-253, 1-285, 250-285, 250-292, and 134-292. A WUS mutation series with mutations in the Acidic Motif (AMM), WUS-Box Motif (WBM), and EAR-Like Motif (EARM) was generated based on the mutations previously described via PCR site-directed mutagenesis (Ikeda et al., 2009). These pGBKT7 constructs were co-transformed with SUMO1/SUMO2 CDS cloned into pGADT7 and plated as described in Chapter 1. Growth on non-selective SD-(L/W) plates was used to

determine transformation efficiency and growth on SD-(L/W/H/A) was used to determine interaction status. For dilution series analysis, overnight culture of each co-transformation was grown to OD 0.4 and diluted ten-fold three successive times. From each dilution 4µL was plated and grown for 7 days at 30^{o}C.

BiFC constructs for SUMO1/SUMO2 were generated as described in Chapter 1. Co-IP experiments were performed as described in Chapter 1 using a commercially available antibody for SUMO1/SUMO2 (Abcam).

Generation of *sumo1/2* Lines with WUS and *CLV3* Reporter Constructs and Confocal Imaging

sumo1/2 lines were crossed with lines containing *pWUS::eGFP*, *pWUS::NLS-eGFP*, *pWUS::eGFP-WUS*, *pWUS::eGFP-WUS WBM*, *pWUS::eGFP-WUS EARM*, *pWUS::eGFP-WUS WBM/EARM*, *pWUS::eGFP-WUS229-292*, and *p35S::WUS-GR*, *pCLV3::H2B-YFP* (van den Burg et al., 2010, unpublished data). *sumo1/2* lines were selected on MS+10µM Basta+50µM Kanamycin plates. A modified cetyltrimethylammonium bromide (CTAB) gDNA extraction was performed (Murray and Thompson, 1980). PCR was performed with specific primers for SUMO1/SUMO2 CDS, LB1 SAIL, pGreen0029 plasmid, WUS-GR, H2B-YFP, and eGFP-WUS (Table S3.2) (Mullis et al., 1980). Fluorescent reporters were also screened via fluorescence excitation at 488nm and a GFP filter using the Zeiss Axio Imager and the SAM dissection protocol described in Chapter 2. F_2 plants were grown in continuous light and imaged via Zeiss 510 (inflorescence) at four weeks or Leica SP5 (vegetative) at 7-10 days. Excitation was

performed with a 488nm laser, and emission was captured at 500nm-530nm for eGFP and 500nm-575nm for YFP.

Seedling Sectioning and Image Analysis

Seedlings were grown on appropriate MS plates for 7-10 days under continuous light. Prior to sectioning, 1mL pipette tips were cut in half to use as vessels for seedling preparation. A 5% agarose solution was prepared and kept at 60^{o}C to prevent solidification. Seedlings were removed from the plates with forceps and the roots removed with a sharp razor. A cut 1mL pipette tip was filled with 5% agarose and the seedling immersed in the agarose. The seedling/agarose preparation was allowed to solidify at room temperature and repeated for all seedlings analyzed. Under a stereo dissection microscope, agarose was trimmed from the seedling to create a block. The seedling was oriented in a vertical position such that the SAM could be seen in the stereo dissection microscope. Using a feather sharp razor and forceps, a vertical slice through the SAM and length of the stem was cut and the two halves of the seedling immediately transferred to a slide with water to prevent dehydration. A coverslip was placed after 6-8 seedling sections were placed on a slide, and the slide imaged via confocal microscopy as stated previously.

Confocal images were processed using the ROI manager and Measurement tools in ImageJ for relative nuclear fluorescence measurements, along with the Overlay and Measure tools in Zeiss LSM Image Browser for SAM area measurements.

Semi-Quantitative RT-PCR Analysis of *WUS* and *CLV3* Expression

SAMs from 40-50 *Wt, Wt p35S::WUS-GR*, *sumo1/2*, and *sumo1/2 p35S::WUS-GR* were collected and RNA extracted via a Quiagen RNeasy Plant Mini Kit. cDNA synthesis was performed using the Protoscript II Reverse Transcriptase protocol. *WUS* and *CLV3* specific primers were used and normalized to the *TUB2* reference gene and to Mock treatments, respectively.

Supplemental Figures

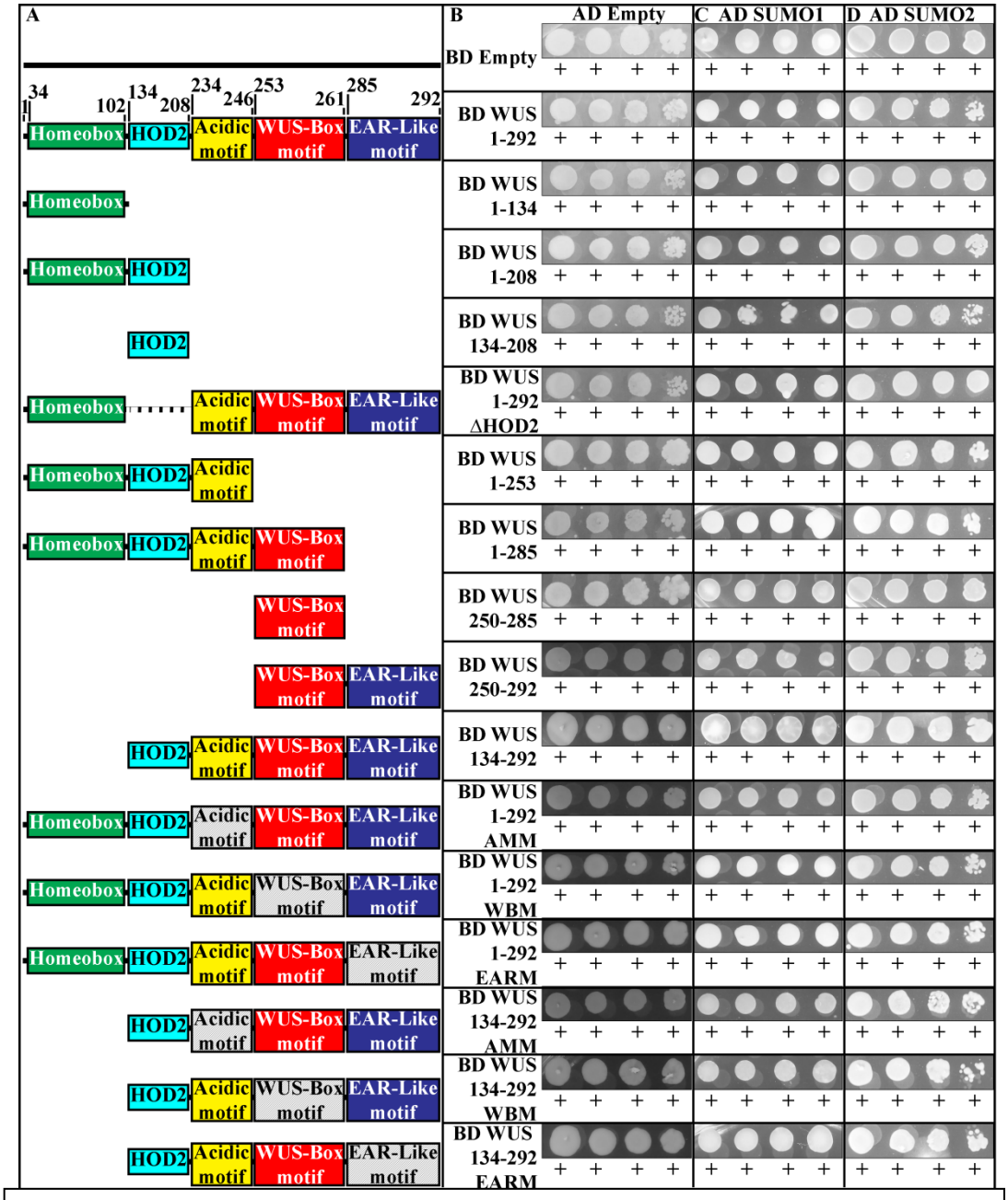

Figure S3.1: Non-Selective Controls for Mapping the Interaction Region of WUS and SUMO1/SUMO2. Each of the WUS truncation and mutation constructs is diagramed (A) with including the amino acid boundaries of the following domains: Homeobox, HOD2 homodimerization domain, Acidic motif, WUS-Box motif, and EAR-Like motif. Mutated domains are marked with grey hashed boxes and annotated as AMM (Acidic motif mutant), WBM (WUS-Box mutant), and EARM (EAR-Like motif mutant). Yeast two-hybrid 10-fold serial dilution analysis of each WUS truncation and mutation construct interaction with and empty control vector (B), SUMO1 (C), and SUMO2 (D). Plus signs show the strength of interaction based on the number of serial dilutions for which positive interaction growth is present.

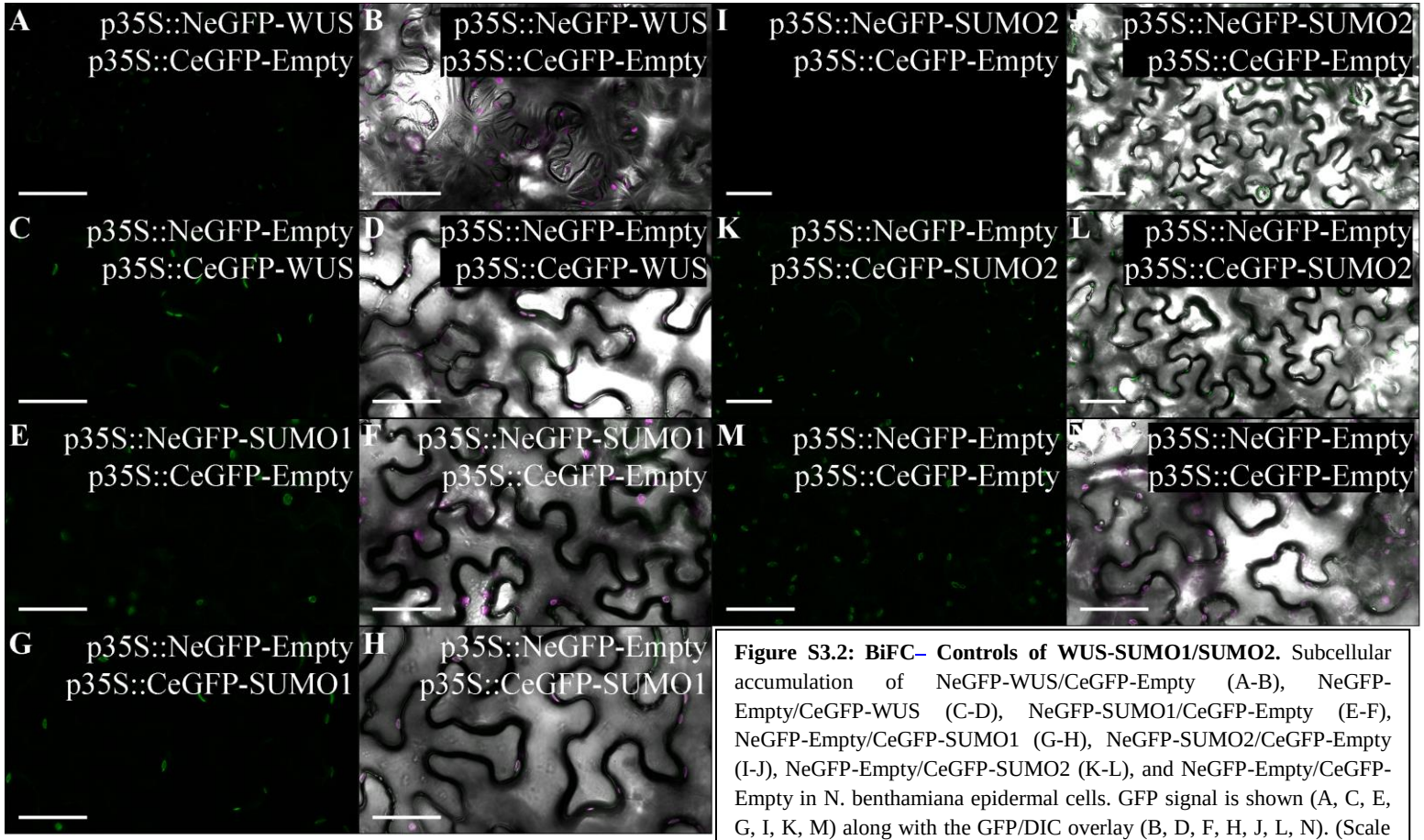

Figure S3.2: BiFC– Controls of WUS-SUMO1/SUMO2. Subcellular accumulation of NeGFP-WUS/CeGFP-Empty (A-B), NeGFP-Empty/CeGFP-WUS (C-D), NeGFP-SUMO1/CeGFP-Empty (E-F), NeGFP-Empty/CeGFP-SUMO1 (G-H), NeGFP-SUMO2/CeGFP-Empty (I-J), NeGFP-Empty/CeGFP-SUMO2 (K-L), and NeGFP-Empty/CeGFP-Empty in N. benthamiana epidermal cells. GFP signal is shown (A, C, E, G, I, K, M) along with the GFP/DIC overlay (B, D, F, H, J, L, N). (Scale bars=50µm).

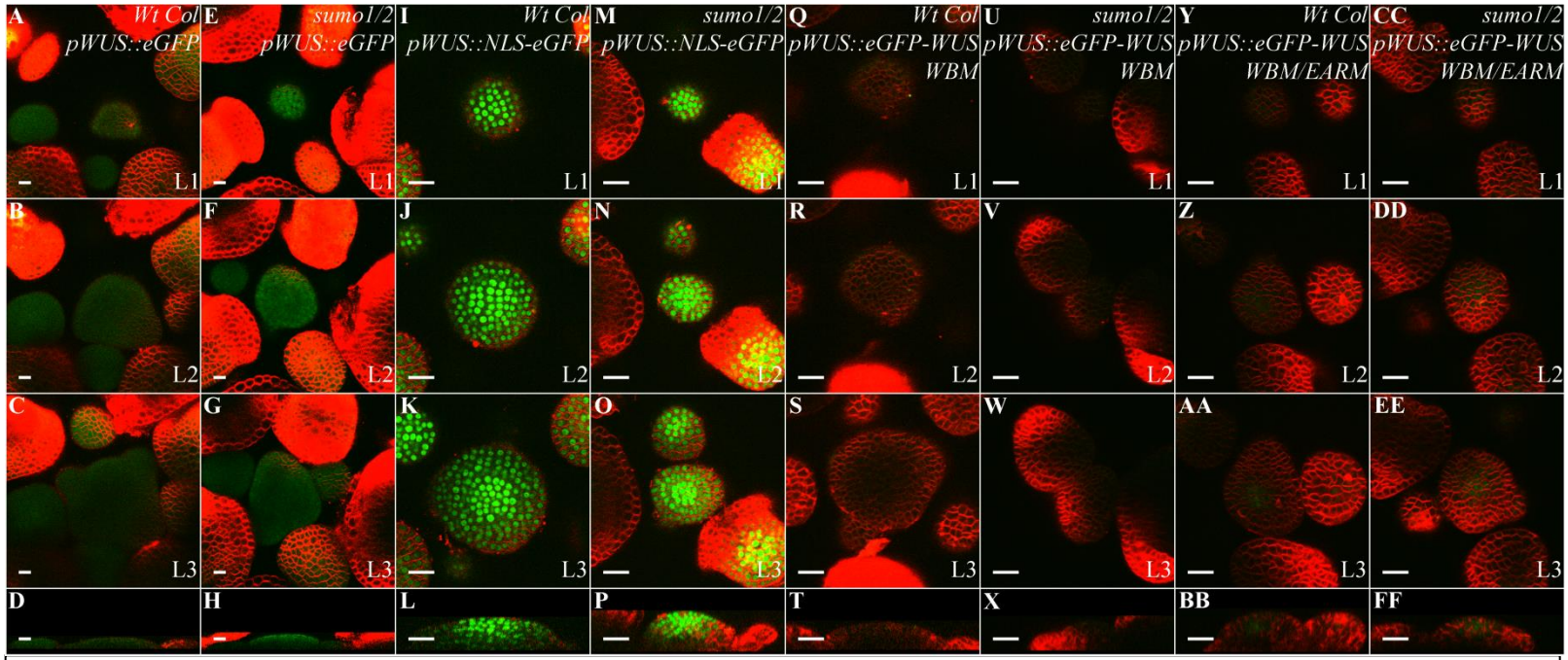

Figure S3.3: Accumulation of WUS and WUS Mutant Variants in *sumo1/2*. *pWUS::eGFP* in *Wt* (A-D) and *sumo1/2* (E-H) has even accumulation across all SAM layers in the nucleus and cytosol. *pWUS::NLS-eGFP* in *Wt* (I-L) and *sumo1/2* (M-P) has even accumulation across all SAM layers in the nucleus. *pWUS::eGFP-WUS WBM* in *Wt* (Q-T) and *sumo1/2* (U-X) showed low WUS accumulation in the cytosol of all SAM layers. *pWUS::eGFP-WUS WBM/EARM* in *Wt* (Y-BB) and *sumo1/2* (CC-FF) had WUS accumulation and distribution, similar to that of *Wt pWUS::eGFP-WUS*, with slightly more accumulation in the nucleus. Green signal is eGFP-WUS, red signal is FM4-64X plasma membrane bound dye. (Scale bars=20μm).

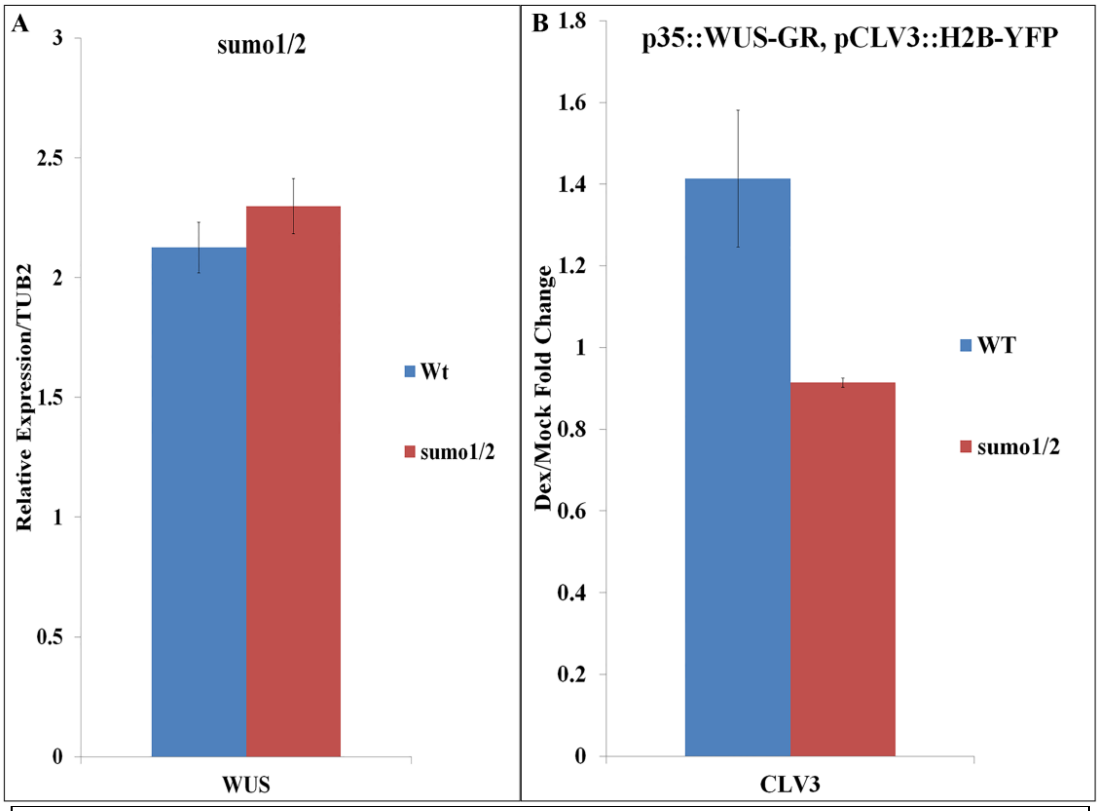

Figure S3.4: Semi- Quantitation of *WUS* and *CLV3* Expression in *Wt* and *sumo1/2* SAMs. The relative expression of *WUS* normalized to *TUB2* in *Wt* and *sumo1/2* SAMs (A). The relative expression of *CLV3* in Dex-treated *p35S::WUS-GR* SAMs normalized to Mock-treated SAMs in *Wt* and *sumo1/2* (B). Error bars represent standard error. (n=3).

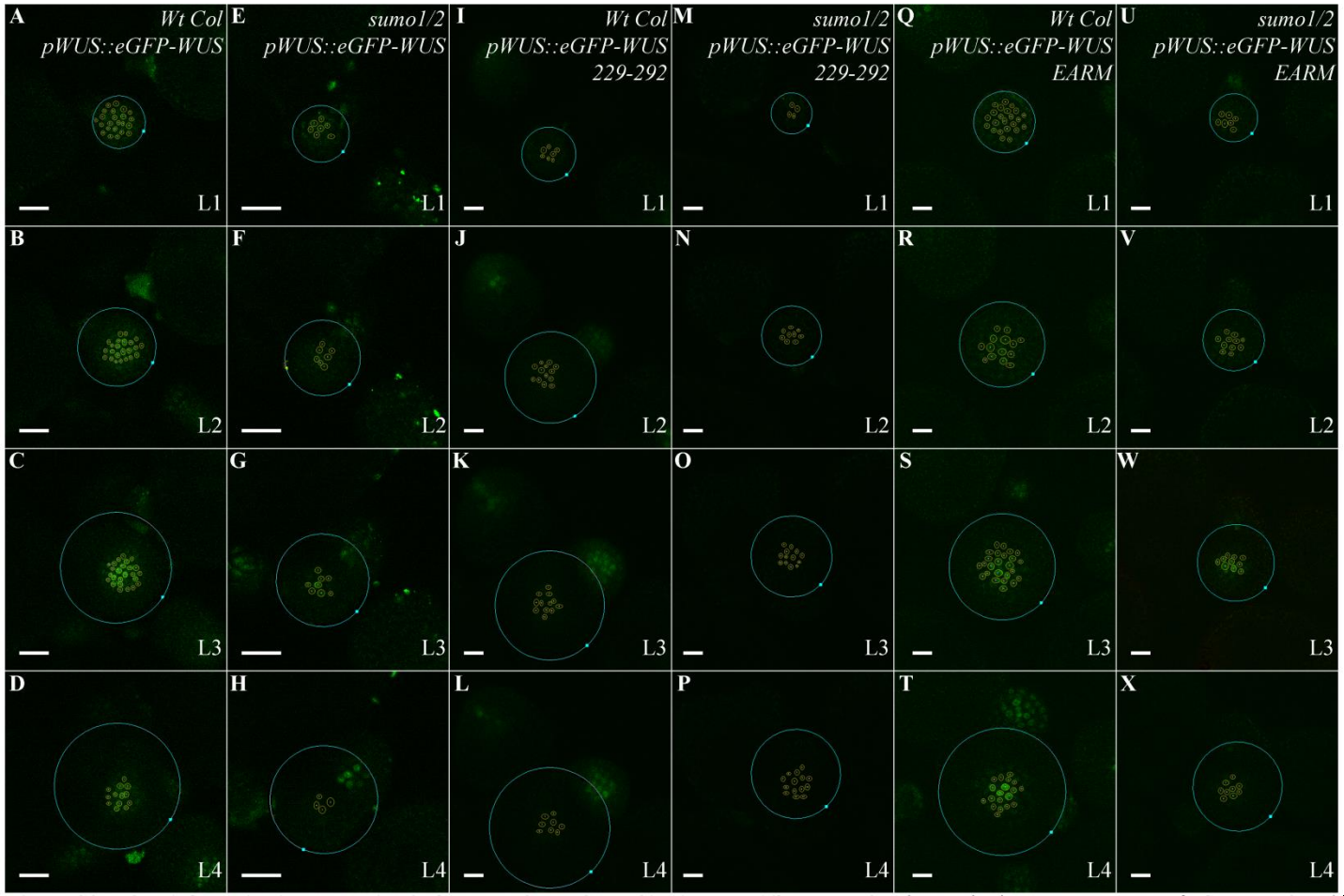

Figure S3.5: Semi-Quantitative Analysis of eGFP-WUS and SAM Size in *sumo1/2* lines. Semi-quantitative measurements of eGFP-WUS and SAM size by layer area in *Wt Col pWUS::eGFP-WUS* (A-D), *sumo1/2 pWUS::eGFP-WUS* (E-H), *Wt Col pWUS::eGFP-WUS229-292* (I-L), *sumo1/2 pWUS::eGFP-WUS229-292* (M-P), *Wt Col pWUS::eGFP-WUS EARM* (Q-T), and *sumo1/2 pWUS::eGFP-WUS EARM* (U-X). Yellow circles with ROIs represent enclosed nuclei from which relative fluorescence signal was obtained from each SAM layer (L1, L2, L3, and L4), and blue circles represent the enclosed area used to calculate SAM area for each layer (Scale bars=20µm, n=3).

Supplemental Tables

Table S3.1: Predicted SUMOylation and SIM Sites on WUS

WUS Location	WUS Sequence	Interaction Type
24	SGNNNNNKSGSGGYT	SUMOylation
46 - 50	WTPTTEQ IKILK ELYYNNA	SIM
47	TPTTEQIKILKELYY	SUMOylation
50	TEQIKILKELYYNNA	SUMOylation
68	PTADQIQKITARLRQ	SUMOylation
78	ARLRQFGKIEGKNVF	SUMOylation
82	QFGKIEGKNVFYWFQ	SUMOylation
92	FYWFQNHKARERQKK	SUMOylation
98	HKARERQKKRFNGTN	SUMOylation
99	KARERQKKRFNGTNM	SUMOylation
143 - 147	MQRPANS VNVKL NQDHHLY	SIM
146	PANSVNVKLNQDHHL	SUMOylation
158	HHLYHHNKPYPSFNN	SUMOylation
229	YNFFDRAKPLFGLEG	SUMOylation
275	GGSGAIWKYGQSEVR	SUMOylation
287 - 291	EVRPCAS LELRL N******	SIM

Table S3.2: Primers

Primer Name	Primer Sequence
5'p Fwd Acidic domainM	GCATGTGGTGGCGCTGCT
5'p Rev Acidic domainM	TGCTGCGGCTTGATGACC
C-eGFP-WUS-F	GACAAGCAGAAGAACGGCATCAAGGTG
C-eGFP-WUS-R	CATGGCGCGCCATGGTGAAGGAGCCCTG
EGFP Fwd Gateway	CACCATGGTGAGCAAGGGCGAGGAGCTG
EGFP-WUS-BOX-mut-Fwd	CGACGTACGGCTCCTG
EGFP-WUS-BOX-mut-Rev	ATGTTCCAGATAAGCAT
GR-Rev	GTGGTAATGCTGCAGGAACTATT
H2BYFP Fwd	CGGATCCACAATGGCGAAGGCAGATAAG
H2BYFP Rev	CGGATCCTTATTTGTATAGTTCATCCAT
LB1_SAIL	GCCTTTTCAGAAATGGATAAATAGCCTTGCTTCC
N-eGFP-WUS-F	GGATCCATGGAGCCGCCACAGCATCAG
N-eGFP-WUS-R	CATGGCGCGCCATGGTGAAGGAGCCCTG
pCR-Blunt SP MCS	CCTGAATTCTGCAGATATCCATCACACTGGCG
pGreen0029/1501-1900 Fwd	GTGCGGGCCTCTTCGCTATTACGC
pGreen0029/1501-1900 Rev	TAGGCACCCCAGGCTTTACACTTTATG
SUMO1 3'CDS StuI	GCAAGGCCTTCAGGCCGTAGCACCACCACCG
SUMO1 5'CDS BamHl	GCAGGATCCATGTCTGCAAACCAGGAGGAAG
SUMO-1-ecor-R	GAATTCTCAGGCCGTAGCACC
SUMO-1-nde-F	CATATGATGTCTGCAAACCAGGAGGAAG
SUMO2 Fwd BamHI	GGATCCATGTCTGCTACTCCGGA
SUMO2 Fwd NdeI	CATATGTCTGCTACTCCGGAAGA
SUMO2 Rev EcoRI	GAATTCCTAAAAGCAGAAGAGCT
SUMO2 Rev StuI	AGGCCTCTAAAAGCAGAAGAGC
TUB2-F	GAGCCTTACAACGCTACTCTGTCTG
TUB2-R	GAAGACGGGGGAATGGGATGAGATT
WUS 134 Fwd	CTGGAATTCTGCCCATCCTCCACCTACGTTG
WUS 208 Fwd	GGATGGGCAAACATGGATCATCATTAC
WUS 253 fwd NdeI	CATATGCATCGACGTACGCTTCCTCTC
WUS CDS 253 ASP	GAATTCACGTCGATGTTCCAGATAAGCATCGCC

759-733	
WUS CDS 285 ASP 858-831	GAATTCAGAAGCGCAAGGGCGAACTTCCGATTGG
WUS NDE-Fwd	CATATGATGGAGCCGCCACAG
WUSCHEL 134 EcoR1 Reverse	GAATTCGGAACACCGTGATGATGGTGAAG
WUSCHEL 208 EcoR1 Reverse	GAATTCCCTCCACCTACGTTGTTGTAATTC
WUS-EARlike-mut-F	TTCTGCTGAGGCACGTGCGAACTAG
WUS-EARlike-mut-R	GCGCAAGGGCGAACTTCCGATTGGCC
WUSFL-ECOR1 Rev	GAATTCCTAGTTCAGACGTAG

References

[1] F. G. Acevedo, A. Gamboa, J. Paez Valencia, L. F. Jimenez Garcia, M. Izaguirre Sierra, and E. R. Alvarez Buylla. FLOR1, a putative interaction partner of the floral homeotic protein AGAMOUS, is a plant-specific intracellular LRR. *Plant Science*, 167(2):225 – 231, 2004.

[2] J. M. Alonso and J. R. Ecker. Moving forward in reverse: Genetic technologies to enable genome-wide phenomic screens in *Arabidopsis*. *Nat. Rev. Genet.*, 7(7):524–536, 2006.

[3] E. Baena Gonzalez, F. Rolland, J. M. Thevelein, and J. Sheen. A central integrator of transcription networks in plant stress and energy signalling. *Nature*, 448(7156):938–942, Aug. 2007.

[4] W. B. Barbazuk, S. J. Emrich, H. D. Chen, L. Li, and P. S. Schnable. SNP discovery via 454 transcriptome sequencing. *The Plant Journal*, 51(5):910–918, 2007.

[5] M. K. Barton and R. S. Poethig. Formation of the shoot apical meristem in *Arabidopsis thaliana*: An analysis of development in the wild type and in the *shoot meristemless* mutant. *Development*, 119(3):823–831, 1993.

[6] D. Bauer, F. Buske, and T. Bailey. Dual-functioning transcription factors in the developmental gene network of *Drosophila melanogaster*. *BMC Bioinformatics*, 11(1):366, 2010.

[7] N. Baumberger and D. C. Baulcombe. *Arabidopsis* ARGONAUTE1 is an RNA slicer that selectively recruits microRNAs and short interfering RNAs. *Proc. Natl. Acad. Sci. U. S. A.*, 102(33):11928–11933, 2005.

[8] S. Beeckmans and L. Kanarek. Demonstration of physical interactions between consecutive enzymes of the citric acid cycle and of the Aspartate-Malate shuttle. *Eur. J. Biochem.*, 117(3):527–535, 1981.

[9] G. T. Beemster, L. De Veylder, S. Vercruysse, G. West, D. Rombaut, P. Van Hummelen, A. Galichet, W. Gruissem, D. Inzé, and M. Vuylsteke. Genome-wide analysis of gene expression profiles associated with cell cycle transitions in growing organs of *Arabidopsis*. *Plant Physiol.*, 138(2):734–743, 2005.

[10] O. Berkowitz, R. Jost, S. Pollmann, and J. Masle. Characterization of TCTP, the Translationally Controlled Tumor Protein, from *Arabidopsis thaliana*. *The Plant Cell*, 20(12):3430–3447, 2008.

[11] K. M. Bollman, M. J. Aukerman, M.-Y. Park, C. Hunter, T. Z. Berardini, and R. S. Poethig. HASTY, the *Arabidopsis* ortholog of exportin 5/MSN5, regulates phase change and morphogenesis. *Development*, 130(8):1493–1504, 2003.

[12] U.-A. Bommer and B.-J. Thiele. The translationally controlled tumour protein (TCTP). *Int. J. Biochem. Cell Biol.*, 36(3):379 – 385, 2004.

[13] J. L. Bowman, J. Alvarez, D. Weigel, E. M. Meyerowitz, and D. R. Smyth. Control of flower development in *Arabidopsis thaliana* by *APETALA1* and interacting genes. *Development*, 119(3):721–743, 1993.

[14] U. Brand, J. C. Fletcher, M. Hobe, E. M. Meyerowitz, and R. Simon. Dependence of stem cell fate in *Arabidopsis* on a feedback loop regulated by CLV3 activity. *Science*, 289(5479):617–619, 2000.

[15] U. Brand, M. Grünewald, M. Hobe, and R. Simon. Regulation of CLV3 expression by two homeobox genes in *Arabidopsis*. *Plant Physiol.*, 129(2):565–575, 2002.

[16] F. Brioudes, A.-M. Thierry, P. Chambrier, B. Mollereau, and M. Bendahmane. Translationally controlled tumor protein is a conserved mitotic growth integrator in animals and plants. *Proc. Natl. Acad. Sci. U. S. A.*, 107(37):16384–16389, 2010.

[17] A. Bruckner, C. Polge, N. Lentze, D. Auerbach, and U. Schlattner. Yeast two-hybrid, a powerful tool for systems biology. *Int. J. Mol. Sci.*, 10(6):2763–2788, June 2009.

[18] R. Budhiraja, R. Hermkes, S. Müller, J. Schmidt, T. Colby, K. Panigrahi, G. Coupland, and A. Bachmair. Substrates related to chromatin and to RNA-dependent processes are modified by *Arabidopsis* SUMO isoforms that differ in a conserved residue with influence on desumoylation. *Plant Physiol.*, 149(3):1529–1540, 2009.

[19] P. Bundock and P. Hooykaas. An *Arabidopsis* hAT-like transposase is essential for plant development. *Nature*, 436(7048):282–284, July 2005.

[20] W. Busch, A. Miotk, F. D. Ariel, Z. Zhao, J. Forner, G. Daum, T. Suzaki, C. Schuster, S. J. Schultheiss, A. Leibfried, et al. Transcriptional control of a plant stem cell niche. *Dev. Cell*, 18(5):841–853, 2010.

[21] C. C. Carles, D. Choffnes Inada, K. Reville, K. Lertpiriyapong, and J. C. Fletcher. ULTRAPETALA1 encodes a SAND domain putative transcriptional regulator that

controls shoot and floral meristem activity in *Arabidopsis*. *Development*, 132(5):897–911, 2005.

[22] B. Causier, M. Ashworth, W. Guo, and B. Davies. The TOPLESS interactome: A framework for gene repression in *Arabidopsis*. *Plant Physiol.*, 158(1):423–438, 2012.

[23] B. Causier, J. Lloyd, L. Stevens, and B. Davies. TOPLESS co-repressor interactions and their evolutionary conservation in plants. *Plant Signaling & Behavior*, 7(3):325–328, 2012.

[24] E. Chae, Q. K.-G. Tan, T. A. Hill, and V. F. Irish. An *Arabidopsis* F-box protein acts as a transcriptional co-factor to regulate floral development. *Development*, 135(7):1235–1245, 2008.

[25] M. Chalfie, Y. Tu, G. Euskirchen, W. Ward, and D. Prasher. Green fluorescent protein as a marker for gene expression. *Science*, 263(5148):802–805, 1994.

[26] V. Chau, J. Tobias, A. Bachmair, D. Marriott, D. Ecker, D. Gonda, and A. Varshavsky. A multiubiquitin chain is confined to specific lysine in a targeted short-lived protein. *Science*, 243(4898):1576–1583, 1989.

[27] C.-F. Chuang and E. M. Meyerowitz. Specific and heritable genetic interference by double-stranded RNA in *Arabidopsis thaliana*. *Proc. Natl. Acad. Sci. U. S. A.*, 97(9):4985–4990, 2000.

[28] S. Chupreta, S. Holmstrom, L. Subramanian, and J. A. Iñiguez Lluhí. A small conserved surface in SUMO is the critical structural determinant of its transcriptional inhibitory properties. *Mol. Cell. Biol.*, 25(10):4272–4282, 2005.

[29] S. E. Clark, M. P. Running, and E. M. Meyerowitz. CLAVATA3 is a specific regulator of shoot and floral meristem development affecting the same processes as CLAVATA1. *Development*, 121(7):2057–2067, 1995.

[30] F. Crick. Central dogma of molecular biology. *Nature*, 227(5258):561–563, 1970.

[31] H. Cui, M. P. Levesque, T. Vernoux, J. W. Jung, A. J. Paquette, K. L. Gallagher, J. Y. Wang, I. Blilou, B. Scheres, and P. N. Benfey. An evolutionarily conserved mechanism delimiting SHR movement defines a single layer of endodermis in plants. *Science*, 316(5823):421–425, 2007.

[32] G. Daum, A. Medzihradszky, T. Suzaki, and J. U. Lohmann. A mechanistic framework for noncell autonomous stem cell induction in *Arabidopsis*. *Proc. Natl. Acad. Sci. U. S. A.*, 111(40):14619–14624, 2014.

[33] R. N. Day. Visualization of Pit-1 transcription factor interactions in the living cell nucleus by fluorescence resonance energy transfer microscopy. *Mol. Endocrinol.*, 12(9):1410–1419, 1998. PMID: 9731708.

[34] J. C. Dohm, C. Lottaz, T. Borodina, and H. Himmelbauer. Substantial biases in ultra-short read data sets from high-throughput DNA sequencing. *Nucleic Acids Res.*, 36(16):e105, 2008.

[35] R. J. Dohmen. SUMO protein modification. *Biochim. Biophys. Acta*, 1695(1):113 – 131, 2004. The Ubiquitin-Proteasome System.

[36] J. X. Du, A. B. Bialkowska, B. B. McConnell, and V. W. Yang. SUMOylation regulates nuclear localization of Kruppel-like Factor 5. *J. Biol. Chem.*, 283(46):31991–32002, Sept. 2008.

[37] N. Elrouby, M. V. Bonequi, A. Porri, and G. Coupland. Identification of *Arabidopsis* SUMO-interacting proteins that regulate chromatin activity and developmental transitions. *Proc. Natl. Acad. Sci. U. S. A.*, 110(49):19956–19961, 2013.

[38] R. Farras, A. Ferrando, J. Jasik, T. Kleinow, L. Okresz, A. Tiburcio, K. Salchert, C. del Pozo, J. Schell, and C. Koncz. SKP1-SnRK protein kinase interactions mediate proteasomal binding of a plant SCF ubiquitin ligase. *The EMBO Journal*, 20(11):2742–2756, 2001.

[39] J. Field, J. Nikawa, D. Broek, B. MacDonald, L. Rodgers, I. A. Wilson, R. A. Lerner, and M. Wigler. Purification of a RAS-responsive adenylyl cyclase complex from *Saccharomyces cerevisiae* by use of an epitope addition method. *Mol. Cell. Biol.*, 8(5):2159–2165, 1988.

[40] S. Fields and O.-k. Song. A novel genetic system to detect protein-protein interactions. *Nature*, 340(6230):245–246, July 1989.

[41] A. Fire, S. Xu, M. K. Montgomery, S. A. Kostas, S. E. Driver, and C. C. Mello. Potent and specific genetic interference by double-stranded RNA in *Caenorhabditis elegans*. *Nature*, 391(6669):806–811, Feb. 1998.

[42] J. Fletcher. The ULTRAPETALA gene controls shoot and floral meristem size in *Arabidopsis*. *Development*, 128(8):1323–1333, 2001.

[43] A. P. Fordham Skelton, P. Chilley, V. Lumbreras, S. Reignoux, T. R. Fenton, C. C. Dahm, M. Pages, and J. A. Gatehouse. A novel higher plant protein tyrosine phosphatase interacts with SNF1-related protein kinases via a KIS (kinase interaction sequence) domain. *The Plant Journal*, 29(6):705–715, 2002.

[44] K. L. Gallagher, A. J. Paquette, K. Nakajima, and P. N. Benfey. Mechanisms regulating SHORT-ROOT intercellular movement. *Curr. Biol.*, 14(20):1847 – 1851, 2004.

[45] J.-L. Gallois, F. R. Nora, Y. Mizukami, and R. Sablowski. WUSCHEL induces shoot stem cell activity and developmental plasticity in the root meristem. *Genes Dev.*, 18(4):375–380, 2004.

[46] J.-L. Gallois, C. Woodward, G. V. Reddy, and R. Sablowski. Combined SHOOT MERISTEMLESS and WUSCHEL trigger ectopic organogenesis in *Arabidopsis*. *Development*, 129(13):3207–3217, 2002.

[47] Gerald W. Gordon, Gail Berry, Xiao Huan Liang, Beth Levine, and Brian Herman. Quantitative fluorescence resonance energy transfer measurements using fluorescence microscopy. *Biophys. J.*, 74(5):2702 – 2713, 1998.

[48] R. Gietz, A. Robbins, K. Graham, B. Triggs Raine, and R. Woods. Identification of proteins that interact with a protein of interest: Applications of the yeast two-hybrid system. *Mol. Cell. Biochem.*, 20:67–79, 1997.

[49] A. Goldshmidt, J. P. Alvarez, J. L. Bowman, and Y. Eshed. Signals derived from YABBY gene activities in organ primordia regulate growth and partitioning of *Arabidopsis* shoot apical meristems. *The Plant Cell*, 20(5):1217–1230, 2008.

[50] G. Goldstein, M. Scheid, U. Hammerling, D. H. Schlesinger, H. D. Niall, and E. A. Boyse. Isolation of a polypeptide that has lymphocyte-differentiating properties and is probably represented universally in living cells. *Proc. Natl. Acad. Sci. U. S. A.*, 72(1):11–15, 1975.

[51] F. Golebiowski, I. Matic, M. H. Tatham, C. Cole, Y. Yin, A. Nakamura, J. Cox, G. J. Barton, M. Mann, and R. T. Hay. System-wide changes to SUMO modifications in response to heat shock. *Science Signaling*, 2(72):ra24–ra24, 2009.

[52] S. P. Gordon, M. G. Heisler, G. V. Reddy, C. Ohno, P. Das, and E. M. Meyerowitz. Pattern formation during de novo assembly of the *Arabidopsis* shoot meristem. *Development*, 134(19):3539–3548, 2007.

[53] E. D. Green and M. V. Olson. Systematic screening of yeast artificial-chromosome libraries by use of the polymerase chain reaction. *Proc. Natl. Acad. Sci. U. S. A.*, 87(3):1213–1217, 1990.

[54] A. Grishok, A. E. Pasquinelli, D. Conte, N. Li, S. Parrish, I. Ha, D. L. Baillie, A. Fire, G. Ruvkun, and C. C. Mello. Genes and mechanisms related to RNA interference regulate expression of the small temporal RNAs that control *C. elegans* developmental timing. *Cell*, 106(1):23–34, 2001.

[55] Y. Guo, L. Han, M. Hymes, R. Denver, and S. E. Clark. CLAVATA2 forms a distinct CLE-binding receptor complex regulating *Arabidopsis* stem cell specification. *The Plant Journal*, 63(6):889–900, 2010.

[56] A. J. Hamilton and D. C. Baulcombe. A species of small antisense RNA in posttranscriptional gene silencing in plants. *Science*, 286(5441):950–952, 1999.

[57] J. T. Hannich, A. Lewis, M. B. Kroetz, S.-J. Li, H. Heide, A. Emili, and M. Hochstrasser. Defining the SUMO-modified proteome by multiple approaches in *Saccharomyces cerevisiae*. *J. Biol. Chem.*, 280(6):4102–4110, 2005.

[58] J. L. Heazlewood, R. E. Verboom, J. Tonti Filippini, I. Small, and A. H. Millar. SUBA: the *Arabidopsis* Subcellular Database. *Nucleic Acids Res.*, 35(suppl 1):D213–D218, 2007.

[59] C.-M. Hecker, M. Rabiller, K. Haglund, P. Bayer, and I. Dikic. Specification of SUMO1- and SUMO2-interacting motifs. *J. Biol. Chem.*, 281(23):16117–16127, 2006.

[60] A. Hershko, H. Heller, S. Elias, and A. Ciechanover. Components of ubiquitin-protein ligase system. resolution, affinity purification, and role in protein breakdown. *J. Biol. Chem.*, 258(13):8206–14, 1983.

[61] P. Hilson, J. Allemeersch, T. Altmann, S. Aubourg, A. Avon, J. Beynon, R. P. Bhalerao, F. Bitton, M. Caboche, B. Cannoot, V. Chardakov, C. Cognet Holliger, V. Colot, M. Crowe, C. Darimont, S. Durinck, H. Eickhoff, A. F. de Longevialle, E. E. Farmer, M. Grant, M. T. Kuiper, H. Lehrach, C. Léon, A. Leyva, J. Lundeberg, C. Lurin, Y. Moreau, W. Nietfeld, J. Paz Ares, P. Reymond, P. Rouzé, G. Sandberg, M. D. Segura, C. Serizet, A. Tabrett, L. Taconnat, V. Thareau, P. Van Hummelen, S. Vercruysse, M. Vuylsteke, M. Weingartner, P. J. Weisbeek, V. Wirta, F. R. Wittink, M. Zabeau, and I. Small. Versatile gene-specific sequence tags for *Arabidopsis* functional genomics: Transcript profiling and reverse genetics applications. *Genome Res.*, 14(10b):2176–2189, 2004.

[62] M. Hirst, C. Ho, L. Sabourin, M. Rudnicki, L. Penn, and I. Sadowski. A two-hybrid system for transactivator bait proteins. *Proc. Natl. Acad. Sci. U. S. A.*, 98(15):8726–8731, 2001.

[63] A. Hoffmann and R. Roeder. Purification of his-tagged proteins in non-denaturing conditions suggests a convenient method for protein interaction studies. *Nucleic Acids Res.*, 19(22):6337, 1991.

[64] R. M. Hofmann and C. M. Pickart. Noncanonical MMS2-encoded ubiquitin-conjugating enzyme functions in assembly of novel polyubiquitin chains for DNA repair. *Cell*, 96(5):645 – 653, 1999.

[65] B. Hook, D. Bernstein, B. Zhang, and M. Wickens. RNA–protein interactions in the yeast three-hybrid system: Affinity, sensitivity, and enhanced library screening. *RNA*, 11(2):227–233, 2005.

[66] T. P. Hopp, K. S. Prickett, V. L. Price, R. T. Libby, C. J. March, D. Pat Cerretti, D. L. Urdal, and P. J. Conlon. A short polypeptide marker sequence useful for recombinant protein identification and purification. *Nat. Biotechnol.*, 6(10):1204–1210, Oct. 1988.

[67] C.-D. Hu, Y. Chinenov, and T. K. Kerppola. Visualization of interactions among bZIP and Rel family proteins in living cells using bimolecular fluorescence complementation. *Mol. Cell*, 9(4):789 – 798, 2002.

[68] L. Huang, S. Yang, S. Zhang, M. Liu, J. Lai, Y. Qi, S. Shi, J. Wang, Y. Wang, Q. Xie, and C. Yang. The arabidopsis SUMO E3 ligase AtMMS21, a homologue of NSE2/MMS21, regulates cell proliferation in the root. *The Plant Journal*, 60(4):666–678, 2009.

[69] M. Ikeda, N. Mitsuda, and M. Ohme Takagi. Arabidopsis WUSCHEL is a bifunctional transcription factor that acts as a repressor in stem cell regulation and as an activator in floral patterning. *The Plant Cell*, 21(11):3493–3505, 2009.

[70] T. Ishida, S. Fujiwara, K. Miura, N. Stacey, M. Yoshimura, K. Schneider, S. Adachi, K. Minamisawa, M. Umeda, and K. Sugimoto. SUMO E3 ligase HIGH PLOIDY2 regulates endocycle onset and meristem maintenance in *Arabidopsis*. *The Plant Cell*, 21(8):2284–2297, 2009.

[71] E. Isono and C. Schwechheimer. *Plant Developmental Biology: Methods and Protocols*, chapter Co-immunoprecipitation and Protein Blots, pages 377–387. Humana Press, Totowa, NJ, 2010.

[72] T. Ito, T. Chiba, R. Ozawa, M. Yoshida, M. Hattori, and Y. Sakaki. A comprehensive two-hybrid analysis to explore the yeast protein interactome. *Proc. Natl. Acad. Sci. U. S. A.*, 98(8):4569–4574, 2001.

[73] P. James, J. Halladay, and E. A. Craig. Genomic libraries and a host strain designed for highly efficient two-hybrid selection in yeast. *Genetics*, 144(4):1425–1436, 1996.

[74] P. Kaiser, K. Flick, C. Wittenberg, and S. I. Reed. Regulation of transcription by ubiquitination without proteolysis: Cdc34/SCFMet30-mediated inactivation of the transcription factor Met4. *Cell*, 102(3):303 – 314, 2000.

[75] S. Kalve, J. Fotschki, T. Beeckman, K. Vissenberg, and G. T. Beemster. Three-dimensional patterns of cell division and expansion throughout the development of *Arabidopsis thaliana* leaves. *J. Exp. Bot.*, 2014.

[76] S. Kaul, H. L. Koo, J. Jenkins, M. Rizzo, T. Rooney, L. J. Tallon, T. Feldblyum, W. Nierman, M.-I. Benito, X. Lin, C. D. Town, J. C. Venter, C. M. Fraser, S. Tabata, Y. Nakamura, T. Kaneko, S. Sato, E. Asamizu, T. Kato, H. Kotani, S. Sasamoto, J. R. Ecker, A. Theologis, N. A. Federspiel, C. J. Palm, B. I. Osborne, P. Shinn, A. B. Conway, V. S. Vysotskaia, K. Dewar, L. Conn, C. A. Lenz, C. J. Kim, N. F. Hansen, S. X. Liu, E. Buehler, H. Altafi, H. Sakano, P. Dunn, B. Lam, P. K. Pham, Q. Chao, M. Nguyen, G. Yu, H. Chen, A. Southwick, J. M. Lee, M. Miranda, M. J. Toriumi, R. W. Davis, R. Wambutt, G. Murphy, A. Dusterhoft, W. Stiekema, T. Pohl, K.-D. Entian, N. Terryn, G. Volckaert, M. Salanoubat, N. Choisne, M. Rieger, W. Ansorge, M. Unseld, B. Fartmann, G. Valle, F. Artiguenave, J. Weissenbach, F. Quetier, R. K. Wilson, M. de la Bastide, M. Sekhon, E. Huang, L. Spiegel, L. Gnoj, K. Pepin, J. Murray, D. Johnson, K. Habermann, N. Dedhia, L. Parnell, R. Preston, L. Hillier, E. Chen, M. Marra, R. Martienssen, W. R. McCombie, K. Mayer, O. White, M. Bevan, K. Lemcke, T. H. Creasy, C. Bielke, B. Haas, D. Haase, R. Maiti, S. Rudd, J. Peterson, H. Schoof, D. Frishman, B. Morgenstern, P. Zaccaria, M. Ermolaeva, M. Pertea, J. Quackenbush, N. Volfovsky, D. Wu, T. M. Lowe, S. L. Salzberg, H.-W. Mewes, S. Rounsley, D. Bush, S. Subramaniam, I. Levin, S. Norris, R. Schmidt, A. Acarkan, I. Bancroft, F. Quetier, A. Brennicke, J. Eisen, T. Bureau, B.-A. Legault, Q.-H. Le, N. Agrawal, Z. Yu, R. Martienssen, G. Copenhaver, S. Luo, C. Pikaard, D. Preuss, I. Paulsen, M. Sussman, A. Britt, D. Selinger, R. Pandey, D. Mount, V. Chandler, R. Jorgensen, C. Pikaard, G. Juergens, E. Meyerowitz, A. Theologis, J. Dangl, J. Jones, M. Chen, J. Chory, and M. Somerville. Analysis of the genome sequence of the flowering plant *Arabidopsis thaliana*. *Nature*, 408(6814):796–815, 2000.

[77] T. K. Kerppola. Bimolecular fluorescence complementation (BiFC) analysis as a probe of protein interactions in living cells. *Annu. Rev. of Biophys.*, 37(1):465–487, 2008. PMID: 18573091.

[78] M. Kieffer, Y. Stern, H. Cook, E. Clerici, C. Maulbetsch, T. Laux, and B. Davies. Analysis of the transcription factor WUSCHEL and its functional homologue in *Antirrhinum* reveals a potential mechanism for their roles in meristem maintenance. *The Plant Cell*, 18(3):560–573, 2006.

[79] J.-Y. Kim, Y. Rim, J. Wang, and D. Jackson. A novel cell-to-cell trafficking assay indicates that the KNOX homeodomain is necessary and sufficient for intercellular protein and mRNA trafficking. *Genes Dev.*, 19(7):788–793, 2005.

[80] U.-J. Kim, B. W. Birren, T. Slepak, V. Mancino, C. Boysen, H.-L. Kang, M. I. Simon, and H. Shizuya. Construction and characterization of a Human bacterial artificial chromosome library. *Genomics*, 34(2):213 – 218, 1996.

[81] Koji Koizumi, Shuang Wu, Aurora MacRae Crerar, and Kimberly L. Gallagher. An essential protein that interacts with endosomes and promotes movement of the SHORT-ROOT transcription factor. *Curr. Biol.*, 21(18):1559 – 1564, 2011.

[82] T. Kondo, S. Sawa, A. Kinoshita, S. Mizuno, T. Kakimoto, H. Fukuda, and Y. Sakagami. A plant peptide encoded by CLV3 identified by in Situ MALDI-TOF MS analysis. *Science*, 313(5788):845–848, 2006.

[83] M. Koornneeff, L. Dellaert, and J. van der Veen. EMS- and relation-induced mutation frequencies at individual loci in *Arabidopsis thaliana* (l.) heynh. *Mutat. Res.*, 93(1):109 – 123, 1982.

[84] K. Kremer, D. Kamin, E. Rittweger, J. Wilkes, H. Flammer, S. Mahler, J. Heng, C. J. Tonkin, G. Langsley, S. W. Hell, V. B. Carruthers, D. J. P. Ferguson, and M. Meissner. An overexpression screen of *Toxoplasma gondii* Rab-GTPases reveals distinct transport routes to the micronemes. *PLoS Pathog.*, 9(3):e1003213, 2013.

[85] P. J. Krysan, J. C. Young, and M. R. Sussman. T-DNA as an insertional mutagen in *Arabidopsis*. *The Plant Cell*, 11(12):2283–2290, 1999.

[86] J. Kurepa, J. M. Walker, J. Smalle, M. M. Gosink, S. J. Davis, T. L. Durham, D.-Y. Sung, and R. D. Vierstra. The small ubiquitin-like modifier (SUMO) protein modification system in *Arabidopsis* : Accumulation of SUMO1 and -2 conjugates is increased by stress. *J. Biol. Chem.*, 278(9):6862–6872, 2003.

[87] F. Lamoliatte, D. Caron, C. Durette, L. Mahrouche, M. A. Maroui, O. Caron Lizotte, E. Bonneil, M. K. Chelbi Alix, and P. Thibault. Large-scale analysis of lysine SUMOylation by SUMO remnant immunoaffinity profiling. *Nat. Commun.*, 5:–, Nov. 2014.

[88] B. Langmead, C. Trapnell, M. Pop, and S. Salzberg. Ultrafast and memory-efficient alignment of short DNA sequences to the human genome. *Genome Biol.*, 10(3):R25, 2009.

[89] T. Laux, K. Mayer, J. Berger, and G. Jurgens. The WUSCHEL gene is required for shoot and floral meristem integrity in *Arabidopsis*. *Development*, 122(1):87–96, 1996.

[90] A. Leibfried, J. P. C. To, W. Busch, S. Stehling, A. Kehle, M. Demar, J. J. Kieber, and J. U. Lohmann. WUSCHEL controls meristem function by direct regulation of cytokinin-inducible response regulators. *Nature*, 438(7071):1172–1175, Dec. 2005.

[91] M. Lenhard, G. Jürgens, and T. Laux. The WUSCHEL and SHOOTMERISTEMLESS genes fulfil complementary roles in *Arabidopsis* shoot meristem regulation. *Development*, 129(13):3195–3206, 2002.

[92] J. Li and I. Herskowitz. Isolation of ORC6, a component of the yeast origin recognition complex by a one-hybrid system. *Science*, 262(5141):1870–1874, 1993.

[93] C. Liu, W. Xi, L. Shen, C. Tan, and H. Yu. Regulation of floral patterning by flowering time genes. *Dev. Cell*, 16(5):711 – 722, 2009.

[94] F. Liu, W. Ni, M. E. Griffith, Z. Huang, C. Chang, W. Peng, H. Ma, and D. Xie. The ASK1 and ASK2 genes are essential for *Arabidopsis* early development. *The Plant Cell*, 16(1):5–20, 2004.

[95] L. Liu, Y. Li, S. Li, N. Hu, Y. He, R. Pong, D. Lin, L. Lu, and M. Law. Comparison of next-generation sequencing systems. *J. Biomed. Biotech.*, 2012, 2012.

[96] X. Liu, Y. J. Kim, R. Müller, R. E. Yumul, C. Liu, Y. Pan, X. Cao, J. Goodrich, and X. Chen. AGAMOUS terminates floral stem cell maintenance in *Arabidopsis* by directly repressing WUSCHEL through recruitment of polycomb group proteins. *The Plant Cell*, 23(10):3654–3670, 2011.

[97] J. A. Long, C. Ohno, Z. R. Smith, and E. M. Meyerowitz. TOPLESS regulates apical embryonic fate in *Arabidopsis*. *Science*, 312(5779):1520–1523, 2006.

[98] R. Mahajan, C. Delphin, T. Guan, L. Gerace, and F. Melchior. A small ubiquitin-related polypeptide involved in targeting RanGAP1 to nuclear pore complex protein RanBP2. *Cell*, 88(1):97 – 107, 1997.

[99] I. Maldonado Mendoza and C. Nessler. Molecular characterization of the AP19 gene family in *Arabidopsis thaliana*: Components of the golgi AP-1 clathrin assembly protein complex. *Plant Mol. Biol.*, 35(6):865–872, 1997.

[100] J. C. Marioni, C. E. Mason, S. M. Mane, M. Stephens, and Y. Gilad. RNA-seq: An assessment of technical reproducibility and comparison with gene expression arrays. *Genome Res.*, 18(9):1509–1517, 2008.

[101] T. Matsumura, T. Suzuki, K. Aizawa, Y. Munemasa, S. Muto, M. Horikoshi, and R. Nagai. The deacetylase HDAC1 negatively regulates the cardiovascular transcription factor Krüppel-like factor 5 through direct interaction. *J. Biol. Chem.*, 280(13):12123–12129, 2005.

[102] K. F. Mayer, H. Schoof, A. Haecker, M. Lenhard, G. Jurgens, and T. Laux. Role of WUSCHEL in regulating stem cell fate in the *Arabidopsis* shoot meristem. *Cell*, 95(6):805 – 815, 1998.

[103] M. J. Mazur and H. A. van den Burg. Global SUMO proteome responses guide gene regulation, mRNA biogenesis, and plant stress responses. *Front. Plant Sci.*, 3:215–, Aug. 2012.

[104] M. J. Miller, G. A. Barrett Wilt, Z. Hua, and R. D. Vierstra. Proteomic analyses identify a diverse array of nuclear processes affected by small ubiquitin-like modifier conjugation in *Arabidopsis*. *Proc. Natl. Acad. Sci. U. S. A.*, 107(38):16512–16517, 2010.

[105] A. Minty, X. Dumont, M. Kaghad, and D. Caput. Covalent modification of p73 by SUMO-1: Two-hybrid screening with p73 identifies novel SUMO-1-interacting proteins and a SUMO-1 interaction motif. *J. Biol. Chem.*, 275(46):36316–36323, 2000.

[106] K. Miura and P. M. Hasegawa. Sumoylation and other ubiquitin-like post-translational modifications in plants. *Trends Cell Biol.*, 20(4):223 – 232, 2010.

[107] K. Miura, J. B. Jin, and P. M. Hasegawa. Sumoylation, a post-translational regulatory process in plants. *Curr. Opin. Plant Biol.*, 10(5):495 – 502, 2007. Cell Signalling and Gene Regulation Edited by Jian-Kang Zhu and Ko Shimamoto.

[108] K. Miura, J. B. Jin, J. Lee, C. Y. Yoo, V. Stirm, T. Miura, E. N. Ashworth, R. A. Bressan, D.-J. Yun, and P. M. Hasegawa. SIZ1-mediated sumoylation of ICE1 controls

CBF3/DREB1A expression and freezing tolerance in *Arabidopsis*. *The Plant Cell*, 19(4):1403–1414, 2007.

[109] T. C. Mockler, X. Yu, D. Shalitin, D. Parikh, T. P. Michael, J. Liou, J. Huang, Z. Smith, J. M. Alonso, J. R. Ecker, J. Chory, and C. Lin. Regulation of flowering time in *Arabidopsis* by K homology domain proteins. *Proc. Natl. Acad. Sci. U. S. A.*, 101(34):12759–12764, 2004.

[110] S. Muller, C. Hoege, G. Pyrowolakis, and S. Jentsch. SUMO, Ubiquitin's mysterious cousin. *Nat. Rev. Mol. Cell Biol.*, 2(3):202–213, Mar. 2001.

[111] K. Mullis, F. Faloona, S. Scharf, R. Saiki, G. Horn, and H. Erlich. Specific enzymatic amplification of DNA in vitro: The polymerase chain reaction. In *Cold Spring Harbor Symposia on Quantitative Biology*, volume 51, pages 263–273. Cold Spring Harbor Laboratory Press, 1986.

[112] T. Murashige and F. Skoog. A revised medium for rapid growth and bio assays with tobacco tissue cultures. *Physiol. Plant.*, 15(3):473–497, 1962.

[113] M. Murray and W. Thompson. Rapid isolation of high molecular weight plant DNA. *Nucleic Acids Res.*, 8(19):4321–4326, 1980.

[114] K. Nakajima, G. Sena, T. Nawy, and P. N. Benfey. Intercellular movement of the putative transcription factor SHR in root patterning. *Nature*, 413(6853):307–311, Sept. 2001.

[115] K. Ohyama, H. Shinohara, M. Ogawa Ohnishi, and Y. Matsubayashi. A glycopeptide regulating stem cell fate in *Arabidopsis thaliana*. *Nat. Chem. Biol.*, 5(8):578–580, 2009.

[116] S. Okada, M. Nagabuchi, Y. Takamura, T. Nakagawa, K. Shinmyozu, J.-i. Nakayama, and K. Tanaka. Reconstitution of *Arabidopsis thaliana* SUMO pathways in *E. coli*: Functional evaluation of SUMO machinery proteins and mapping of SUMOylation sites by mass spectrometry. *Plant Cell Physiol.*, 50(6):1049–1061, 2009.

[117] D. R. Page and U. Grossniklaus. The art and design of genetic screens: *Arabidopsis thaliana*. *Nat. Rev. Genet.*, 3(2):124–136, Feb. 2002.

[118] S. W. Park, X. Hu, P. Gupta, Y.-P. Lin, S. G. Ha, and L.-N. Wei. SUMOylation of Tr2 orphan receptor involves Pml and fine-tunes Oct4 expression in stem cells. *Nat. Struct. Mol. Biol.*, 14(1):68–75, Jan. 2007.

[119] H. R. Pires, M. M. Monfared, E. A. Shemyakina, and J. C. Fletcher. ULTRAPETALA trxG genes interact with KANADI transcription factor genes to regulate *Arabidopsis* gynoecium patterning. *The Plant Cell*, 26(11):4345–4361, 2014.

[120] D. C. Prasher, V. K. Eckenrode, W. W. Ward, F. G. Prendergast, and M. J. Cormier. Primary structure of the *Aequorea victoria* green-fluorescent protein. *Gene*, 111(2):229 – 233, 1992.

[121] J. Prober, G. Trainor, R. Dam, F. Hobbs, C. Robertson, R. Zagursky, A. Cocuzza, M. Jensen, and K. Baumeister. A system for rapid DNA sequencing with fluorescent chain-terminating dideoxynucleotides. *Science*, 238(4825):336–341, 1987.

[122] G. Queval, E. Issakidis Bourguet, F. A. Hoeberichts, M. Vandorpe, B. Gakiere, H. Vanacker, M. Miginiac Maslow, F. Van Breusegem, and G. Noctor. Conditional oxidative stress responses in the *Arabidopsis* photorespiratory mutant cat2 demonstrate that redox state is a key modulator of daylength-dependent gene expression, and define photoperiod as a crucial factor in the regulation of H2O2-induced cell death. *The Plant Journal*, 52(4):640–657, 2007.

[123] G. V. Reddy. Live-imaging stem-cell homeostasis in the *Arabidopsis* shoot apex. *Curr. Opin. Plant Biol.*, 11(1):88 – 93, 2008. Growth and Development Edited by Christian Hardtke and Keiko Torii.

[124] G. V. Reddy, M. G. Heisler, D. W. Ehrhardt, and E. M. Meyerowitz. Real-time lineage analysis reveals oriented cell divisions associated with morphogenesis at the shoot apex of *Arabidopsis thaliana*. *Development*, 131(17):4225–4237, 2004.

[125] G. V. Reddy and E. M. Meyerowitz. Stem-cell homeostasis and growth dynamics can be uncoupled in the arabidopsis shoot apex. *Science*, 310(5748):663–667, 2005.

[126] S. B. Reffey, J. U. Wurthner, W. T. Parks, A. B. Roberts, and C. S. Duckett. X-linked inhibitor of apoptosis protein functions as a cofactor in transforming growth factor-B signaling. *J. Biol. Chem.*, 276(28):26542–26549, 2001.

[127] D. Reinhardt, M. Frenz, T. Mandel, and C. Kuhlemeier. Microsurgical and laser ablation analysis of interactions between the zones and layers of the tomato shoot apical meristem. *Development*, 130(17):4073–4083, 2003.

[128] J. Ren, X. Gao, C. Jin, M. Zhu, X. Wang, A. Shaw, L. Wen, X. Yao, and Y. Xue. Systematic study of protein sumoylation: Development of a site-specific predictor of SUMOsp 2.0. *Proteomics*, 9(12):3409–3412, 2009.

[129] D. Robertson. VIGS vectors for gene silencing: Many targets, many tools. *Annu. Rev. Plant Biol.*, 55(1):495–519, 2004. PMID: 15377229.

[130] J. T. Robinson, H. Thorvaldsdottir, W. Winckler, M. Guttman, E. S. Lander, G. Getz, and J. P. Mesirov. Integrative genomics viewer. *Nat. Biotechnol.*, 29(1):24–26, Jan. 2011.

[131] M. S. Rodriguez, C. Dargemont, and R. T. Hay. SUMO-1 conjugation in vivo requires both a consensus modification motif and nuclear targeting. *J. Biol. Chem.*, 276(16):12654–12659, 2001.

[132] E. Rojo, V. K. Sharma, V. Kovaleva, N. V. Raikhel, and J. C. Fletcher. CLV3 is localized to the extracellular space, where it activates the *Arabidopsis* CLAVATA stem cell signaling pathway. *The Plant Cell*, 14(5):969–977, 2002.

[133] F. Sanger, S. Nicklen, and A. R. Coulson. DNA sequencing with chain-terminating inhibitors. *Proc. Natl. Acad. Sci. U. S. A.*, 74(12):5463–5467, Dec. 1977.

[134] S. A. Saracco, M. J. Miller, J. Kurepa, and R. D. Vierstra. Genetic analysis of SUMOylation in *Arabidopsis*: Conjugation of SUMO1 and SUMO2 to nuclear proteins is essential. *Plant Physiol.*, 145(1):119–134, 2007.

[135] D. Sarkar, R. Gentleman, M. Lawrence, and Z. Yao. Chipseq: A package for analyzing chipseq data. Technical report.

[136] D. H. Schlesinger, G. Goldstein, and H. D. Niall. Complete amino acid sequence of ubiquitin, an adenylate cyclase stimulating polypeptide probably universal in living cells. *Biochemistry*, 14(10):2214–2218, 1975.

[137] H. Schoof, M. Lenhard, A. Haecker, K. F. Mayer, G. Jurgens, and T. Laux. The stem cell population of *Arabidopsis* shoot meristems is maintained by a regulatory loop between the *CLAVATA* and *WUSCHEL* genes. *Cell*, 100(6):635 – 644, 2000.

[138] A. Sessions, M. F. Yanofsky, and D. Weigel. Cell-cell signaling and movement by the floral transcription factors LEAFY and APETALA1. *Science*, 289(5480):779–781, 2000.

[139] N. C. Shaner, P. A. Steinbach, and R. Y. Tsien. A guide to choosing fluorescent proteins. *Nat. Methods*, 2(12):905–909, Dec. 2005.

[140] P. Shannon, A. Markiel, O. Ozier, N. S. Baliga, J. T. Wang, D. Ramage, N. Amin, B. Schwikowski, and T. Ideker. Cytoscape: A software environment for integrated models of biomolecular interaction networks. *Genome Res.*, 13(11):2498–2504, 2003.

[141] Z. Shen, P. E. Pardington Purtymun, J. C. Comeaux, R. K. Moyzis, and D. J. Chen. UBL1, a human ubiquitin-like protein associating with human RAD51/RAD52 proteins. *Genomics*, 36(2):271 – 279, 1996.

[142] J. Shendure, G. J. Porreca, N. B. Reppas, X. Lin, J. P. McCutcheon, A. M. Rosenbaum, M. D. Wang, K. Zhang, R. D. Mitra, and G. M. Church. Accurate multiplex polony sequencing of an evolved bacterial genome. *Science*, 309(5741):1728–1732, 2005.

[143] J. Song, L. K. Durrin, T. A. Wilkinson, T. G. Krontiris, and Y. Chen. Identification of a SUMO-binding motif that recognizes SUMO-modified proteins. *Proc. Natl. Acad. Sci. U. S. A.*, 101(40):14373–14378, 2004.

[144] J. Spence, S. Sadis, A. L. Haas, and D. Finley. A ubiquitin mutant with specific defects in DNA repair and multiubiquitination. *Mol. Cell. Biol.*, 15(3):1265–73, 1995.

[145] T. A. Steeves and I. M. Sussex. *Patterns in plant development*. Cambridge University Press, 1989.

[146] I. Sussex. Regeneration of the potato shoot apex. *Nature*, 1952.

[147] I. M. Sussex. Developmental programming of the shoot meristem. *Cell*, 56(2):225 – 229, 1989.

[148] S. Tahmasebi, M. Ghorbani, P. Savage, G. Gocevski, and X.-J. Yang. The SUMO conjugating enzyme Ubc9 is required for inducing and maintaining stem cell pluripotency. *Stem Cells*, 32(4):1012–1020, 2014.

[149] H. Thorvaldsdóttir, J. T. Robinson, and J. P. Mesirov. Integrative Genomics Viewer (IGV): High-performance genomics data visualization and exploration. *Brief. Bioinform.*, 14(2):178–192, 2013.

[150] S. Torti, F. Fornara, C. Vincent, F. Andrés, K. Nordström, U. Göbel, D. Knoll, H. Schoof, and G. Coupland. Analysis of the *Arabidopsis* shoot meristem transcriptome during floral transition identifies distinct regulatory patterns and a Leucine-rich repeat protein that promotes flowering. *The Plant Cell*, 24(2):444–462, 2012.

[151] S. Tsuruzoe, K. Ishihara, Y. Uchimura, S. Watanabe, Y. Sekita, T. Aoto, H. Saitoh, Y. Yuasa, H. Niwa, M. Kawasuji, H. Baba, and M. Nakao. Inhibition of DNA binding of Sox2 by the SUMO conjugation. *Biochem. Biophys. Res. Commun.*, 351(4):920 – 926, 2006.

[152] Y. Ueno, T. Ishikawa, K. Watanabe, S. Terakura, H. Iwakawa, K. Okada, C. Machida, and Y. Machida. Histone deacetylases and ASYMMETRIC LEAVES2 are involved in the establishment of polarity in leaves of *Arabidopsis*. *The Plant Cell*, 19(2):445–457, 2007.

[153] P. Uetz, L. Giot, G. Cagney, T. A. Mansfield, R. S. Judson, J. R. Knight, D. Lockshon, V. Narayan, M. Srinivasan, P. Pochart, A. Qureshi Emili, Y. Li, B. Godwin, D. Conover, T. Kalbfleisch, G. Vijayadamodar, M. Yang, M. Johnston, S. Fields, and J. M. Rothberg. A comprehensive analysis of protein-protein interactions in *Saccharomyces cerevisiae*. *Nature*, 403(6770):623–627, Feb. 2000.

[154] R. Ullmann, C. Chien, M. Avantaggiati, and S. Muller. An acetylation switch regulates SUMO-dependent protein interaction networks. *Mol. Cell*, 46(6):759 – 770, 2012.

[155] H. A. van den Burg, R. K. Kini, R. C. Schuurink, and F. L. Takken. *Arabidopsis* Small Ubiquitin-Like Modifier paralogs have distinct functions in development and defense. *The Plant Cell*, 22(6):1998–2016, 2010.

[156] J. C. Venter, M. D. Adams, G. G. Sutton, A. R. Kerlavage, H. O. Smith, and M. Hunkapiller. Shotgun sequencing of the human genome. *Science*, 280(5369):1540, 1998.

[157] A. Visel, M. J. Blow, Z. Li, T. Zhang, J. A. Akiyama, A. Holt, I. Plajzer Frick, M. Shoukry, C. Wright, F. Chen, V. Afzal, B. Ren, E. M. Rubin, and L. A. Pennacchio. ChIP-seq accurately predicts tissue-specific activity of enhancers. *Nature*, 457(7231):854–858, 2009.

[158] M. Walter, C. Chaban, K. Schutze, O. Batistic, K. Weckermann, C. Nake, D. Blazevic, C. Grefen, K. Schumacher, C. Oecking, K. Harter, and J. Kudla. Visualization of protein interactions in living plant cells using bimolecular fluorescence complementation. *The Plant Journal*, 40(3):428–438, 2004.

[159] R. H. Webb. Confocal optical microscopy. *Rep. Prog. Phys.*, 59(3):427, 1996.

[160] R. K. Yadav, T. Girke, S. Pasala, M. Xie, and G. V. Reddy. Gene expression map of the *Arabidopsis* shoot apical meristem stem cell niche. *Proc. Natl. Acad. Sci. U. S. A.*, 106(12):4941–4946, 2009.

[161] R. K. Yadav, M. Perales, J. Gruel, T. Girke, H. Jönsson, and G. V. Reddy. WUSCHEL protein movement mediates stem cell homeostasis in the *Arabidopsis* shoot apex. *Genes Dev.*, 25(19):2025–2030, 2011.

[162] R. K. Yadav, M. Perales, J. Gruel, C. Ohno, M. Heisler, T. Girke, H. Jonsson, and G. V. Reddy. Plant stem cell maintenance involves direct transcriptional repression of differentiation program. *Mol. Syst. Biol.*, 9(1), 2013.

[163] R. K. Yadav, M. Tavakkoli, and G. V. Reddy. WUSCHEL mediates stem cell homeostasis by regulating stem cell number and patterns of cell division and differentiation of stem cell progenitors. *Development*, 137(21):3581–3589, 2010.

[164] R. K. Yadav, M. Tavakkoli, M. Xie, T. Girke, and G. V. Reddy. A high-resolution gene expression map of the *Arabidopsis* shoot meristem stem cell niche. *Development*, 141(13):2735–2744, 2014.

[165] Y. Yoneda, M. Hieda, E. Nagoshi, and Y. Miyamoto. Nucleocytoplasmic protein transport and recycling of Ran. *Cell Struct. Funct.*, 24(6):425–433, 1999.

[166] H. Yu, L. Tardivo, S. Tam, E. Weiner, F. Gebreab, C. Fan, N. Svrzikapa, T. Hirozane Kishikawa, E. Rietman, X. Yang, J. Sahalie, K. Salehi Ashtiani, T. Hao, M. E. Cusick, D. E. Hill, F. P. Roth, P. Braun, and M. Vidal. Next-generation sequencing to generate interactome datasets. *Nat. Methods*, 8(6):478–480, J 2011.

[167] L. Yu, E. Simon, A. Trotochaud, and S. Clark. POLTERGEIST functions to regulate meristem development downstream of the CLAVATA loci. *Development*, 127(8):1661–1670, 2000.

[168] M. Zdarska, P. Zatloukalova, M. Benitez, O. S edo, D. Potesil, O. Novak, J. Svacinova, B. Pesek, J. Malbeck, J. Vasickova, Z. Zdrahal, and J. Hejatko. Proteome analysis in *Arabidopsis* reveals shoot- and root-specific targets of cytokinin action and differential regulation of hormonal homeostasis. *Plant Physiol.*, 161(2):918–930, Nov. 2012.

[169] J. Zhang and S. Lautar. A yeast three-hybrid method to clone ternary protein complex components. *Anal. Biochem.*, 242(1):68–72, 1996.

[170] Q. Zhao, Y. Xie, Y. Zheng, S. Jiang, W. Liu, W. Mu, Z. Liu, Y. Zhao, Y. Xue, and J. Ren. GPS-SUMO: A tool for the prediction of sumoylation sites and SUMO-interaction motifs. *Nucleic Acids Res.*, 42(W1):W325–W330, 2014.

[171] S. Zhong, Z. Lin, R. Fray, and D. Grierson. Improved plant transformation vectors for fluorescent protein tagging. *Transgenic Res.*, 17(5):985–989, 2008.

[172] Y. Zhou, X. Liu, E. M. Engstrom, Z. L. Nimchuk, J. L. Pruneda Paz, P. T. Tarr, A. Yan, S. A. Kay, and E. M. Meyerowitz. Control of plant stem cell function by conserved interacting transcriptional regulators. *Nature*, 517(7534):377–380, Jan. 2015.

[173] L. Zhu, C. Gazin, N. Lawson, H. Pages, S. Lin, D. Lapointe, and M. Green. ChIPpeakAnno: A bioconductor package to annotate ChIP-seq and ChIP-chip data. *BMC Bioinformatics*, 11(1):237, 2010.

[174] L. J. Zhu. Integrative analysis of ChIP-Chip and ChIP-Seq dataset. In T.-L. Lee and A. C. Shui Luk, editors, *Tiling Arrays*, volume 1067 of *Methods in Molecular Biology*, pages 105–124. Humana Press, 2013.